

Theory of phonon angular momentum transport across smooth interfaces between crystals

Yuta Suzuki,^{1,*} Shuntaro Sumita,^{2,3,4,†} and Yusuke Kato^{2,5,6,‡}

¹*Department of Physics, Tokyo Institute of Technology, 2-12-1 Ookayama, Tokyo 152-8551, Japan*

²*Department of Basic Science, The University of Tokyo, 3-8-1 Komaba, Tokyo 153-8902, Japan*

³*Komaba Institute for Science, The University of Tokyo, 3-8-1 Komaba, Tokyo 153-8902, Japan*

⁴*Condensed Matter Theory Laboratory, RIKEN CPR, Wako, Saitama 351-0198, Japan*

⁵*Quantum Research Center for Chirality, Institute for Molecular Science, Okazaki, Aichi 444-8585, Japan*

⁶*Department of Physics, Graduate School of Science,
The University of Tokyo, 7-3-1 Hongo, Tokyo 113-0033, Japan*

(Dated: September 16, 2024)

We study the spatial profile of phonon angular momentum in a junction between a chiral crystal and a non-chiral (achiral) crystal with a smooth, flat contact at low temperatures. In this junction, the angular momentum is generated by an imbalance in non-equilibrium distributions between transverse acoustic modes. We incorporate the Fresnel coefficients for elastic waves to establish a boundary condition for the phonon distributions, for which we also provide a proof. We demonstrate that the spin angular momentum of phonon induced by a thermal gradient in the chiral crystal diffuses into the adjacent achiral crystal. This diffusion is accompanied by a finite orbital angular momentum stemming from an acoustic analog of the Imbert–Fedorov shift in reflected/transmitted wave packets. Concerning angular momentum fluxes that are polarized normal to the interface, the sum of the spin and orbital components is continuous at the interface. This continuity confirms the conservation law of total phonon angular momentum.

I. INTRODUCTION

The existence of circularly-polarized phonon modes in which atoms rotate around their stable positions has been predicted theoretically [1–4] and ensured by subsequent detection [5–8]. These phonon modes have been dubbed the “chiral phonons.” Triggered by these studies on the chiral phonon, much effort has been devoted to understanding its role in transport [9–15], which stems from phonon angular momentum (AM) [2, 16–19]. In particular, spin angular momentum (SAM) is an extensive quantity characteristic to the chiral phonon, defined as a statistical average of the sum of mechanical AM over all atoms [2, 16–19]. Although the chiral phonon is also characterized by discrete pseudo AM [3, 6, 7, 20–23], which is related to SAM in helical chains [24], we confine ourselves in the present paper to the phonon SAM in crystals.

One of the key features of the chiral-phonon transport is the coupling between electron spin and the phonon spin [25–30], which is studied by injecting phonon spin from one crystal to another. It has been recognized that the AM of chiral phonons is transferred to that of electrons in ferromagnets [25, 27], ferrimagnet [26], magnetic oxide heterostructure [28], copper [29], and non-magnetic heavy metals [30]. In addition, some mechanisms of spin-dependent coupling between phonons and electrons [31, 32], and phonons and magnons [33], as well as a spin conversion theory at the interface by virtue of spin–vorticity coupling [34] have been proposed recently.

In contrast to the conversion from phonon spin to electron spin, the transport of phonon spin itself between two different crystals has yet to be discussed. In practice, as a sound wave propagates between media, it is plausible that chiral phonons of acoustic modes transmit across the interface. Since the chiral phonon is regarded as a source of the electron-spin polarization, it is essential to provide the transmission ratio of phonon SAM as well as its spatial distribution in the junction of two crystals.

In the present paper we build a theoretical framework for the phonon AM diffusion from a chiral crystal (CC) to an adjacent achiral crystal (ACC), as illustrated in Fig. 1(a). Here the CC is subject to a thermal gradient in an arbitrary direction. We consider that the CC/ACC junction is at a sufficiently low temperature, and phonon transport is dominated by low-energy acoustic phonons with long wavelengths. For simplicity, we neglect any excitations in the crystals other than the acoustic phonons, such as electrons and magnons.

We further approximate each crystal as an isotropic medium in the long-wavelength limit. Then the SAM survives in non-equilibrium states where the numbers of phonons are different between the left-handed (LH) and right-handed (RH) circularly polarized acoustic modes. The two modes are exactly degenerate in the ACC, and approximately degenerate in the CC in the long-wavelength limit, as shown in Fig. 1(b). Here the CC allows the imbalance in the number of phonons between the LH and RH modes under the thermal gradient ∇T ; this imbalance results in phonon-spin polarization parallel to ∇T [9]. Our model of the CC may correspond to a chiral polycrystal with the same handedness that satisfies both macroscopic isotropy and microscopic chirality.

We determine the spatial distribution of phonons for

* suzuki.y.ep@m.titech.ac.jp

† s-sumita@g.ecc.u-tokyo.ac.jp

‡ yusuke@phys.c.u-tokyo.ac.jp

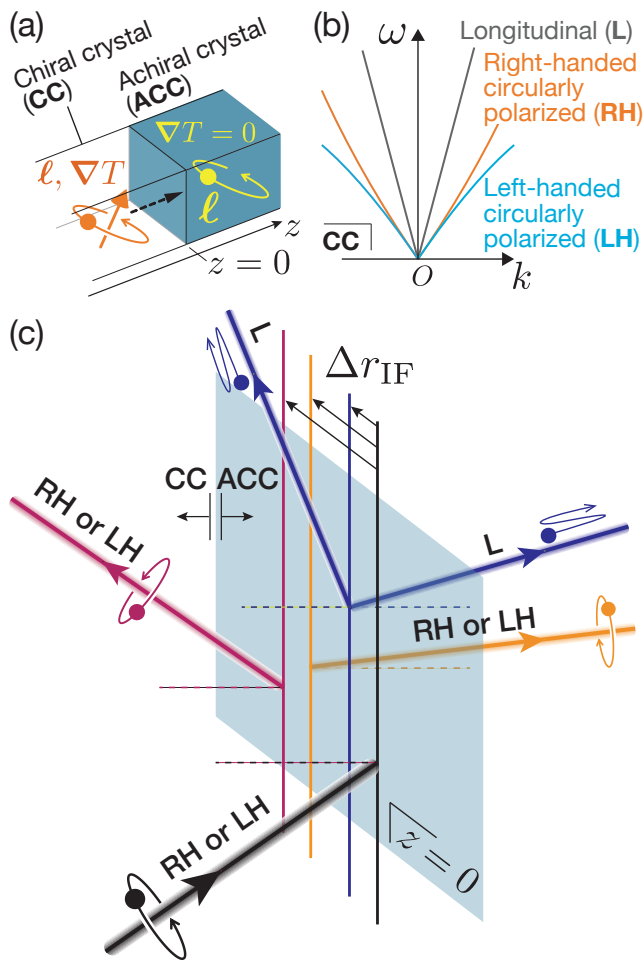


FIG. 1. Schematic view of (a) diffusion of phonon angular momentum (AM) ℓ through interface, (b) dispersion relation of acoustic modes in the chiral crystal (CC), and (c) detailed reflection/transmission of phonon at the interface. In the CC, the phonon AM ℓ is generated by the thermal gradient ∇T [(a)], since the degeneracy of transverse modes is slightly lifted [(b)]. At the interface seen in (c), an enlarged view of (a), the number of phonons in the incident wave (shown in black) is redistributed to the number of phonons in the reflected and transmitted waves (shown in colored). The angle of reflection/refraction obeys the laws of reflection/refraction, while the plane of reflection/refraction deviates from that of incidence by a distance Δr_{IF} .

each mode on the basis of the Boltzmann formalism, while imposing a boundary condition for the phonon distributions in the CC and ACC. We here assume that the interface is smooth and flat; its surface roughness is negligible compared to the wavelength. For the smooth and flat interface, the acoustic mismatch model [35–37] is often adopted to explain interfacial phonon transport. With this idea, we introduce a boundary condition that consists of linear equations among phonon distributions of incident and reflected/transmitted waves; the coefficients of the equations are taken from elastic power reflectance and transmittance. We include mode conver-

sions by the interfacial scattering in order to fully account for the transmittance without losing any information about the phonon polarization. Explicit expression will be shown later in Eqs. (68) and (87). We also provide a derivation of the boundary condition in Sect. IV.

Elastic waves transmit easily between two media when their acoustic impedances and velocities match each other. We demonstrate that the diffusion of phonon SAM polarized *parallel* to the interface shows the same behavior. We can, however, increase the diffusion of SAM density polarized *normal* to the interface by choosing the ACC so that its transverse-wave velocity is relatively low. Detailed explanations are given in Sect. VI.

We emphasize that the interfacial scattering conserves the phonon AM polarized normal to the interface. Since the smooth and flat interface has a continuous rotational symmetry, neither the source nor sink of AM polarized normal to the interface exists at the interface. In steady state, the flux of AM is continuous at the interface as a result.

We thus examine the AM conservation for phonons at the interface, for which the SAM alone is not sufficient. There are two kinds of AM involved in the conservation law in acoustics [38]: one is the SAM stemming from the circular polarization; the other is the orbital angular momentum (OAM) [39, 40]. The OAM is further divided into intrinsic contribution accompanied by acoustic vortex beams [41–44] and extrinsic contribution. In particular, we focus on the extrinsic OAM stemming from boundary scatterings. When a wave packet enters the interface, the plane of reflection/refraction generally deviates from that of incidence [see Fig. 1(c) and the deviation Δr_{IF} shown in it]. This spatial deviation (transverse shift), which is termed the Imbert–Fedorov (IF) shift [45–47] or the spin Hall effect of light [48] in optics, results in the extrinsic OAM in the wave packets. In the absence of the intrinsic OAM, the sum of the SAM and extrinsic OAM is predicted to be conserved even at the sharp boundary [38]. To the best of our knowledge, however, an exact expression of the acoustic transverse shift when a circularly polarized beam is incident has been left unnoticed. We provide the expression of the acoustic transverse shift in Sect. III. We also apply the AM conservation law to phonons. We confirm that the total phonon AM flux is continuous at the interface, and predict the accumulation of phonon OAM near the interface.

The rest of the present paper is organized in the manner shown in Fig. 2. In Sect. II we review the reflection/transmission of monochromatic plane waves. In Sect. III we address elastic beams and derive their transverse shifts as well as total AM conservation at the interface. Section IV is devoted to the derivation of the boundary condition for phonon distribution functions. Readers with a specific interest in phonon transport in junctions should start reading from Sect. V and VI: the formulation of phonon SAM transport is given in Sect. V, and we demonstrate the diffusion of the SAM across the interface in Sect. VI. We then introduce the extrinsic

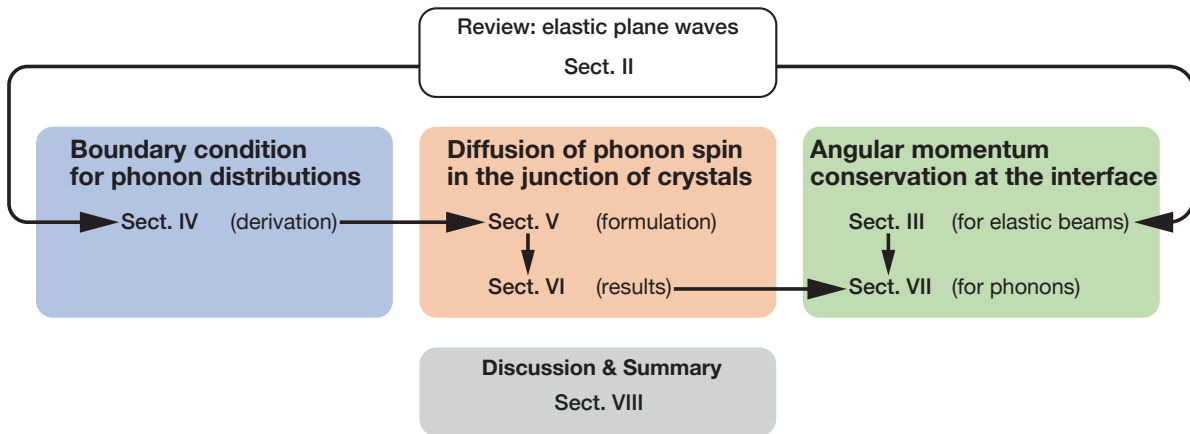
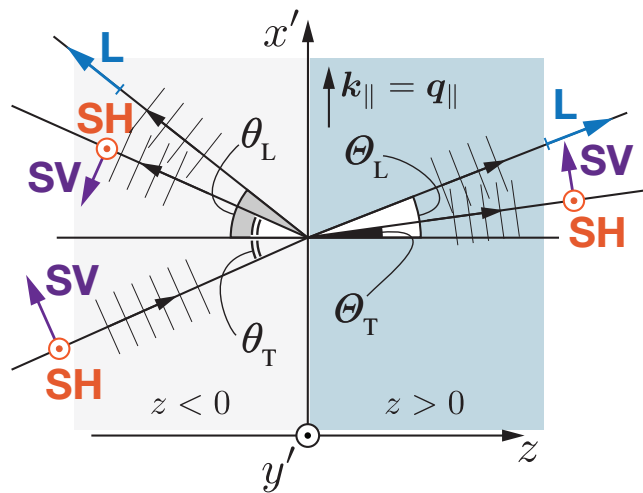


FIG. 2. Overview of the present paper.

OAM of phonons and describe the continuity of the total phonon AM flux in Sect. VII. We finally summarize the present paper and give outlooks in Sect. VIII. In Supplemental Material [49], we illustrate the behavior of the power reflectance/transmittance of elastic waves and the spatial profile of phonon energy transport.

II. REFLECTION AND TRANSMISSION OF ELASTIC PLANE WAVES

We start with a short review of the boundary scattering of elastic plane waves at an interface plane between two elastic bodies in contact; the interface is schematically shown in Figs. 1(a) and 3. It is worth noting that the two elastic bodies occupy semi-infinite regions $z < 0$ and $z > 0$, and the wavevector and frequency of elastic waves

FIG. 3. Interface ($x'y'$ -plane), incident plane (zx' -plane) and modes of elastic plane waves (L, SH, SV) with their polarization vectors.

take continuous values.

A. Setup and boundary condition for elastic waves

Suppose that the whole medium vibrates with a single frequency ω , while the two bodies in $z < 0$ and $z > 0$ vibrate with wavevectors \mathbf{k} and \mathbf{q} , respectively. We specify wavevector components parallel to the interface, denoted by \mathbf{k}_{\parallel} and \mathbf{q}_{\parallel} . As a requirement of the translational symmetry along the interface, the components are the same: $\mathbf{k}_{\parallel} = \mathbf{q}_{\parallel}$. The plane of incidence is then spanned by the interface normal \hat{z} and the wavevector \mathbf{k}_{\parallel} , as shown in Fig. 3. We take a (x', y', z) -coordinate with x' -axis in the direction of \mathbf{k}_{\parallel} and y' -axis in the direction of $\hat{z} \times \mathbf{k}_{\parallel}$. Later in Sect. VI, we will also use a laboratory coordinate (x, y, z) without primes that is independent of the direction of wavevectors.

We next focus on the left-hand side of the medium $z < 0$ with mass density ρ . For simplicity, we approximate the elastic body to be isotropic. Dispersion and polarization of three acoustic modes are then determined by two Lamé parameters λ and μ [50, 51]. Their linear dispersions are denoted by $\Omega_{\mathbf{k},L} = v_L |\mathbf{k}|$ and $\Omega_{\mathbf{k},T} = v_T |\mathbf{k}|$, where $v_L = \sqrt{(\lambda + 2\mu)/\rho}$ is a velocity of a longitudinal wave (L mode) and $v_T = \sqrt{\mu/\rho}$ is a velocity of doubly degenerated transverse waves. We decompose the transverse waves into two modes, one of whose polarization is normal to the plane of incidence and the other of whose polarization is within the incident plane. We shall call the former SH mode and the latter SV mode in accordance with geophysical conventions. (The SH/SV mode means a horizontally/vertically polarized shear mode.) We also introduce circularly polarized waves denoted as RH (right-handed) and LH (left-handed) modes later on.

For given ω , \mathbf{k}_{\parallel} and mode $n = L, SH, SV$, the dispersion relation $\omega = \Omega_{\mathbf{k},n} = v_n \sqrt{|\mathbf{k}_{\parallel}|^2 + |\mathbf{k}_z|^2}$ yields two

solutions of \mathbf{k}_z , given as

$$\mathbf{k}_{z,s,n} = s\omega\hat{\mathbf{z}} \cdot \begin{cases} \cos\theta_L/v_L & n = L \\ \cos\theta_T/v_T & n = \text{SH, SV} \end{cases} \quad (1)$$

with $s = \pm$. The angles θ_n of incidence, reflection, and refraction are defined by $\sin\theta_L = v_L|\mathbf{k}_{\parallel}|/\omega$ and $\sin\theta_T = v_T|\mathbf{k}_{\parallel}|/\omega$. The plane wave component characterized by (s, n) propagates into $s \cdot \hat{\mathbf{z}}$ direction with polarization vector

$$\mathbf{e}_{\mathbf{k},n} = \mathbf{e}_{s,n} = \begin{cases} \hat{\mathbf{x}}' \sin\theta_L + s\hat{\mathbf{z}} \cos\theta_L & n = L \\ \hat{\mathbf{y}}' & n = \text{SH} \\ -\hat{\mathbf{z}} \sin\theta_T + s\hat{\mathbf{x}}' \cos\theta_T & n = \text{SV} \end{cases} \quad (2)$$

The displacement field for the region $z < 0$ over time $\mathbf{u}^{\text{ela}}(\mathbf{r}, t)$ is a sum of the plane wave components (s, n)

with amplitudes $u_{s,n}$, expressed as

$$\mathbf{u}^{\text{ela}} = 2\text{Re} \left[\sum_{s=\pm} \sum_{n=L,\text{SH},\text{SV}} u_{s,n} \mathbf{e}_{s,n} e^{i(\mathbf{k}_{\parallel} + \mathbf{k}_{z,s,n}) \cdot \mathbf{r} - i\omega t} \right]. \quad (3)$$

The stress tensor takes the form $\sigma_{ik} = \sum_{l,m} a_{iklm} \partial u_l^{\text{ela}} / \partial r_m$ with $a_{iklm} = \rho v_T^2 (\delta_{il} \delta_{km} + \delta_{im} \delta_{kl}) + \rho (v_L^2 - 2v_T^2) \delta_{ik} \delta_{lm}$ for the isotropic elastic body in $z < 0$ [38, 50].

In the same way, elastic waves in the right-hand side of the medium $z > 0$ are characterized by the sign of propagating direction $s = \pm$ and the mode $n = L, \text{SH}, \text{SV}$. The model parameters in this region are represented as follows: mass density $\tilde{\rho}$, dispersion relation $\omega_{\mathbf{q},n} = c_n |\mathbf{q}|$, velocities c_L and c_T , angles of incidence, reflection, and refraction Θ_L and Θ_T , polarization vector $\tilde{\boldsymbol{\xi}}_{s,n}$, amplitude of each plane wave component $\tilde{u}_{s,n}$, and stress tensor $\tilde{\sigma}_{ik}$.

In the case of perfect contact, the displacements and the stresses are continuous at the interface $z = 0$ for arbitrary time [50, 51]. The equalities $\sum_{s,n} u_{s,n} \mathbf{e}_{s,n} = \sum_{s,n} \tilde{u}_{s,n} \tilde{\boldsymbol{\xi}}_{s,n}$, $\sigma_{zz} = \tilde{\sigma}_{zz}$, $\sigma_{zx'} = \tilde{\sigma}_{zx'}$, and $\sigma_{zy'} = \tilde{\sigma}_{zy'}$ yield the boundary condition:

$$\begin{bmatrix} \cos\theta_L & -\sin\theta_T & -\cos\theta_L & -\sin\theta_T \\ \sin\theta_L & \cos\theta_T & \sin\theta_L & -\cos\theta_T \\ Z_L \cos 2\theta_T & -Z_T \sin 2\theta_T & Z_L \cos 2\theta_T & Z_T \sin 2\theta_T \\ Z_L \left(\frac{\sin\theta_T}{\sin\theta_L}\right)^2 \sin 2\theta_L & Z_T \cos 2\theta_T & -Z_L \left(\frac{\sin\theta_T}{\sin\theta_L}\right)^2 \sin 2\theta_L & Z_T \cos 2\theta_T \end{bmatrix} \begin{bmatrix} u_{+,L} \\ u_{+,SV} \\ u_{-,L} \\ u_{-,SV} \end{bmatrix} = \begin{bmatrix} \cos\Theta_L & -\sin\Theta_T & -\cos\Theta_L & -\sin\Theta_T \\ \sin\Theta_L & \cos\Theta_T & \sin\Theta_L & -\cos\Theta_T \\ \zeta_L \cos 2\Theta_T & -\zeta_T \sin 2\Theta_T & \zeta_L \cos 2\Theta_T & \zeta_T \sin 2\Theta_T \\ \zeta_L \left(\frac{\sin\Theta_T}{\sin\Theta_L}\right)^2 \sin 2\Theta_L & \zeta_T \cos 2\Theta_T & -\zeta_L \left(\frac{\sin\Theta_T}{\sin\Theta_L}\right)^2 \sin 2\Theta_L & \zeta_T \cos 2\Theta_T \end{bmatrix} \begin{bmatrix} \tilde{u}_{+,L} \\ \tilde{u}_{+,SV} \\ \tilde{u}_{-,L} \\ \tilde{u}_{-,SV} \end{bmatrix}, \quad (4a)$$

$$\begin{bmatrix} 1 & 1 \\ Z_T \cos\theta_T & -Z_T \cos\theta_T \end{bmatrix} \begin{bmatrix} u_{+,\text{SH}} \\ u_{-,\text{SH}} \end{bmatrix} = \begin{bmatrix} 1 & 1 \\ \zeta_T \cos\Theta_T & -\zeta_T \cos\Theta_T \end{bmatrix} \begin{bmatrix} \tilde{u}_{+,\text{SH}} \\ \tilde{u}_{-,\text{SH}} \end{bmatrix} \quad (4b)$$

with acoustic impedances

$$Z_L = \rho v_L, \quad Z_T = \rho v_T, \quad \zeta_L = \tilde{\rho} c_L, \quad \zeta_T = \tilde{\rho} c_T. \quad (5)$$

The first equation (4a) is known as the Zoeppritz equations [52, 53]. Analytical solution of it is available in geophysics textbooks [54].

It is worth noting that perfect transmission of transverse waves is possible when the two bodies in contact share common acoustic impedance and velocity for the

transverse waves:

$$\frac{c_T}{v_T} = \frac{\zeta_T}{Z_T} = 1. \quad (6)$$

In this case, $\rho = \tilde{\rho}$ and $\theta_T = \Theta_T$ hold and it follows from Eqs. (4) that $u_{\pm,\text{SV}} = \tilde{u}_{\pm,\text{SV}}$ and $u_{\pm,\text{SH}} = \tilde{u}_{\pm,\text{SH}}$. Since transverse modes carry circular polarization of elastic waves, the condition (6) maximizes the diffusion of the SAM density and flux polarized parallel to the interface,

as will be mentioned in Sect. VI.

When there is no incident wave from $z > 0$, i.e., $\tilde{u}_{-,n} = 0$, we can transform Eqs. (4) as another matrix

$$\begin{bmatrix} u_{-,L} \\ u_{-,SH} \\ u_{-,SV} \\ \tilde{u}_{+,L} \\ \tilde{u}_{+,SH} \\ \tilde{u}_{+,SV} \end{bmatrix} = \begin{bmatrix} \rho_{L,L} & 0 & \rho_{L,SV} \\ 0 & \rho_{SH,SH} & 0 \\ \rho_{SV,L} & 0 & \rho_{SV,SV} \\ \tau_{L,L} & 0 & \tau_{L,SV} \\ 0 & \tau_{SH,SH} & 0 \\ \tau_{SV,L} & 0 & \tau_{SV,SV} \end{bmatrix} \begin{bmatrix} u_{+,L} \\ u_{+,SH} \\ u_{+,SV} \end{bmatrix}, \quad (7)$$

elements of which we will use in Sect. III.

B. Circularly polarized modes and their reflection/transmission

In the isotropic two elastic bodies, dispersions of the two transverse modes (SH and SV) are degenerate. We can thus take a new basis of rotational modes as $\mathbf{e}_{s,RH} \equiv (\mathbf{e}_{s,SV} + i\mathbf{e}_{s,SH})/\sqrt{2}$, $\mathbf{e}_{s,LH} \equiv \mathbf{e}_{s,RH}^*$, $\boldsymbol{\xi}_{s,RH} \equiv (\boldsymbol{\xi}_{s,SV} + i\boldsymbol{\xi}_{s,SH})/\sqrt{2}$, and $\boldsymbol{\xi}_{s,LH} \equiv \boldsymbol{\xi}_{s,RH}^*$. Here RH and LH stand for right-handed circularly polarized waves and left-handed circularly polarized waves, respectively. The amplitudes of the circularly polarized waves with $s = \pm$ are then given as

$$\begin{bmatrix} u_{s,L} \\ u_{s,RH} \\ u_{s,LH} \end{bmatrix} = \begin{bmatrix} 1 \\ -i/\sqrt{2} & 1/\sqrt{2} \\ +i/\sqrt{2} & 1/\sqrt{2} \end{bmatrix} \begin{bmatrix} u_{s,L} \\ u_{s,SH} \\ u_{s,SV} \end{bmatrix}. \quad (8)$$

We apply the same transformation for $\tilde{u}_{s,n}$ by inserting tildes above each $u_{s,n}$ in Eq. (8).

Let us now consider energy flux for each mode with its flow normal to the interface. This is derived from a long-time average of power that each elastic wave makes on the interface. When the angle of incidence is small enough to satisfy $\sin \theta_n < 1$ and $\sin \Theta_n < 1$ for any mode n , no evanescent wave appears in the scattering problem, and the energy flux per unit area for each mode (s, n) with $n = L, RH, LH$ is given as $2s\omega^2 Z_n \cos \theta_n |u_{s,n}|^2$ in $z < 0$ and $2s\omega^2 \zeta_n \cos \Theta_n |\tilde{u}_{s,n}|^2$ in $z > 0$ [55]. The conservation of energy at the interface then reduces to an equality

$$\begin{aligned} J_u^{\text{ela}} &\equiv \sum_{s,n} 2s\omega^2 Z_n \cos \theta_n |u_{s,n}|^2 \\ &= \sum_{s,n} 2s\omega^2 \zeta_n \cos \Theta_n |\tilde{u}_{s,n}|^2. \end{aligned} \quad (9)$$

Here the subscript u indicates that the quantity is related to energy.

We now transform the boundary condition (4) into a linear response to the amplitudes of incident waves on

the new basis

$$Z^{1/2} \begin{bmatrix} u_{-,L} \\ u_{-,RH} \\ u_{-,LH} \\ \tilde{u}_{+,L} \\ \tilde{u}_{+,RH} \\ \tilde{u}_{+,LH} \end{bmatrix} = S(\omega, \mathbf{k}_{\parallel}) \cdot Z^{1/2} \begin{bmatrix} u_{+,L} \\ u_{+,RH} \\ u_{+,LH} \\ \tilde{u}_{-,L} \\ \tilde{u}_{-,RH} \\ \tilde{u}_{-,LH} \end{bmatrix}, \quad (10)$$

with a diagonal matrix made up of the acoustic impedances (5)

$$Z = \text{diag} [Z_L \cos \theta_L, Z_T \cos \theta_T, Z_T \cos \theta_T, \zeta_L \cos \Theta_L, \zeta_T \cos \Theta_T, \zeta_T \cos \Theta_T]. \quad (11)$$

It follows from the energy conservation law (9) that the S -matrix in Eq. (10), denoted by

$$S(\omega, \mathbf{k}_{\parallel}) = \begin{bmatrix} r_{L,L} & r_{L,RH} & r_{L,LH} & t'_{L,L} & t'_{L,RH} & t'_{L,LH} \\ r_{RH,L} & r_{RH,RH} & r_{RH,LH} & t'_{RH,L} & t'_{RH,RH} & t'_{RH,LH} \\ r_{LH,L} & r_{LH,RH} & r_{LH,LH} & t'_{LH,L} & t'_{LH,RH} & t'_{LH,LH} \\ \hline t_{L,L} & t_{L,RH} & t_{L,LH} & r'_{L,L} & r'_{L,RH} & r'_{L,LH} \\ t_{RH,L} & t_{RH,RH} & t_{RH,LH} & r'_{RH,L} & r'_{RH,RH} & r'_{RH,LH} \\ t_{LH,L} & t_{LH,RH} & t_{LH,LH} & r'_{LH,L} & r'_{LH,RH} & r'_{LH,LH} \end{bmatrix}, \quad (12)$$

is unitary.

When the angle of incidence becomes large, Snell's law may require that some angles of reflection/refraction satisfy $\sin \theta_n > 1$ or $\sin \Theta_n > 1$. These evanescent waves, localized in the vicinity of the interface, do not contribute to the energy flux normal to the interface.

We thus obtain the power reflectance \mathcal{R}_{nm} and \mathcal{R}'_{nm} and transmittance \mathcal{T}_{nm} and \mathcal{T}'_{nm} , i.e., ratios of the energy flux of incident wave with mode m to the energy flux of reflected and transmitted waves with mode n . They are expressed as

$$\mathcal{R}_{nm} = |r_{nm}|^2 \cdot \Theta_H(1 - \sin \theta_n) \Theta_H(1 - \sin \theta_m), \quad (13a)$$

$$\mathcal{R}'_{nm} = |r'_{nm}|^2 \cdot \Theta_H(1 - \sin \Theta_n) \Theta_H(1 - \sin \Theta_m), \quad (13b)$$

$$\mathcal{T}_{nm} = |t_{nm}|^2 \cdot \Theta_H(1 - \sin \Theta_n) \Theta_H(1 - \sin \theta_m), \quad (13c)$$

$$\mathcal{T}'_{nm} = |t'_{nm}|^2 \cdot \Theta_H(1 - \sin \theta_n) \Theta_H(1 - \sin \Theta_m), \quad (13d)$$

where $\Theta_H(w)$ is the Heaviside step function

$$\Theta_H(w) = \begin{cases} 1 & w > 0 \\ 0 & w < 0 \end{cases}. \quad (14)$$

In Supplemental Material [49], we have plotted the behavior of the reflectance/transmittance with respect to the angle of incidence for some pairs of elastic bodies in contact.

With the help of the energy conservation law (9), the above coefficients follow the next constraints for any mode m :

$$\sum_n (\mathcal{R}_{nm} + \mathcal{T}_{nm}) = 1, \quad (15a)$$

$$\sum_n (\mathcal{T}'_{nm} + \mathcal{R}'_{nm}) = 1. \quad (15b)$$

We also notice that the coefficients satisfy two symmetries: one is the Helmholtz reciprocity $\mathcal{R}_{nm} = \mathcal{R}_{mn}$, $\mathcal{R}'_{nm} = \mathcal{R}'_{mn}$ and $\mathcal{T}_{nm} = \mathcal{T}'_{mn}$; the other is an invariance under a replacement of subscripts (n, m) from (L, RH, LH) into (L, LH, RH):

$$\mathcal{R}_{\text{RH,RH}} = \mathcal{R}_{\text{LH,LH}}, \quad \mathcal{T}_{\text{RH,RH}} = \mathcal{T}_{\text{LH,LH}}, \quad (16a)$$

$$\mathcal{R}_{\text{RH,LH}} = \mathcal{R}_{\text{LH,RH}}, \quad \mathcal{T}_{\text{RH,LH}} = \mathcal{T}_{\text{LH,RH}}, \quad (16b)$$

$$\mathcal{R}_{\text{RH,L}} = \mathcal{R}_{\text{LH,L}}, \quad \mathcal{T}_{\text{RH,L}} = \mathcal{T}_{\text{LH,L}}. \quad (16c)$$

Note that these symmetries hold only for the reflectance/transmittance with the same ω and \mathbf{k}_{\parallel} .

III. ACOUSTIC ANALOG OF IMBERT-FEDOROV SHIFT AND ANGULAR MOMENTUM CONSERVATION

In the previous section we have reviewed interfacial scattering of a monochromatic plane wave in elastic medium. In this section we shall consider interfacial scattering of successive elastic wave packets, i.e., acoustic beams with a finite spatial extent lying in the system with infinite spatial volume.

The aim of this section is to determine the transverse shift of the reflected or transmitted beams at the interface [see Δr_{IF} shown in Fig. 1(c)] when a circularly polarized beam is incident. We also derive orbital angular momentum (OAM) from the trajectory of the beam. We finally summarize the total AM conservation for the acoustic beam at the interface [38]. The following formulation is based on a review article in optics [56], but we extend it to acoustics by including both longitudinal and transverse modes. We expect that the derived spatial shift and OAM is still valid for wave packets or phonons. We will apply these results for later discussion of the AM conservation for phonons at the interface in Sect. VII.

A. Plane wave components in the incident beam

Let us introduce a paraxial beam of transverse modes incident upon the interface plane $z = 0$ from the region $z < 0$. We first specify the central wavevector of the incident beam as $\mathbf{k}_c = \mathbf{k}_{c,\parallel} + k_{c,\perp} \hat{z}$. Here $\mathbf{k}_{c,\parallel}$ is parallel to the interface. We then take a (x', y', z) -coordinate with x' -axis in the direction of $\mathbf{k}_{c,\parallel}$ and y' -axis in the direction of $\hat{z} \times \mathbf{k}_{c,\parallel}$, in the same way as Sect. II A. We also define a center coordinate of the incident beam (X, y', Z)

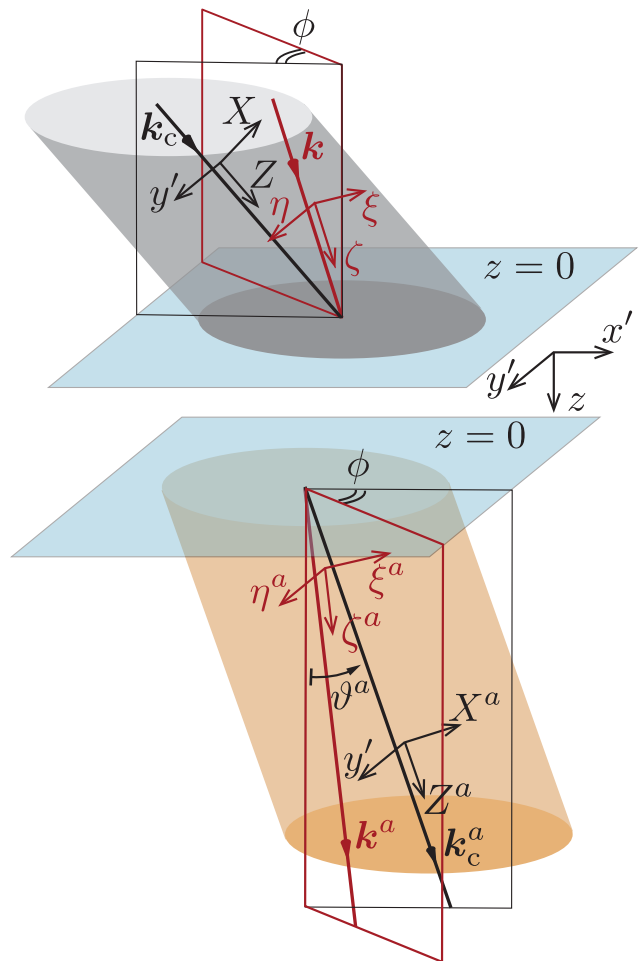


FIG. 4. Schematic view of coordinate frames attached to the incident (top) and transmitted beam (bottom). The coordinate frames attached to the reflected beam is also introduced in the same way as the transmitted beam (bottom); the only difference is that the z -components of the wavevectors are negative with obtuse angle ϑ^a . The central wavevector of each beam is represented by the black bold line with an arrow, and the wavevector of an off-center plane wave component inside each beam is represented by the red bold line with an arrow. The reflected/transmitted waves are labeled by a for each mode (see the beginning of Sect. III B).

by rotating the original frame (x', y', z) around the y' -axis by the angle of incidence (see Fig. 4). The polarization of the beam is in the Xy' -plane, since transverse waves are incident.

We then describe an off-center plane wave component within the incident beam. The component is characterized by a wavevector with small orthogonal deflection from the central wavevector $\mathbf{k} = \mathbf{k}_c + k_c(\mu \hat{X} + \nu \hat{y}')$. Here $k_c = |\mathbf{k}_c|$, and \hat{X} and \hat{y}' are unit vectors in the direction of X -axis and y' -axis, respectively. A new coordinate (ξ, η, ζ) with ζ along the wavevector \mathbf{k} is then taken as shown in Fig. 4.

We now write down the displacement of the incident

beam as a superposition of all the plane wave components. Since we consider a paraxial beam with definite polarization, the displacement of the off-center plane wave component is parallel to the displacement of the central plane wave component. The amplitude of the displacement, at the same time, attenuates as the degree of deflection $\mu^2 + \nu^2$ increases. The superposition of plane wave components within the beam is thus

$$\mathbf{u}(\mathbf{r}, t) = 2\text{Re} \int_{-\infty}^{\infty} \frac{k_c d\mu}{2\pi} \int_{-\infty}^{\infty} \frac{k_c d\nu}{2\pi} \cos \vartheta \cdot e^{i(\mathbf{k} \cdot \mathbf{r} - \omega t)} \times \sqrt{G(\mu, \nu)} \left(u_X \hat{\mathbf{X}} + u_{y'} \hat{\mathbf{y}}' + u_Z \hat{\mathbf{Z}} \right) \quad (17)$$

with $u_Z = 0$, since we consider the incidence of transverse modes. The amplitudes u_X and $u_{y'}$ are independent of \mathbf{k} . We inserted $\cos \vartheta$ in Eq. (17) with the angle of incidence $\vartheta = \theta_T$ for later convenience. The envelope function $G(\mu, \nu) = G(|\mu|, |\nu|)$ represents the attenuation in the radial direction of the beam. We can also consider an asymmetric beam with $G(\mu, \nu) \neq G(|\mu|, |\nu|)$ or insert a \mathbf{k} -dependent phase factor in the expression (17), as in the case of the acoustic vortex beam [41–44], but in the present paper we neglect such contributions. Furthermore, we assume $G(\mu, \nu) \propto \delta(\mu)$ and neglect the deviation $\mu \neq 0$, since we focus only on the transverse shift of beams and μ does not contribute to the lowest order of the transverse shift [56].

Before we consider the reflection/transmission of each off-center plane wave, we transform the displacement observed from (X, y', Z) -coordinate $\sqrt{G(\mu, \nu)} \cdot (u_X, u_{y'}, u_Z)$ into the displacement observed from (ξ, η, ζ) -coordinate, denoted by (u_ξ, u_η, u_ζ) . The transformation is represented as a product of rotation matrices

$$\begin{aligned} \begin{bmatrix} u_\xi \\ u_\eta \\ u_\zeta \end{bmatrix} &= \begin{bmatrix} \cos \vartheta & 0 & -\sin \vartheta \\ 0 & 1 & 0 \\ \sin \vartheta & 0 & \cos \vartheta \end{bmatrix} \begin{bmatrix} \cos \phi & \sin \phi & 0 \\ -\sin \phi & \cos \phi & 0 \\ 0 & 0 & 1 \end{bmatrix} \\ &\times \begin{bmatrix} \cos \vartheta & 0 & \sin \vartheta \\ 0 & 1 & 0 \\ -\sin \vartheta & 0 & \cos \vartheta \end{bmatrix} \begin{bmatrix} u_X \\ u_{y'} \\ u_Z \end{bmatrix} \cdot \sqrt{G(\mu, \nu)} \quad (18) \\ &\simeq \begin{bmatrix} 1 & \nu \cot \vartheta & 0 \\ -\nu \cot \vartheta & 1 & -\nu \\ 0 & \nu & 1 \end{bmatrix} \begin{bmatrix} u_X \\ u_{y'} \\ u_Z \end{bmatrix} \cdot \sqrt{G(\mu, \nu)}, \end{aligned} \quad (19)$$

where the angle of incidence of the center plane wave is denoted by $\vartheta = \theta_T$ and the azimuthal angle of \mathbf{k} in the $x'y'$ -plane by $\phi \simeq \tan \phi = \nu / \sin \vartheta$. In the last line, we take terms up to the first order in ν . The 3×3 matrix in the last line is denoted by $U(\nu, \vartheta)$.

B. Plane wave components in the reflected/transmitted beam

Let us now consider reflected and transmitted beams. The wavevectors of their central plane waves are denoted by $\mathbf{k}_c^{\text{r-L}}, \mathbf{k}_c^{\text{r-T}}, \mathbf{k}_c^{\text{t-L}},$ and $\mathbf{k}_c^{\text{t-T}}$, or simply \mathbf{k}_c^a . Here

$a = \text{r-L}, \text{r-T}, \text{t-L}, \text{t-T}$ stand for reflected longitudinal, reflected transverse, transmitted longitudinal, and transmitted transverse waves, respectively. For convenience, angles that these wavevectors form with the z -axis are denoted by $\vartheta^{\text{r-L}} = \pi - \theta_L$, $\vartheta^{\text{r-T}} = \pi - \theta_T$, $\vartheta^{\text{t-L}} = \theta_L$, and $\vartheta^{\text{t-T}} = \theta_T$. The amplitudes and angles of the wavevectors follow Snell's law $k_c^a \sin \vartheta^a = k_c \sin \vartheta$ with $k_c^a = |\mathbf{k}_c^a|$. We further define a center coordinate of the reflected/transmitted beam (X^a, y', Z^a) as shown in Fig. 4. The polarization of transverse waves is in the $X^a y'$ -plane, while the polarization of longitudinal waves is in the Z^a -direction.

We next consider reflected or transmitted plane waves by the incidence of the off-center component. They have wavevectors $\mathbf{k}^a = \mathbf{k}_c^a + k_c^a (\mu^a \hat{\mathbf{X}}^a + \nu^a \hat{\mathbf{y}}')$, where the small deflection is given by Snell's law as $k_c^a \mu^a |\cos \vartheta^a| = k_c \mu \cos \vartheta = 0$ and $k_c^a \nu^a = k_c \nu$. We, again, define a coordinate (ξ^a, η^a, ζ^a) with ζ^a along the wavevector \mathbf{k}^a as shown in Fig. 4.

The superposition of the plane wave components with the reflected/transmitted beam is expressed in the same way as Eq. (17):

$$\mathbf{u}^a(\mathbf{r}, t) = 2\text{Re} \int \frac{k_c^{a2} |\cos \vartheta^a| d\mu^a d\nu^a}{(2\pi)^2} e^{i(\mathbf{k}^a \cdot \mathbf{r} - \omega t)} \times \left(u_X^a \hat{\mathbf{X}}^a + u_{y'}^a \hat{\mathbf{y}}' + u_Z^a \hat{\mathbf{Z}}^a \right), \quad (20)$$

where we have introduced an area element in common with the incident and scattered beams:

$$\begin{aligned} k_c^{a2} |\cos \vartheta^a| d\mu^a d\nu^a &= d^2 \mathbf{k}_\parallel^a = dk_{x'}^a dk_{y'}^a \\ &= dk_{x'} dk_{y'} = d^2 \mathbf{k}_\parallel = k_c^2 \cos \vartheta d\mu d\nu. \end{aligned} \quad (21)$$

Here \mathbf{k}_\parallel and \mathbf{k}_\parallel^a are components of \mathbf{k} and \mathbf{k}^a parallel to the interface. The displacement observed from (ξ^a, η^a, ζ^a) -coordinate denoted as $(u_\xi^a, u_\eta^a, u_\zeta^a)$ is again given in the same way as Eq. (19):

$$\begin{bmatrix} u_\xi^a \\ u_\eta^a \\ u_\zeta^a \end{bmatrix} \simeq \begin{bmatrix} 1 & \nu^a \cot \vartheta^a & 0 \\ -\nu^a \cot \vartheta^a & 1 & -\nu^a \\ 0 & \nu^a & 1 \end{bmatrix} \begin{bmatrix} u_X^a \\ u_{y'}^a \\ u_Z^a \end{bmatrix}. \quad (22)$$

The 3×3 matrix in the last line is denoted by $U^a(\nu^a, \vartheta^a)$.

C. Transfer matrix for displacements

Now elastic Fresnel coefficients ρ_{nm} and τ_{nm} , shown in Eq. (7), relates the displacement of incident off-center plane waves (u_ξ, u_η, u_ζ) and that of reflected/transmitted

waves $(u_\xi^a, u_\eta^a, u_\zeta^a)$:

$$\begin{bmatrix} u_\xi^{r-L} \\ u_\eta^{r-L} \\ u_\zeta^{r-L} \end{bmatrix} = \begin{bmatrix} 0 & 0 & 0 \\ 0 & 0 & 0 \\ \rho_{L,SV} & 0 & 0 \end{bmatrix} \begin{bmatrix} u_\xi \\ u_\eta \\ u_\zeta \end{bmatrix} \equiv F^{r-L} \begin{bmatrix} u_\xi \\ u_\eta \\ u_\zeta \end{bmatrix}, \quad (23a)$$

$$\begin{bmatrix} u_\xi^{r-T} \\ u_\eta^{r-T} \\ u_\zeta^{r-T} \end{bmatrix} = \begin{bmatrix} \rho_{SV,SV} & 0 & 0 \\ 0 & \rho_{SH,SH} & 0 \\ 0 & 0 & 0 \end{bmatrix} \begin{bmatrix} u_\xi \\ u_\eta \\ u_\zeta \end{bmatrix} \equiv F^{r-T} \begin{bmatrix} u_\xi \\ u_\eta \\ u_\zeta \end{bmatrix}, \quad (23b)$$

$$\begin{bmatrix} u_\xi^{t-L} \\ u_\eta^{t-L} \\ u_\zeta^{t-L} \end{bmatrix} = \begin{bmatrix} 0 & 0 & 0 \\ 0 & 0 & 0 \\ \tau_{L,SV} & 0 & 0 \end{bmatrix} \begin{bmatrix} u_\xi \\ u_\eta \\ u_\zeta \end{bmatrix} \equiv F^{t-L} \begin{bmatrix} u_\xi \\ u_\eta \\ u_\zeta \end{bmatrix}, \quad (23c)$$

$$\begin{bmatrix} u_\xi^{t-T} \\ u_\eta^{t-T} \\ u_\zeta^{t-T} \end{bmatrix} = \begin{bmatrix} \tau_{SV,SV} & 0 & 0 \\ 0 & \tau_{SH,SH} & 0 \\ 0 & 0 & 0 \end{bmatrix} \begin{bmatrix} u_\xi \\ u_\eta \\ u_\zeta \end{bmatrix} \equiv F^{t-T} \begin{bmatrix} u_\xi \\ u_\eta \\ u_\zeta \end{bmatrix}. \quad (23d)$$

Let us summarize the interfacial scattering of plane wave components observed from the center coordinate frames of the paraxial beams. With the help of Eqs. (19), (22), and (23), the scattering process follows

$$\begin{bmatrix} u_X^a \\ u_{y'}^a \\ u_Z^a \end{bmatrix} = P^a U^{a\dagger} F^a U P \begin{bmatrix} u_X \\ u_{y'} \\ u_Z \end{bmatrix} \cdot \sqrt{G} \quad (24)$$

$$\equiv T^a \begin{bmatrix} u_X \\ u_{y'} \\ u_Z \end{bmatrix} \cdot \sqrt{G}. \quad (25)$$

Here we introduced projection matrices onto the longitudinal displacement or the transverse displacement

$$P^{r-L} = P^{t-L} = \begin{bmatrix} 0 \\ 0 \\ 1 \end{bmatrix}, \quad (26a)$$

$$P = P^{r-T} = P^{t-T} = \begin{bmatrix} 1 \\ 1 \\ 0 \end{bmatrix}. \quad (26b)$$

D. Transverse shift of beams

We derive the shift of the reflected/transmitted beam in the y' -direction. Note that the longitudinal shift, i.e., shift of the reflected/transmitted beam in the x' -direction is also known as the Schoch shift [57], analogous to the Goos-Hänchen shift in optics [58], but we omit its derivation and focus only on the transverse shift.

We measure the transverse shift weighted by the energy flux across the interface. With the help of Eq. (9), the shift is expressed as

$$\Delta r_{IF}^a = \frac{\int dx' dy' \omega^2 Z^a \cos \vartheta^a \overline{|\mathbf{u}^a(\mathbf{r}, t)|^2} \cdot y'}{\int dx' dy' \omega^2 Z^a \cos \vartheta^a \overline{|\mathbf{u}^a(\mathbf{r}, t)|^2}} \Bigg|_{z=0}. \quad (27)$$

Here acoustic impedance Z^a is given as $Z^{r-L} = Z_L$, $Z^{r-T} = Z_T$, $Z^{t-L} = \zeta_L$, and $Z^{t-T} = \zeta_T$. The long-time average is denoted by a bar over a symbol, s.t., $\overline{O(t)} = \lim_{T \rightarrow \infty} T^{-1} \int_0^T O(t) dt$.

With the help of Eqs. (20), (21), (25), and the property $G(\mu, \nu) = G(|\mu|, |\nu|)$, we transform the numerator of Eq. (27) as

$$\begin{aligned} & \omega^2 Z^a \cos \vartheta^a \int dx' dy' \int \frac{d^2 \mathbf{k}_{1,\parallel}^a}{(2\pi)^2} \int \frac{d^2 \mathbf{k}_{2,\parallel}^a}{(2\pi)^2} \\ & \times \sqrt{G(\mu_1, \nu_1) G(\mu_2, \nu_2)} \begin{bmatrix} u_X \\ u_{y'} \\ u_Z \end{bmatrix}^\dagger T^{a\dagger}(\mathbf{k}_1) T^a(\mathbf{k}_2) \begin{bmatrix} u_X \\ u_{y'} \\ u_Z \end{bmatrix} \\ & \times \left(-i \frac{\partial}{\partial k_{2,y'}^a} \right) e^{i(\mathbf{k}_{2,\parallel}^a - \mathbf{k}_{1,\parallel}^a) \cdot \mathbf{r}} + \text{c.c.} \quad (28) \\ & = \omega^2 Z^a \cos \vartheta^a \int \frac{d^2 \mathbf{k}_{1,\parallel}^a}{(2\pi)^2} \int \frac{d^2 \mathbf{k}_{2,\parallel}^a}{(2\pi)^2} \delta(\mathbf{k}_{1,\parallel}^a - \mathbf{k}_{2,\parallel}^a) G(\mu_1, \nu_1) \\ & \times \begin{bmatrix} u_X \\ u_{y'} \\ u_Z \end{bmatrix}^\dagger T^{a\dagger}(\mathbf{k}_1) \left(\frac{-i}{k_c} \frac{\partial}{\partial \nu_2} \right) T^a(\mathbf{k}_2) \begin{bmatrix} u_X \\ u_{y'} \\ u_Z \end{bmatrix} + \text{c.c.} \quad (29) \\ & = \frac{2\omega^2 Z^a \cos \vartheta^a}{k_c} \text{Re} \int \frac{d^2 \mathbf{k}_{\parallel}}{(2\pi)^2} G(\mu, \nu) \\ & \times \begin{bmatrix} u_X \\ u_{y'} \\ u_Z \end{bmatrix}^\dagger T^{a\dagger}(\nu) i \frac{\partial T^a(\nu)}{\partial \nu} \begin{bmatrix} u_X \\ u_{y'} \\ u_Z \end{bmatrix}, \quad (30) \end{aligned}$$

where c.c. denotes the complex conjugate of the previous terms.

The denominator of Eq. (27), on the other hand, provides total energy flux of a beam labeled a ,

$$J_u^{\text{beam}} = 2\omega^2 Z^a \cos \vartheta^a \int \frac{d^2 \mathbf{k}_{\parallel}}{(2\pi)^2} G(\mu, \nu) \left| T^a(\nu) \begin{bmatrix} u_X \\ u_{y'} \\ u_Z \end{bmatrix} \right|^2 \quad (31)$$

$$= 2\omega^2 Z^a \cos \vartheta^a \left| T^a(0) \begin{bmatrix} u_X \\ u_{y'} \\ u_Z \end{bmatrix} \right|^2 \cdot N^{\text{beam}} \quad (32)$$

with

$$N^{\text{beam}} \equiv \int \frac{d^2 \mathbf{k}_{\parallel}}{(2\pi)^2} G(\mu, \nu). \quad (33)$$

Here we neglect second or higher order terms in ν of $T^a(\nu)$. The first order terms in ν also vanish in the integral over the symmetric interval (31).

The same calculation applies to the integral in Eq. (30), and as a result, the factors N^{beam} in both numerator and denominator of Eq. (27) cancel each other out. We thus obtain the transverse shift independent of the detail of

the envelope function of the beam:

$$\Delta r_{\text{IF}}^a = \frac{\text{Re} \left\{ \begin{bmatrix} u_X \\ u_{y'} \\ u_Z \end{bmatrix}^\dagger T^{a\dagger}(\nu) \frac{\partial T^a(\nu)}{\partial \nu} \Big|_{\nu=0} \begin{bmatrix} u_X \\ u_{y'} \\ u_Z \end{bmatrix} \right\}}{k_c \cdot \begin{bmatrix} u_X \\ u_{y'} \\ u_Z \end{bmatrix}^\dagger T^{a\dagger}(0) T^a(0) \begin{bmatrix} u_X \\ u_{y'} \\ u_Z \end{bmatrix}}. \quad (34)$$

The denominator is written by a ratio of the amplitudes between the incident and reflected/transmitted waves

$$(Q^a)^2 \equiv \frac{\begin{bmatrix} u_X \\ u_{y'} \\ u_Z \end{bmatrix}^\dagger T^{a\dagger}(0) T^a(0) \begin{bmatrix} u_X \\ u_{y'} \\ u_Z \end{bmatrix}}{|u_X|^2 + |u_{y'}|^2}, \quad (35)$$

while the numerator is characterized by average helicity $\bar{\sigma}$ and degree of linear polarization inclined at $\pi/4$ angle

$\bar{\rho}$, defined as

$$\bar{\sigma} \equiv \frac{2\text{Im}[u_X^* u_{y'}]}{|u_X|^2 + |u_{y'}|^2}, \quad \bar{\rho} \equiv \frac{2\text{Re}[u_X^* u_{y'}]}{|u_X|^2 + |u_{y'}|^2}. \quad (36)$$

Let us write down $(Q^a)^2$ and Δr_{IF}^a :

$$(Q^{\text{r-L}})^2 = \frac{|\rho_{\text{L,SV}}|^2 |u_X|^2}{|u_X|^2 + |u_{y'}|^2}, \quad (37a)$$

$$(Q^{\text{r-T}})^2 = \frac{|\rho_{\text{SV,SV}}|^2 |u_X|^2 + |\rho_{\text{SH,SH}}|^2 |u_{y'}|^2}{|u_X|^2 + |u_{y'}|^2}, \quad (37b)$$

$$(Q^{\text{t-L}})^2 = \frac{|\tau_{\text{L,SV}}|^2 |u_X|^2}{|u_X|^2 + |u_{y'}|^2}, \quad (37c)$$

$$(Q^{\text{t-T}})^2 = \frac{|\tau_{\text{SV,SV}}|^2 |u_X|^2 + |\tau_{\text{SH,SH}}|^2 |u_{y'}|^2}{|u_X|^2 + |u_{y'}|^2}, \quad (37d)$$

$$\Delta r_{\text{IF}}^{\text{r-L}} = -\frac{|\rho_{\text{L,SV}}|^2}{2k_c} \cdot \frac{\bar{\sigma} \cot \theta_{\text{T}}}{(Q^{\text{r-L}})^2} = -\frac{|u_X|^2 + |u_{y'}|^2}{|u_X|^2} \cdot \frac{\bar{\sigma} \cot \theta_{\text{T}}}{2k_c}, \quad (38a)$$

$$\Delta r_{\text{IF}}^{\text{r-T}} = -\frac{1}{2k_c} \cdot \frac{\cot \theta_{\text{T}}}{(Q^{\text{r-T}})^2} \left(|\rho_{\text{SV,SV}} + \rho_{\text{SH,SH}}|^2 \cdot \bar{\sigma} + 2\text{Im}[\rho_{\text{SV,SV}}^* \rho_{\text{SH,SH}}] \cdot \bar{\rho} \right), \quad (38b)$$

$$\Delta r_{\text{IF}}^{\text{t-L}} = -\frac{|\tau_{\text{L,SV}}|^2}{2k_c} \cdot \frac{\bar{\sigma} \cot \theta_{\text{T}}}{(Q^{\text{t-L}})^2} = -\frac{|u_X|^2 + |u_{y'}|^2}{|u_X|^2} \cdot \frac{\bar{\sigma} \cot \theta_{\text{T}}}{2k_c}, \quad (38c)$$

$$\Delta r_{\text{IF}}^{\text{t-T}} = -\frac{1}{2k_c} \cdot \frac{\cot \theta_{\text{T}}}{(Q^{\text{t-T}})^2} \left[\left(|\tau_{\text{SV,SV}}|^2 + |\tau_{\text{SH,SH}}|^2 - 2\text{Re}[\tau_{\text{SV,SV}}^* \tau_{\text{SH,SH}}] \cdot \frac{\cos \Theta_{\text{T}}}{\cos \theta_{\text{T}}} \right) \cdot \bar{\sigma} - 2\text{Im}[\tau_{\text{SV,SV}}^* \tau_{\text{SH,SH}}] \frac{\cos \Theta_{\text{T}}}{\cos \theta_{\text{T}}} \cdot \bar{\rho} \right]. \quad (38d)$$

The above expressions are nothing but the transverse shift of beams for both acoustic transverse and longitudinal modes, as an analog of the Imbert–Fedorov (IF) shift [45–47] in optics. In particular, the transverse shifts Δr_{IF}^a are odd in the average helicity, i.e., circular polarization of the incident beam $\bar{\sigma}$. It is worth noting that $(\bar{\sigma}, \bar{\rho}) = (+1, 0)$ holds when the right-handed (RH) circularly polarized beam is incident, while $(\bar{\sigma}, \bar{\rho}) = (-1, 0)$ holds when the left-handed (LH) circularly polarized beam is incident. This spin-dependent property of the transverse shift resembles the spin Hall effect for electrons [48, 59–61]. We also notice that for longitudinal reflected/transmitted waves, their transverse shifts are the same: $\Delta r_{\text{IF}}^{\text{r-L}} = \Delta r_{\text{IF}}^{\text{t-L}}$. In contrast to the case when transverse waves are incident, incidence of longitudinal waves shows no transverse shift in the reflected/transmitted waves, though we omit the derivation here.

E. Total angular momentum conservation of beams

Since we assume a smooth and flat interface $z = 0$, the interface has a continuous rotational symmetry around \hat{z} . Conservation of elastic angular momentum (AM) thus follows from Noether’s theorem. It is confirmed in optics that the AM conservation law is satisfied for the sum of the AM stemming from the circular polarization and the AM stemming from the IF shift at the interface. The former is called spin angular momentum (SAM), while the latter is called extrinsic orbital angular momentum (OAM) [56]. The same conservation law at a sharp interface will hold in acoustics, as has been discussed by Bliokh and Freilikher [38]. Note that there also exists intrinsic OAM that is inherent in optical or acoustic vortex beams but we here omit considering such a special case of incidence.

We first calculate the expectation value of the SAM of the incident, reflected, and transmitted beams. The

component normal to the interface is given as

$$S_z^a \equiv \frac{\begin{bmatrix} u_X \\ u_{y'} \\ u_Z \end{bmatrix}^\dagger T^{a\dagger}(0) \begin{bmatrix} 0 & -i & 0 \\ i & 0 & 0 \\ 0 & 0 & 0 \end{bmatrix} \cos \vartheta^a T^a(0) \begin{bmatrix} u_X \\ u_{y'} \\ u_Z \end{bmatrix}}{\begin{bmatrix} u_X \\ u_{y'} \\ u_Z \end{bmatrix}^\dagger T^{a\dagger}(0) T^a(0) \begin{bmatrix} u_X \\ u_{y'} \\ u_Z \end{bmatrix}}, \quad (39)$$

since the polarization vector of the RH mode and that of the LH mode are eigenvectors of the 3×3 matrix given in Eq. (39) with eigenvalues $+1$ and -1 , respectively. We will later define matrices that represent the SAM operator in Eq. (77).

The SAM for each transverse wave is expressed as

$$S_z^{r-T} = \frac{\text{Re} [\rho_{\text{SV},\text{SV}}^* \rho_{\text{SH},\text{SH}}] \bar{\sigma} + \text{Im} [\rho_{\text{SV},\text{SV}}^* \rho_{\text{SH},\text{SH}}] \bar{\rho}}{(Q^{r-T})^2} \times (-\cos \theta_T), \quad (40a)$$

$$S_z^{t-T} = \frac{\text{Re} [\tau_{\text{SV},\text{SV}}^* \tau_{\text{SH},\text{SH}}] \bar{\sigma} + \text{Im} [\tau_{\text{SV},\text{SV}}^* \tau_{\text{SH},\text{SH}}] \bar{\rho}}{(Q^{t-T})^2} \times \cos \Theta_T, \quad (40b)$$

and $S_z = \bar{\sigma} \cos \theta_T$ for the incident beam. The longitudinal waves have no SAM: $S_z^{r-L} = S_z^{t-L} = 0$.

We next focus on the OAM that arises from the transverse shift Δr_{IF}^a . Since each wave has the same x' -component of the momentum $k_{c,x'}^a = k_c \sin \theta_T$, the OAM is determined mechanically by a cross product of the spatial shift and the momentum of the beam:

$$L_z^a = (\Delta \mathbf{r}^a \times \mathbf{k}_c^a)_z = -\Delta r_{\text{IF}}^a k_c \sin \theta_T. \quad (41)$$

We now construct the AM flux of each beam according to the expression of the energy flux of each beam (32). Since the absolute value of the energy flux is proportional to the number of phonons in the beam, we replace energy quanta $\hbar\omega$ in the energy flux formula with the sum of the SAM and OAM to obtain the total AM flux

$$\mathcal{J}^a \equiv \frac{S_z^a + L_z^a}{\hbar\omega} 2\omega^2 Z^a \cos \vartheta^a (Q^a)^2 (|u_X|^2 + |u_{y'}|^2) N^{\text{beam}} \quad (42)$$

for the reflected/transmitted beam and $\mathcal{J} \equiv (S_z/\hbar\omega) \cdot 2\omega^2 Z_T \cos \vartheta (|u_X|^2 + |u_{y'}|^2) N^{\text{beam}}$ for the incident beam. Here all of the AM flux have flow and polarization normal to the interface.

The ratio of \mathcal{J}^a to \mathcal{J} is derived as follows:

$$\frac{\mathcal{J}^{r-L}}{\mathcal{J}} = -\frac{|\rho_{\text{L},\text{SV}}|^2}{2} \frac{Z_{\text{L}} \cos \theta_{\text{L}}}{Z_{\text{T}} \cos \theta_{\text{T}}} = -\mathcal{R}_{\text{L},\text{RH}}, \quad (43a)$$

$$\begin{aligned} \frac{\mathcal{J}^{r-T}}{\mathcal{J}} &= -\frac{|\rho_{\text{SV},\text{SV}}|^2 + |\rho_{\text{SH},\text{SH}}|^2}{2} \\ &= -\mathcal{R}_{\text{RH},\text{RH}} - \mathcal{R}_{\text{LH},\text{RH}}, \end{aligned} \quad (43b)$$

$$\frac{\mathcal{J}^{t-L}}{\mathcal{J}} = \frac{|\tau_{\text{L},\text{SV}}|^2}{2} \frac{\zeta_{\text{L}} \cos \Theta_{\text{L}}}{Z_{\text{T}} \cos \theta_{\text{T}}} = \mathcal{T}_{\text{L},\text{RH}}, \quad (43c)$$

$$\begin{aligned} \frac{\mathcal{J}^{t-T}}{\mathcal{J}} &= \frac{|\tau_{\text{SV},\text{SV}}|^2 + |\tau_{\text{SH},\text{SH}}|^2}{2} \frac{\zeta_{\text{T}} \cos \Theta_{\text{T}}}{Z_{\text{T}} \cos \theta_{\text{T}}} \\ &= \mathcal{T}_{\text{RH},\text{RH}} + \mathcal{T}_{\text{LH},\text{RH}}. \end{aligned} \quad (43d)$$

Since the Fresnel coefficients satisfy unitarity due to the energy conservation law (15), i.e., $\mathcal{R}_{\text{L},\text{RH}} + \mathcal{R}_{\text{RH},\text{RH}} + \mathcal{R}_{\text{LH},\text{RH}} + \mathcal{T}_{\text{L},\text{RH}} + \mathcal{T}_{\text{RH},\text{RH}} + \mathcal{T}_{\text{LH},\text{RH}} = 1$, the continuity of the AM flux follows accordingly: $\mathcal{J} + \mathcal{J}^{r-L} + \mathcal{J}^{r-T} = \mathcal{J}^{t-L} + \mathcal{J}^{t-T}$. Clearly, the total AM of the incident beam is divided into the scattered beams in the same manner as the division of energy at the interface. The transverse shift of each mode thus compensates the difference between the division of total AM and the division of SAM with the extrinsic OAM.

IV. LATTICE VIBRATION, PHONON, AND THEIR BOUNDARY CONDITION

In the previous sections we have discussed the boundary scattering of elastic plane waves or beams in an infinite volume space. In this section we consider low-energy acoustic modes of lattice vibration in crystals with a finite volume and discuss boundary condition at the interface between the crystals. We construct the boundary condition according to a principle that a wave packet composed of the acoustic modes with almost the same wavevector and frequency simulates a monochromatic plane wave in the elastic medium. We then apply the boundary condition to phonons.

A. Classical lattice vibration in the elastic limit

Let us first take both low-energy and long-wavelength limit of the classical lattice vibration in the region $z < 0$. The stable position, displacement, and weight of an atomic site at a sublattice α in a unit cell labeled j are denoted by $\mathbf{R}_{j\alpha}$, $\mathbf{u}_{j\alpha}$, and M_α , respectively. The expansion of the lattice vibration then becomes

$$\mathbf{u}_{j\alpha}(t) = \sum_{\mathbf{k},n} e^{i(\mathbf{k} \cdot \mathbf{R}_{j\alpha} - \Omega_{\mathbf{k}n} t)} \sqrt{\frac{\hbar}{2NM_\alpha\Omega_{\mathbf{k}n}}} a_{\mathbf{k}n} \mathbf{e}_{\mathbf{k}n\alpha} + \text{c.c.} \quad (44)$$

$$\rightarrow \mathbf{u}(\mathbf{r}, t) = \sum_{\mathbf{k},n=L,\text{RH},\text{LH}} e^{i(\mathbf{k} \cdot \mathbf{r} - \Omega_{\mathbf{k}n} t)} \sqrt{\frac{\hbar}{2\rho V\Omega_{\mathbf{k}n}}} a_{\mathbf{k}n} \mathbf{e}_{\mathbf{k}n} + \text{c.c.} \quad (45)$$

Here N is the number of unit cells and c.c. denotes the complex conjugate of all preceding terms. The details of the sublattice degree of freedom are averaged out to the mass density ρ and the volume of the crystal V . Other than the dimensionless amplitude $a_{\mathbf{k}n}$, we introduce an auxiliary amplitude

$$A_{\mathbf{k}n}^{\text{lat}} \equiv \sqrt{\frac{\hbar}{2\rho\Omega_{\mathbf{k}n}}} a_{\mathbf{k}n}, \quad (46)$$

with which the lattice vibration is expressed without using the reduced Planck constant \hbar :

$$\mathbf{u}(\mathbf{r}, t) = \sum_{\mathbf{k}'n} \frac{e^{i(\mathbf{k}' \cdot \mathbf{r} - \Omega_{\mathbf{k}'n} t)}}{\sqrt{V}} A_{\mathbf{k}'n}^{\text{lat}} \mathbf{e}_{\mathbf{k}'n} + \text{c.c.} \quad (47)$$

In contrast to elastic waves, lattice vibrations in crystals with finite volumes are characterized by discrete wavevectors \mathbf{k} or discrete spectra of frequency $\Omega_{\mathbf{k}n}$. As a result, for two different crystals, their discrete wavevector components or discrete spectra of frequency do not coincide perfectly. This mismatch makes it difficult to establish a boundary condition at interfaces between different crystals.

Of course, normal vibrational modes in each crystal will be modulated into those in the junction system in reality. It is thus possible for the two crystals in contact to vibrate at the same frequency ω . If the interface still has discrete translational symmetry, we can also introduce wavevector components parallel to the interface \mathbf{k}_{\parallel} . The analysis of the coupled oscillation involving two different crystals, however, depends on the details of the interface and will require extensive calculations.

Instead, we shall here derive the boundary condition for the lattice vibrations on the basis of interfacial scattering of elastic waves. This is because details of the interface do not affect the reflection/transmission of waves with sufficiently long wavelengths. More importantly, we focus on a wave packet, not a monochromatic plane wave, with its central frequency ω and wavevector parallel to the interface \mathbf{k}_{\parallel} . The wave packet consists of some vibrational states with discrete frequencies and wavevectors. Let $\Delta\omega$ be the range in the frequency of the wave packet and $\Delta^2\mathbf{k}_{\parallel} = \Delta k_x \Delta k_y$ be the range in the wavevector component parallel to the interface. If we take a limit $\Delta\omega \Delta^2\mathbf{k}_{\parallel} \rightarrow 0$, the wave packet becomes indistinguishable from a plane wave characterized by $(\omega, \mathbf{k}_{\parallel})$. This correspondence leads to equalities between the wave packet and the plane wave in terms of the energy flux and in terms of the power reflectance/transmittance at the interface. These equalities yield the boundary condition for amplitudes of the lattice vibration in two crystals, as derived in the following.

B. Wave packet reflection/transmission in crystals

Let us slice the sum over all the vibrational states (47) into patches of wave packets. Each wave packet consists of a mode n propagating in $s \cdot \hat{\mathbf{z}}$ -direction ($s = \pm$) in the region $z < 0$, and is a superposition of plane waves around a frequency ω and a wavevector component parallel to the interface \mathbf{k}_{\parallel} . We assume that amplitude of the lattice vibrations within the wave packet is uniformly distributed in a range of frequency $[\omega - \Delta\omega/2, \omega + \Delta\omega/2]$ and a range of wavevector component parallel to the interface spread around \mathbf{k}_{\parallel} with area $\Delta^2\mathbf{k}_{\parallel}$. The condition of the uniform distribution will be satisfied if the width

$\Delta\omega \Delta^2\mathbf{k}_{\parallel}$ is sufficiently small. We thus describe the displacement of the wave packet $\mathbf{w}_{s,n}$ and its amplitude by

$$\mathbf{w}_{s,n}(\omega, \mathbf{k}_{\parallel}; \mathbf{r}, t) = \sum_{\mathbf{k}'} \frac{e^{i(\mathbf{k}' \cdot \mathbf{r} - \Omega_{\mathbf{k}'n} t)}}{\sqrt{V}} A_{\mathbf{k}'n}^{\text{w.p.}} \mathbf{e}_{\mathbf{k}'n} + \text{c.c.}, \quad (48a)$$

$$A_{\mathbf{k}'n}^{\text{w.p.}} = \sqrt{G(\Omega_{\mathbf{k}'n} - \omega, \mathbf{k}'_{\parallel} - \mathbf{k}_{\parallel})} u_{\mathbf{k}n}, \quad (48b)$$

where the superscript inequality $s \cdot k'_z > 0$ denotes a restriction on the range of the \mathbf{k}' -summation. The envelope function G for each wave packet takes the form of

$$G(\delta\omega, \delta\mathbf{k}_{\parallel}) \equiv \begin{cases} g(\omega, \mathbf{k}_{\parallel}) & \max \left\{ \frac{|\delta\omega|}{\Delta\omega}, \frac{|\delta k_x|}{\Delta k_x}, \frac{|\delta k_y|}{\Delta k_y} \right\} \leq \frac{1}{2} \\ 0 & \text{otherwise} \end{cases} \quad (48c)$$

Here we introduced an undermined factor $g(\omega, \mathbf{k}_{\parallel})$ for convenience.

We then calculate the energy flux per unit area of the interface, carried by the wave packet. Let S be the area of the interface. Then we obtain

$$J_{u;s,n}^{\text{w.p.}} = \int \frac{dx dy}{S} s \omega^2 Z_n \cos \theta_n \overline{|\mathbf{w}_{s,n}(\omega, \mathbf{k}_{\parallel}; \mathbf{r}, t)|^2} \Big|_{z=0} \quad (49)$$

$$= \frac{2s\omega^2 Z_n \cos \theta_n |u_{\mathbf{k}n}|^2}{V} \sum_{\mathbf{k}'}^{s \cdot k'_z > 0} G(\delta\omega, \delta\mathbf{k}_{\parallel}). \quad (50)$$

Here a bar over a symbol denotes the long-time average, as defined after Eq. (27). In the derivation of (50), we assumed discrete translational symmetry of the interface. The sum in the last line is reduced to the number of lattice vibrations included in the wave packet. We write it as $N_n(\omega, \mathbf{k}_{\parallel}) \Delta\omega \Delta^2\mathbf{k}_{\parallel}$ for infinitesimal $\Delta\omega$ and $\Delta^2\mathbf{k}_{\parallel}$, which gives

$$\sum_{\mathbf{k}'}^{s \cdot k'_z > 0} G(\delta\omega, \delta\mathbf{k}_{\parallel}) = g(\omega, \mathbf{k}_{\parallel}) \cdot N_n(\omega, \mathbf{k}_{\parallel}) \Delta\omega \Delta^2\mathbf{k}_{\parallel}. \quad (51)$$

Since acoustic modes have linear dispersions in the long-wavelength limit, N_n is obtained as

$$N_n(\omega, \mathbf{k}_{\parallel}) = \sum_{\mathbf{k}'}^{s \cdot k'_z > 0} \delta(\Omega_{\mathbf{k}'n} - \omega) \cdot \delta(\mathbf{k}'_{\parallel} - \mathbf{k}_{\parallel}) \quad (52)$$

$$= V \int \frac{dk'_z d^2\mathbf{k}'_{\parallel}}{(2\pi)^3} \frac{\delta\left(k'_z - s \sqrt{\frac{\omega^2}{v_n^2} - |\mathbf{k}'_{\parallel}|^2}\right)}{\left| \frac{\partial \Omega_{\mathbf{k},n}}{\partial k_z} \right|} \delta(\mathbf{k}'_{\parallel} - \mathbf{k}_{\parallel}) \quad (53)$$

$$= \frac{V}{(2\pi)^3} \cdot \frac{1}{v_n \cos \theta_n}. \quad (54)$$

Here we have transformed the discrete sum of \mathbf{k}' into an integral by assuming periodic boundary condition, since

details of the boundary condition are irrelevant to the density of states in the bulk [62].

We now assume that the energy flux density is uniquely determined when the system size $V^{1/3}$ is larger than the wavelength. The energy flux density for a wave packet, given as

$$J_{u;s,n}^{\text{w.p.}} = 2s\omega^2 Z_n \cos \theta_n |u_{\mathbf{k}n}|^2 \times g(\omega, \mathbf{k}_{\parallel}) \cdot \frac{N_n(\omega, \mathbf{k}_{\parallel}) \Delta\omega \Delta^2 \mathbf{k}_{\parallel}}{V}, \quad (55)$$

is thus equivalent to the energy flux density for the plane wave characterized by a mode n propagating in $s \cdot \hat{z}$ -direction in $z < 0$, given as $2s\omega^2 Z_n \cos \theta_n |u_{s,n}|^2$ [see Eq. (9)]. It follows that the wave packet defined by Eqs. (48) with amplitudes

$$A_{\mathbf{k}'n}^{\text{w.p.}} = \sqrt{g(\omega, \mathbf{k}_{\parallel})} \cdot u_{\mathbf{k}n} = \sqrt{\frac{V}{N_n \Delta\omega \Delta^2 \mathbf{k}_{\parallel}}} u_{\mathbf{k}n} \quad (56)$$

carries the same energy flux density as the plane wave characterized by $(\omega, \mathbf{k}_{\parallel})$ and an amplitude $u_{s,n} = u_{\mathbf{k}n}$. In the limit $\Delta\omega \Delta^2 \mathbf{k}_{\parallel} \rightarrow 0$, the wave packet becomes indistinguishable from the plane wave and we can identify $u_{\mathbf{k}n}$ to be $u_{s,n}$ on condition that $g(\omega, \mathbf{k}_{\parallel}) = V/(N_n \Delta\omega \Delta^2 \mathbf{k}_{\parallel})$.

We then transform the S -matrix between the amplitudes of plane waves $u_{s,n}$ at the interface, shown in Eqs. (10) and (12), into a boundary condition for amplitudes of wave packets at the interface. Let us consider wave packets expressed as Eqs. (48) in both regions $z < 0$ and $z > 0$ with the same the width $\Delta\omega$ and $\Delta^2 \mathbf{k}_{\parallel}$ as well as the same center values ω and \mathbf{k}_{\parallel} . The amplitude of the wave packet consist of a mode n propagating in $s \cdot \hat{z}$ -direction is denoted by $A_{\mathbf{k}'n}^{\text{w.p.}} = A_{s,n}^{\text{w.p.}}$ in $z < 0$ and $\tilde{A}_{\mathbf{q}'n}^{\text{w.p.}} = \tilde{A}_{s,n}^{\text{w.p.}}$ in $z > 0$. The mass density in the region $z < 0$ and $z > 0$ are ρ and $\tilde{\rho}$, respectively.

In accordance with the plane wave-wave packet correspondence (56), the elements of the vectors shown in Eq. (10) are translated into the amplitudes of incident waves or scattered waves as

$$\begin{aligned} & \sqrt{Z_n \cos \theta_n} u_{s,n} \\ & \rightarrow \sqrt{Z_n \cos \theta_n} \sqrt{\frac{N_n \Delta\omega \Delta^2 \mathbf{k}_{\parallel}}{V}} A_{\mathbf{k}'n}^{\text{w.p.}} \end{aligned} \quad (57)$$

$$= \sqrt{\frac{\Delta\omega \Delta^2 \mathbf{k}_{\parallel}}{(2\pi)^3}} \sqrt{\rho} A_{s,n}^{\text{w.p.}} \quad (58)$$

and $\sqrt{\frac{\Delta\omega \Delta^2 \mathbf{k}_{\parallel}}{(2\pi)^3}} \sqrt{\tilde{\rho}} \tilde{A}_{s,n}^{\text{w.p.}}$. Here we used Eq. (5). We then find a relation between them around the interface

$$\begin{bmatrix} \sqrt{\rho} A_{+,L}^{\text{w.p.}} \\ \sqrt{\rho} A_{-,RH}^{\text{w.p.}} \\ \sqrt{\rho} A_{-,LH}^{\text{w.p.}} \\ \sqrt{\tilde{\rho}} \tilde{A}_{+,L}^{\text{w.p.}} \\ \sqrt{\tilde{\rho}} \tilde{A}_{+,RH}^{\text{w.p.}} \\ \sqrt{\tilde{\rho}} \tilde{A}_{+,LH}^{\text{w.p.}} \end{bmatrix} = S(\omega, \mathbf{k}_{\parallel}) \begin{bmatrix} \sqrt{\rho} A_{+,L}^{\text{w.p.}} \\ \sqrt{\rho} A_{+,RH}^{\text{w.p.}} \\ \sqrt{\rho} A_{+,LH}^{\text{w.p.}} \\ \sqrt{\tilde{\rho}} \tilde{A}_{-,L}^{\text{w.p.}} \\ \sqrt{\tilde{\rho}} \tilde{A}_{-,RH}^{\text{w.p.}} \\ \sqrt{\tilde{\rho}} \tilde{A}_{-,LH}^{\text{w.p.}} \end{bmatrix}, \quad (59)$$

which holds independent of the choice of infinitesimal $\Delta\omega \Delta^2 \mathbf{k}_{\parallel}$.

C. Derivation of boundary condition for phonon distributions

We now patch together the wave packets (48) to form the entire lattice vibration (47) again. Let us identify $A_{\mathbf{k}'n}^{\text{w.p.}}$ as $A_{\mathbf{k}'n}^{\text{lat}}$ and apply Eq. (46) to transform them into $a_{\mathbf{k}'n}$. Since the S -matrix for each wave packet (59) still holds for $A_{\mathbf{k}'n}^{\text{lat}} = A_{\mathbf{k}'n}^{\text{w.p.}}$, we can rewrite it as

$$\begin{bmatrix} a_{-,L} \\ a_{-,RH} \\ a_{-,LH} \\ \tilde{a}_{+,L} \\ \tilde{a}_{+,RH} \\ \tilde{a}_{+,LH} \end{bmatrix} = S(\omega, \mathbf{k}_{\parallel}) \begin{bmatrix} a_{+,L} \\ a_{+,RH} \\ a_{+,LH} \\ \tilde{a}_{-,L} \\ \tilde{a}_{-,RH} \\ \tilde{a}_{-,LH} \end{bmatrix}, \quad (60)$$

where $a_{s,n}$ or $\tilde{a}_{s,n}$ instead of $a_{\mathbf{k}'n}$ or $\tilde{a}_{\mathbf{q}'n}$ denotes the dimensionless amplitude for the vibrational state (\mathbf{k}', n) or (\mathbf{q}', n) characterized by common $(\omega, \mathbf{k}_{\parallel})$ and $s = k'_z/|k'_z|$ or $s = q'_z/|q'_z|$, respectively.

We then consider the quantization of the lattice vibration, i.e., phonon, and construct the boundary condition for phonon distribution functions. Let us replace the classical amplitude $a_{\mathbf{k}n}$ (and its complex conjugate $a_{\mathbf{k}n}^*$) with a phonon annihilation (creation) operator $\hat{a}_{\mathbf{k}n}$ ($\hat{a}_{\mathbf{k}n}^\dagger$). They satisfy the commutation relation

$$[\hat{a}_{\mathbf{k}n}, \hat{a}_{\mathbf{k}'n'}^\dagger] = \delta_{\mathbf{k}, \mathbf{k}'} \delta_{nn'}. \quad (61)$$

We consider the classical S -matrix relation (60) provides a restriction not on the phonon annihilation operators but on the Fock space of phonons in the junction system. The corresponding S -matrix relation now requires an equality

$$\begin{bmatrix} \hat{a}_{-,L} |\Psi\rangle \\ \hat{a}_{-,RH} |\Psi\rangle \\ \hat{a}_{-,LH} |\Psi\rangle \\ \hat{\tilde{a}}_{+,L} |\Psi\rangle \\ \hat{\tilde{a}}_{+,RH} |\Psi\rangle \\ \hat{\tilde{a}}_{+,LH} |\Psi\rangle \end{bmatrix} = S(\omega, \mathbf{q}_{\parallel}) \begin{bmatrix} \hat{a}_{+,L} |\Psi\rangle \\ \hat{a}_{+,RH} |\Psi\rangle \\ \hat{a}_{+,LH} |\Psi\rangle \\ \hat{\tilde{a}}_{-,L} |\Psi\rangle \\ \hat{\tilde{a}}_{-,RH} |\Psi\rangle \\ \hat{\tilde{a}}_{-,LH} |\Psi\rangle \end{bmatrix}, \quad (62a)$$

or more concisely

$$\hat{a}_{\mu}^{\text{out}} |\Psi\rangle = \sum_{\nu} S_{\mu\nu}(\omega, \mathbf{q}_{\parallel}) \hat{a}_{\nu}^{\text{in}} |\Psi\rangle, \quad (62b)$$

for any phonon state $|\Psi\rangle$ allowed in the junction. Here annihilation operators labeled with ‘‘in’’ (‘‘out’’) denote incident (scattered) waves at the interface. For long-wavelength phonon excitations, Eqs. (62) exclude classically forbidden vibrational states in the junction system, at least in the vicinity of the interface. It is worth

noting that the vacuum $|\Psi\rangle = |0\rangle$ when the two crystals are apart is still the vacuum after the two crystals are in contact.

Let us introduce a phonon density matrix at the interface, denoted by $\hat{\rho}$. We then consider a reduced density matrix for incident waves and that for scattered waves at the interface. We define them as

$$\rho_{\nu_1\nu_2}^{\text{in}} \equiv \frac{\text{Tr} [\hat{a}_{\nu_1}^{\text{in}} \hat{\rho} \hat{a}_{\nu_2}^{\text{in} \dagger}]}{\text{Tr} [\hat{\rho}]}, \quad \rho_{\mu_1\mu_2}^{\text{out}} \equiv \frac{\text{Tr} [\hat{a}_{\mu_1}^{\text{out}} \hat{\rho} \hat{a}_{\mu_2}^{\text{out} \dagger}]}{\text{Tr} [\hat{\rho}]}, \quad (63)$$

where the trace is taken in the restricted Fock space specified by Eqs. (62). The two reduced density matrices are related by the S -matrix:

$$\rho_{\mu_1\mu_2}^{\text{out}} = \sum_{\Psi, \Phi} \langle \Psi | \hat{a}_{\mu_2}^{\text{out} \dagger} \hat{a}_{\mu_1}^{\text{out}} | \Phi \rangle \frac{\langle \Phi | \hat{\rho} | \Psi \rangle}{\text{Tr} [\hat{\rho}]} \quad (64)$$

$$= \sum_{\Psi, \Phi} \sum_{\nu_1, \nu_2} S_{\mu_2\nu_2}^* \langle \Psi | \hat{a}_{\nu_2}^{\text{in} \dagger} \hat{a}_{\nu_1}^{\text{in}} | \Phi \rangle S_{\mu_1\nu_1} \frac{\langle \Phi | \hat{\rho} | \Psi \rangle}{\text{Tr} [\hat{\rho}]} \quad (65)$$

$$= \sum_{\nu_1, \nu_2} S_{\mu_1\nu_1} \rho_{\nu_1\nu_2}^{\text{in}} (S^\dagger)_{\nu_2\mu_2}. \quad (66)$$

We now make two assumptions: one is that the phonon excitations of different incident waves have no correlation; the other is that the phonon excitations of different scattered waves have no correlation. Then the reduced density matrices have only the diagonal parts [63]

$$\rho_{\nu_1\nu_2}^{\text{in}} \simeq \delta_{\nu_1\nu_2} f_{\nu_1}^{\text{in}}, \quad \rho_{\mu_1\mu_2}^{\text{out}} \simeq \delta_{\mu_1\mu_2} f_{\mu_1}^{\text{out}} \quad (67)$$

and the phonon distribution functions for incident waves f_ν^{in} and for reflected/transmitted waves f_μ^{out} satisfy a relation

$$f_\mu^{\text{out}}(\omega, \mathbf{k}_\parallel) = \sum_\nu |S_{\mu\nu}(\omega, \mathbf{k}_\parallel)|^2 f_\nu^{\text{in}}(\omega, \mathbf{k}_\parallel). \quad (68)$$

This is nothing but the boundary condition for phonon distribution functions at the interface. In the case when off-diagonal elements of the phonon density matrix plays an important role [64], we may rather use the boundary condition (66) instead.

It is worth noting that the boundary condition (68) holds in thermal equilibrium $f_\mu^{\text{out}}(\omega, \mathbf{k}_\parallel) = f_\nu^{\text{in}}(\omega, \mathbf{k}_\parallel) = [e^{\hbar\omega/k_B T} - 1]^{-1} \equiv f^{\text{eq}}(\omega, T)$ because of the unitarity of the S -matrix (15). The conservation of the number of phonons also follows from both (68) and the unitarity of the S -matrix: $\sum_\mu f_\mu^{\text{out}}(\omega, \mathbf{k}_\parallel) = \sum_\nu f_\nu^{\text{in}}(\omega, \mathbf{k}_\parallel)$. We can also transform it as $\sum_{s,n} s F_{s,n}(\omega, \mathbf{k}_\parallel) = \sum_{s,n} s f_{s,n}(\omega, \mathbf{k}_\parallel)$ with $F_{s,n}$ and $f_{s,n}$ the phonon distribution function in $z < 0$ and $z > 0$, respectively.

With the help of this relation, we can further confirm

that the energy flux density is continuous at the interface:

$$\begin{aligned} & \frac{1}{V} \sum_{\mathbf{k}, n} \hbar \Omega_{\mathbf{k}n} v_{\mathbf{k}n}^z F_{\mathbf{k}n} |_{z=-0} \\ &= \int d\omega d^2 \mathbf{k}_\parallel \sum_{s,n} \frac{N_n(\omega, \mathbf{k}_\parallel)}{V} \hbar \omega \cdot s v_n \cos \theta_n \\ & \quad \times F_{s,n}(\omega, \mathbf{k}_\parallel) |_{z=-0} \end{aligned} \quad (69)$$

$$= \int \frac{d\omega d^2 \mathbf{k}_\parallel}{(2\pi)^3} \hbar \omega \sum_{s,n} s F_{s,n}(\omega, \mathbf{k}_\parallel) |_{z=-0} \quad (70)$$

$$= \int \frac{d\omega d^2 \mathbf{k}_\parallel}{(2\pi)^3} \hbar \omega \sum_{s,n} s f_{s,n}(\omega, \mathbf{k}_\parallel) |_{z=+0} \quad (71)$$

$$= \frac{1}{V} \sum_{\mathbf{q}, n} \hbar \omega_{\mathbf{q}n} c_{\mathbf{q}n}^z f_{\mathbf{q}n} |_{z=+0}. \quad (72)$$

Here we write $F_{\mathbf{k}n} = F_{s,n}(\omega, \mathbf{k}_\parallel)$ with $s = k_z/|k_z|$ and $f_{\mathbf{q}n} = f_{s,n}(\omega, \mathbf{q}_\parallel)$ with $s = q_z/|q_z|$ to represent the phonon distribution functions. The energy conservation law thus holds at the interface under the boundary condition (68).

Finally, we conclude this section by comparing the obtained boundary condition (68) with previous studies. The boundary condition given in Refs. [65, 66] is similar to (68) in that their condition consists of linear equations among phonon distributions of incident and reflected/transmitted waves for each frequency ω . Refs. [65, 66], however, have addressed the case of quasi-ballistic phonon transport with diffuse scattering at the interface. The situation is different from that in the present paper, which covers the scattering at the smooth and flat interface. In fact, the boundary condition derived in Refs. [65, 66] differs from that derived in this section.

Considering the case of perfect reflection, the boundary condition for phonon distributions is well explained in Ziman's monograph [67]. The boundary condition for the specular reflection according to the monograph becomes the same as our boundary condition (68). Furthermore, the calculation of the interfacial thermal resistance based on (68) is in agreement with the acoustic mismatch model [35, 36] (see Sect. S3 in the Supplemental Material [49]). These consistencies also support the validity of our boundary condition.

V. FORMULATION OF CHIRAL/ACHIRAL JUNCTION

From this section we start considering the spatial profile of phonon angular momentum (AM) and its transmission across the interface $z = 0$ between the chiral crystal (CC) in $z < 0$ and the achiral crystal (ACC) in $z > 0$. The aim of this section is threefold. First, we provide the Boltzmann transport equation for phonon. Second, we introduce boundary condition for phonon distribution

functions at the interface. Third, we describe the difference in phonon distribution between circularly polarized modes. This difference results in the polarization of spin angular momentum (SAM).

A. Setup and Boltzmann formalism

We first specify phonon states in the CC (ACC) with wavevectors $\mathbf{k} = k \cdot \hat{\mathbf{k}}$ ($\mathbf{q} = q \cdot \hat{\mathbf{q}}$) and modes $n = \text{L, T}$. Since we focus only on acoustic modes, the phonon modes are characterized by one longitudinal mode (L) and two transverse modes (T). We thus use the same symbol n in both crystals.

For simplicity, the two adjacent crystals are modeled as isotropic media. The phonon dispersions and velocities in the CC are denoted by

$$\Omega_{kn} = v_n k, \quad \mathbf{v}_{kn} = v_n \hat{\mathbf{k}} \quad (n = \text{L, T}) \quad (73a)$$

and those for the ACC are denoted by

$$\omega_{qn} = c_n q, \quad \mathbf{c}_{qn} = c_n \hat{\mathbf{q}} \quad (n = \text{L, T}). \quad (73b)$$

We then decompose the degenerate T modes into two modes: one is the right-handed (RH) circularly polarized mode, and the other is the left-handed (LH) circularly polarized mode. Their polarization vectors are denoted by $\mathbf{e}_{\mathbf{k}\text{RH}}$ and $\mathbf{e}_{\mathbf{k}\text{LH}}$ in the CC and $\boldsymbol{\xi}_{\mathbf{q}\text{RH}}$ and $\boldsymbol{\xi}_{\mathbf{q}\text{LH}}$ in the ACC. The polarization vectors for the RH modes are given as

$$\mathbf{e}_{\mathbf{k}\text{RH}} \equiv \frac{\hat{k}_z \hat{\mathbf{k}} - \hat{\mathbf{z}} + i \hat{\mathbf{z}} \times \hat{\mathbf{k}}}{\sqrt{2(1 - \hat{k}_z^2)}}, \quad \boldsymbol{\xi}_{\mathbf{q}\text{RH}} \equiv \frac{\hat{q}_z \hat{\mathbf{q}} - \hat{\mathbf{z}} + i \hat{\mathbf{z}} \times \hat{\mathbf{q}}}{\sqrt{2(1 - \hat{q}_z^2)}}, \quad (74)$$

while those for the LH modes are given as $\mathbf{e}_{\mathbf{k}\text{LH}} = \mathbf{e}_{\mathbf{k}\text{RH}}^*$ and $\boldsymbol{\xi}_{\mathbf{q}\text{LH}} = \boldsymbol{\xi}_{\mathbf{q}\text{RH}}^*$.

For each phonon state (\mathbf{k}, n) in the CC and (\mathbf{q}, n) in the ACC, we define the spin angular momentum (SAM) as

$$\boldsymbol{\ell}_{kn} \equiv \begin{cases} 0 & n = \text{L} \\ +\hbar \hat{\mathbf{k}} & n = \text{RH} \\ -\hbar \hat{\mathbf{k}} & n = \text{LH} \end{cases}, \quad \tilde{\boldsymbol{\ell}}_{qn} \equiv \begin{cases} 0 & n = \text{L} \\ +\hbar \hat{\mathbf{q}} & n = \text{RH} \\ -\hbar \hat{\mathbf{q}} & n = \text{LH} \end{cases}, \quad (75)$$

reflecting the circular polarization. Note that in our convention, a time-reversal pair of (\mathbf{k}, n) and $(-\mathbf{k}, n)$ is characterized by the same phonon band, as shown in Fig. 1(b). The phonon spins $\boldsymbol{\ell}_{kn}$ and $\tilde{\boldsymbol{\ell}}_{qn}$ are thus odd in \mathbf{k} and \mathbf{q} , respectively.

Let us now introduce distribution function and SAM density given by it. The phonon distribution function in the CC and ACC are represented as $F = F_{kn}(z)$ and $f = f_{qn}(z)$, respectively ($n = \text{L, RH, LH}$). Then the phonon SAM density in the CC with the volume V is

defined as [2, 16–19]

$$\boldsymbol{\ell}^{\text{SAM}}(z < 0) = \frac{1}{V} \sum_{j,\alpha} \left\langle \hat{\mathbf{u}}_{j\alpha} \times M_\alpha \frac{d\hat{\mathbf{u}}_{j\alpha}}{dt} \right\rangle \quad (76)$$

$$= \frac{1}{V} \sum_{\mathbf{k},n} \left(F_{kn} + \frac{1}{2} \right) \sum_{\alpha} \mathbf{e}_{\mathbf{k}n\alpha}^\dagger \boldsymbol{\mathfrak{S}} \mathbf{e}_{\mathbf{k}n\alpha}. \quad (77)$$

Here $\hat{\mathbf{u}}_{j\alpha}$ denotes the displacement of an atomic site with weight M_α at a sublattice α in a unit cell labeled j , while $\mathbf{e}_{\mathbf{k}n\alpha}$ denotes polarization vector of the phonon state (\mathbf{k}, n) . Statistical average is represented by the bracket in Eq. (76). The spin-1 matrices $\boldsymbol{\mathfrak{S}} = (\boldsymbol{\mathfrak{S}}_x, \boldsymbol{\mathfrak{S}}_y, \boldsymbol{\mathfrak{S}}_z)$ are represented as $(\boldsymbol{\mathfrak{S}}_a)_{bc} = -i\hbar \epsilon_{abc}$ ($a, b, c = x, y, z$).

Since we are interested in the elastic limit, we consider the polarization vectors to be independent of the sublattice degree of freedom $\mathbf{e}_{\mathbf{k}n\alpha} \rightarrow \mathbf{e}_{\mathbf{k}n}$ while keeping the normalization $\sum_{\alpha} \mathbf{e}_{\mathbf{k}n\alpha}^\dagger \mathbf{e}_{\mathbf{k}n\alpha} = \mathbf{e}_{\mathbf{k}n}^\dagger \mathbf{e}_{\mathbf{k}n} = 1$. The phonon SAM density is then reduced to

$$\boldsymbol{\ell}^{\text{SAM}}(z < 0) \rightarrow \frac{1}{V} \sum_{\mathbf{k},n=\text{L,RH,LH}} \boldsymbol{\ell}_{kn} \left(F_{kn} - F_{kn}^{(0)} \right). \quad (78)$$

Here we used a property $\boldsymbol{\ell}_{kn} = \mathbf{e}_{\mathbf{k}n}^\dagger \boldsymbol{\mathfrak{S}} \mathbf{e}_{\mathbf{k}n}$. We also omitted a constant $1/2$ and the equilibrium part of the distribution function $F_{kn}^{(0)} = f^{\text{eq}}(\Omega_{kn}, T)$ given by Bose distribution $f^{\text{eq}}(\omega, T) = [e^{\hbar\omega/k_B T} - 1]^{-1}$, since $\boldsymbol{\ell}_{kn}$ is odd in \mathbf{k} while $1/2$ and $F_{kn}^{(0)}$ are even in \mathbf{k} . In the same way, the SAM density in the ACC with the volume \tilde{V} is written down as

$$\boldsymbol{\ell}^{\text{SAM}}(z > 0) = \frac{1}{\tilde{V}} \sum_{\mathbf{q},n=\text{L,RH,LH}} \tilde{\boldsymbol{\ell}}_{qn} \left(f_{qn} - f_{qn}^{(0)} \right) \quad (79)$$

with $f_{qn}^{(0)} = f^{\text{eq}}(\omega_{qn}, T)$.

We now consider a steady state where a thermal gradient ∇T is applied to the CC. To describe the spatial variation of a finite phonon SAM density or flux in the non-equilibrium state, let us introduce the Boltzmann equation that F and f follow:

$$v_{kn}^z \frac{\partial F_{kn}^{(1)}}{\partial z} + \mathbf{v}_{kn} \cdot \nabla T \frac{\partial F_{kn}^{(0)}}{\partial T} = -\frac{F_{kn}^{(1)}}{\tau}, \quad (80a)$$

$$c_{qn}^z \frac{\partial f_{qn}^{(1)}}{\partial z} = -\frac{f_{qn}^{(1)}}{\tilde{\tau}}. \quad (80b)$$

Here $F^{(1)} \simeq F - F^{(0)}$ and $f^{(1)} \simeq f - f^{(0)}$ are deviations of the first order of ∇T from the equilibrium distributions. We also assumed that the non-equilibrium steady state is spatially uniform in the direction parallel to the interface (x, y -direction). We hereafter attributes all the dissipation of the system to the time constants τ and $\tilde{\tau}$ in Eqs. (80).

The solution of the Boltzmann equation (80) is given

as [67]

$$F_{\mathbf{k}n}^{(1)}(z < 0) = B_{\mathbf{k}n} + \begin{cases} C_{\mathbf{k}n} \exp \left[z / (-v_{\mathbf{k}n}^z \tau) \right] & v_{\mathbf{k}n}^z < 0 \\ 0 & v_{\mathbf{k}n}^z > 0 \end{cases}, \quad (81a)$$

$$f_{\mathbf{q}n}^{(1)}(z > 0) = \begin{cases} 0 & c_{\mathbf{q}n}^z < 0 \\ D_{\mathbf{q}n} \exp \left[-z / c_{\mathbf{q}n}^z \tilde{\tau} \right] & c_{\mathbf{q}n}^z > 0 \end{cases} \quad (81b)$$

with the bulk part in $z < 0$

$$B_{\mathbf{k}n} = -\tau \mathbf{v}_{\mathbf{k}n} \cdot \nabla T \frac{\partial F_{\mathbf{k}n}^{(0)}}{\partial T}. \quad (81c)$$

With the help of the Boltzmann equation, we can also derive a constitutive equation for the SAM. If we multiply both sides of (80) by $\ell_{\mathbf{k}n}$ or $\tilde{\ell}_{\mathbf{q}n}$ and sum up for states (\mathbf{k}, n) or (\mathbf{q}, n) , it follows that

$$\begin{aligned} \frac{\partial}{\partial z} \left(\frac{1}{V} \sum_{\mathbf{k}, n} \ell_{\mathbf{k}n}^i v_{\mathbf{k}n}^z F_{\mathbf{k}n}^{(1)} \right) - \frac{1}{\tau V} \sum_{\mathbf{k}, n} \ell_{\mathbf{k}n}^i B_{\mathbf{k}n} \\ = -\frac{1}{\tau} \left(\frac{1}{V} \sum_{\mathbf{k}, n} \ell_{\mathbf{k}n}^i F_{\mathbf{k}n}^{(1)} \right), \end{aligned} \quad (82a)$$

$$\frac{\partial}{\partial z} \left(\frac{1}{\tilde{V}} \sum_{\mathbf{q}, n} \tilde{\ell}_{\mathbf{q}n}^i c_{\mathbf{q}n}^z f_{\mathbf{q}n}^{(1)} \right) = -\frac{1}{\tilde{\tau}} \left(\frac{1}{\tilde{V}} \sum_{\mathbf{q}, n} \tilde{\ell}_{\mathbf{q}n}^i f_{\mathbf{q}n}^{(1)} \right) \quad (82b)$$

with $i = x, y, z$. We then introduce the SAM flux that flows along the direction normal to the interface

$$J_i^{\text{SAM}}(z < 0) \equiv \frac{1}{V} \sum_{\mathbf{k}, n} \ell_{\mathbf{k}n}^i v_{\mathbf{k}n}^z F_{\mathbf{k}n}^{(1)}, \quad (83a)$$

$$J_i^{\text{SAM}}(z > 0) \equiv \frac{1}{\tilde{V}} \sum_{\mathbf{q}, n} \tilde{\ell}_{\mathbf{q}n}^i c_{\mathbf{q}n}^z f_{\mathbf{q}n}^{(1)}, \quad (83b)$$

and the bulk SAM density in the CC

$$\ell_0 \equiv \frac{1}{V} \sum_{\mathbf{k}, n} \ell_{\mathbf{k}n} B_{\mathbf{k}n} \quad (84)$$

$$= \hbar \int \frac{d^3 \mathbf{k}}{(2\pi)^3} \hat{\mathbf{k}} (B_{\mathbf{k}, \text{RH}} - B_{\mathbf{k}, \text{LH}}). \quad (85)$$

The constitutive equation between the SAM density and flux is now given as

$$\ell_i^{\text{SAM}}(z) - \ell_{0,i} = -\tau \frac{\partial J_i^{\text{SAM}}}{\partial z} \quad z < 0, \quad (86a)$$

$$\ell_i^{\text{SAM}}(z) = -\tilde{\tau} \frac{\partial J_i^{\text{SAM}}}{\partial z} \quad z > 0, \quad (86b)$$

which represents a balance between the sink of SAM flux and the dissipation of SAM density.

B. Boundary condition for phonon distributions

The phonon distribution incident upon the interface is redistributed into phonon states scattered from the interface. Let us give a boundary condition that determines this redistribution. Since we have assumed the smooth interface, the angle of reflection/refraction follows Snell's law and the wavevector parallel to the interface is conserved during the elastic scattering. The energy of phonon is also conserved during the scattering. We thus write $F_{\mathbf{k}n} = F_{s,n}(\omega, \mathbf{k}_{\parallel})$ with $s = k_z / |k_z|$ to represent the phonon distribution function of a state (\mathbf{k}, n) by using its frequency ω and wavevector parallel to the interface \mathbf{k}_{\parallel} . In the same way, we write $f_{\mathbf{q}n} = f_{s,n}(\omega, \mathbf{q}_{\parallel})$ with $s = q_z / |q_z|$ for convenience. The number of phonons is then redistributed between $F_{s,n}$ and $f_{s,n}$ at $z = \pm 0$ with the same ω and $\mathbf{k}_{\parallel} = \mathbf{q}_{\parallel}$.

We then write down the boundary condition (68) derived in Sect. IV C as follows:

$$\left[\begin{array}{c} F_{-,L}(\omega, \mathbf{k}_{\parallel}) \\ F_{-,RH}(\omega, \mathbf{k}_{\parallel}) \\ F_{-,LH}(\omega, \mathbf{k}_{\parallel}) \\ f_{+,L}(\omega, \mathbf{k}_{\parallel}) \\ f_{+,RH}(\omega, \mathbf{k}_{\parallel}) \\ f_{+,LH}(\omega, \mathbf{k}_{\parallel}) \end{array} \right]_{z=0} = \left[\begin{array}{ccc|ccc} \mathcal{R}_{L,L} & \mathcal{R}_{L,RH} & \mathcal{R}_{L,LH} & \mathcal{T}'_{L,L} & \mathcal{T}'_{L,RH} & \mathcal{T}'_{L,LH} \\ \mathcal{R}_{RH,L} & \mathcal{R}_{RH,RH} & \mathcal{R}_{RH,LH} & \mathcal{T}'_{RH,L} & \mathcal{T}'_{RH,RH} & \mathcal{T}'_{RH,LH} \\ \mathcal{R}_{LH,L} & \mathcal{R}_{LH,RH} & \mathcal{R}_{LH,LH} & \mathcal{T}'_{LH,L} & \mathcal{T}'_{LH,RH} & \mathcal{T}'_{LH,LH} \\ \hline \mathcal{T}_{L,L} & \mathcal{T}_{L,RH} & \mathcal{T}_{L,LH} & \mathcal{R}'_{L,L} & \mathcal{R}'_{L,RH} & \mathcal{R}'_{L,LH} \\ \mathcal{T}_{RH,L} & \mathcal{T}_{RH,RH} & \mathcal{T}_{RH,LH} & \mathcal{R}'_{RH,L} & \mathcal{R}'_{RH,RH} & \mathcal{R}'_{RH,LH} \\ \mathcal{T}_{LH,L} & \mathcal{T}_{LH,RH} & \mathcal{T}_{LH,LH} & \mathcal{R}'_{LH,L} & \mathcal{R}'_{LH,RH} & \mathcal{R}'_{LH,LH} \end{array} \right]_{(\omega, \mathbf{k}_{\parallel})} \left[\begin{array}{c} F_{+,L}(\omega, \mathbf{k}_{\parallel}) \\ F_{+,RH}(\omega, \mathbf{k}_{\parallel}) \\ F_{+,LH}(\omega, \mathbf{k}_{\parallel}) \\ f_{-,L}(\omega, \mathbf{k}_{\parallel}) \\ f_{-,RH}(\omega, \mathbf{k}_{\parallel}) \\ f_{-,LH}(\omega, \mathbf{k}_{\parallel}) \end{array} \right]_{z=0}. \quad (87)$$

The coefficients \mathcal{R}_{nm} , \mathcal{T}_{nm} , \mathcal{R}'_{nm} , \mathcal{T}'_{nm} are the power reflectance/transmittance of elastic waves, defined in Eqs. (13). Our boundary condition (87) determines the amplitudes of the localized distribution of phonon $C_{\mathbf{k}n} = C_{-,n}$ and $D_{\mathbf{q}n} = D_{+,n}$ in Eqs. (81a) and (81b):

$$B_{-,n}(\omega, \mathbf{k}_{\parallel}) + C_{-,n}(\omega, \mathbf{k}_{\parallel})$$

$$= \sum_m \mathcal{R}_{nm}(\omega, \mathbf{k}_{\parallel}) B_{+,m}(\omega, \mathbf{k}_{\parallel}), \quad (88a)$$

$$D_{+,n}(\omega, \mathbf{k}_{\parallel}) = \sum_m \mathcal{T}_{nm}(\omega, \mathbf{k}_{\parallel}) B_{+,m}(\omega, \mathbf{k}_{\parallel}), \quad (88b)$$

which will be used in the next section (Sect. VI).

C. Difference in distribution between circularly polarized modes

We here consider a small splitting between the two circularly polarized acoustic modes in the CC. The splitting results in $B_{\mathbf{k},\text{RH}} \neq B_{\mathbf{k},\text{LH}}$ and a finite SAM density in the bulk according to Eq. (85).

We first introduce the dynamical matrix of the CC. Let us consider the CC to be an elastic body. A plane wave solution of the equation of motion for its deformation $\mathbf{u} \exp(i\mathbf{k} \cdot \mathbf{r} - i\omega t)$ then satisfies an eigenvalue problem $\underline{D}(\mathbf{k})\mathbf{u} = \omega^2\mathbf{u}$. The 3×3 matrix $\underline{D}(\mathbf{k})$ in the left-hand side is termed the dynamical matrix. The phonon dispersions $\omega = \Omega_{\mathbf{k}n}$ are obtained as square roots of the eigenvalues of $\underline{D}(\mathbf{k})$.

We now expand the dynamical matrix $\underline{D}(\mathbf{k})$ of the CC in the long-wavelength limit $|\mathbf{k}| = k \rightarrow 0$:

$$\underline{D}(\mathbf{k}) = \underline{D}^{(0)} + \underline{D}_i^{(1)}k_i + \underline{D}_{ij}^{(2)}k_ik_j + \underline{D}_{ijl}^{(3)}k_ik_jk_l + \dots, \quad (89)$$

where we take sums over multiple indices. Let us examine matrix elements between the circularly polarized modes

$$\langle n; \mathbf{k} | \underline{D}_{i_1, i_2, \dots, i_a}^{(a)} | m; \mathbf{k} \rangle \equiv \mathbf{e}_{\mathbf{k}n}^\dagger \underline{D}_{i_1, i_2, \dots, i_a}^{(a)} \mathbf{e}_{\mathbf{k}m} \quad (90)$$

with $n, m = \text{RH, LH}$. Since the RH and LH modes are acoustic modes following the Nambu–Goldstone theorem and are degenerate up to the quadratic term $\underline{D}_{ij}^{(2)}k_ik_j$ due to the isotropy, it follows that

$$\langle n; \mathbf{k} | \underline{D}^{(0)} | m; \mathbf{k} \rangle = \langle n; \mathbf{k} | \underline{D}_i^{(1)} | m; \mathbf{k} \rangle = 0, \quad (91a)$$

$$\langle n; \mathbf{k} | \underline{D}_{ij}^{(2)} | m; \mathbf{k} \rangle = v_T^2 \delta_{ij} \delta_{nm}. \quad (91b)$$

We remark other physical constraints on the dynamical matrix $\underline{D}(\mathbf{k})$. First, $\underline{D}(\mathbf{k})$ is a positive-definite Hermitian matrix $\underline{D}^\dagger(\mathbf{k}) = \underline{D}(\mathbf{k})$. Second, the time-reversal symmetry requires a reciprocity $\underline{D}(\mathbf{k}) = \underline{D}^\top(-\mathbf{k})$. Third, in centrosymmetric crystals, $\underline{D}(-\mathbf{k}) = \underline{D}(\mathbf{k})$ holds. The anti-symmetric matrix $\underline{D}_{ijl}^{(3)}$, known as the acoustic gyrotropic tensor [1, 5, 68–70], thus exists in non-centrosymmetric crystals, in particular in the CC.

It follows from the above constraints and relations $\mathbf{e}_{\mathbf{k},\text{LH}} = \mathbf{e}_{\mathbf{k},\text{RH}}^* = \mathbf{e}_{-\mathbf{k},\text{RH}}$ [see Eq. (74)] that the matrix elements of $\underline{D}_{ijl}^{(3)}$ for the CC are reduced to

$$\begin{aligned} & \left[\begin{aligned} & \langle \text{RH}; \mathbf{k} | \underline{D}_{ijl}^{(3)} | \text{RH}; \mathbf{k} \rangle \quad \langle \text{RH}; \mathbf{k} | \underline{D}_{ijl}^{(3)} | \text{LH}; \mathbf{k} \rangle \\ & \langle \text{LH}; \mathbf{k} | \underline{D}_{ijl}^{(3)} | \text{RH}; \mathbf{k} \rangle \quad \langle \text{LH}; \mathbf{k} | \underline{D}_{ijl}^{(3)} | \text{LH}; \mathbf{k} \rangle \end{aligned} \right] \\ &= \begin{bmatrix} \Delta_{ijl}(\hat{\mathbf{k}}) & 0 \\ 0 & -\Delta_{ijl}(\hat{\mathbf{k}}) \end{bmatrix}. \end{aligned} \quad (92)$$

Here the element $\Delta_{ijl}(-\hat{\mathbf{k}}) = -\Delta_{ijl}(\hat{\mathbf{k}})$ yields the lifting of the transverse acoustic modes of the order of k^2 in the dispersion relation. In non-centrosymmetric crystals, this splitting along high-symmetry axes in the Brillouin zone is examined by previous studies [1, 5, 68–71]; the matrix element is estimated to be $|\Delta_{zzz}|/v_T^2 \sim$

3×10^{-10} m for α -quartz in the direction close to the optical axis (z -axis) [5, 69, 70].

Since we assume that the CC is non-centrosymmetric but isotropic medium, we put

$$\Delta_{ijl}(\hat{\mathbf{k}}) = \chi v_T \frac{k_ik_jk_l}{k^3}. \quad (93)$$

with a scalar χ and obtain the band dispersion of the RH and LH modes as

$$\Omega_{\mathbf{k},\text{RH}} = \sqrt{v_T^2 k^2 + \Delta_{ijl}k_ik_jk_l} \simeq v_T k + \frac{\chi k^2}{2}, \quad (94a)$$

$$\Omega_{\mathbf{k},\text{LH}} \simeq v_T k - \frac{\chi k^2}{2}. \quad (94b)$$

Here the sign of χ depends on the handedness of the CC. We consider χ to be small: $|\chi| \cdot k_B T / \hbar v_T \ll v_T$. This assumption is valid at low temperatures $T \ll 100$ K for α -quartz.

Since the band dispersions of the RH and LH modes are slightly different, their phonon distributions deviated from the equilibrium under the thermal gradient also become different. With the help of Eq. (81c), this difference in the bulk of the CC is expressed as

$$\begin{aligned} & B_{\mathbf{k},\text{RH}} - B_{\mathbf{k},\text{LH}} \\ &= -\tau (v_T + \chi k) \hat{\mathbf{k}} \cdot \nabla T \frac{\partial f^{\text{eq}}(v_T k + \chi k^2/2, T)}{\partial T} \\ & \quad + \tau (v_T - \chi k) \hat{\mathbf{k}} \cdot \nabla T \frac{\partial f^{\text{eq}}(v_T k - \chi k^2/2, T)}{\partial T} \quad (95) \\ & \simeq \frac{\tau \chi \mathbf{k} \cdot \nabla T}{T} \cdot \frac{w e^w [w + 3 + (w - 3)e^w]}{(e^w - 1)^3} \Bigg|_{w = \hbar v_T k / k_B T}. \end{aligned} \quad (96)$$

VI. DIFFUSION OF SPIN ANGULAR MOMENTUM

In this section we shall derive the spatial distribution of the SAM density and flux in the junction when the CC is subject to the thermal gradient ∇T . The setup is schematically shown in Fig. 1(a). As we have addressed in Sect. VC, the difference in the phonon distribution between the RH and LH modes results from the lifting of their degeneracy of the order of χ . We, however, omit the same-order differences in the reflectance/transmittance, in the density of states, and in the velocity between RH and LH modes for simplicity.

To begin with, a uniform SAM density in the bulk part of the CC is obtained linear in ∇T according to Eqs. (85) and (96)

$$\ell_0 = \frac{4\pi^2}{45} \hbar \cdot \tau \chi \left(\frac{k_B T}{\hbar v_T} \right)^4 \frac{\nabla T}{T} \equiv \alpha(T) \nabla T, \quad (97)$$

which is known as the phonon Edelstein effect [9]. Here we replaced the phonon cutoff energy to the infinity,

since the integrand steeply decreases above the energy $\sim 10k_{\text{B}}T$ and we assume $k_{\text{B}}T$ is much lower than the Debye energy.

Note that $\alpha(T) \propto T^3$ results from the $O(k^2)$ splitting between the transverse modes. If the band splitting is $O(k^4)$, as supposed by Ref. [71] for tellurium, $\alpha(T) \propto T^5$ follows instead. The temperature dependence and any other details of the coefficient $\alpha(T)$ are, however, not important to the later discussion.

We then consider the SAM density and flux in the vicinity of the interface. Since the constitutive equation (86) allows us to derive $\ell^{\text{SAM}}(z)$ as a spatial derivative of $J_i^{\text{SAM}}(z)$, we first derive the SAM flux. With the help of Eqs. (75), (81a), and (83a), it follows that

$$J_i^{\text{SAM}}(z < 0) = \frac{\hbar}{V} \sum_{\mathbf{k}} \hat{k}_i \left(v_{\mathbf{k},\text{RH}}^z F_{\mathbf{k},\text{RH}}^{(1)} - v_{\mathbf{k},\text{LH}}^z F_{\mathbf{k},\text{LH}}^{(1)} \right) \quad (98)$$

$$\simeq \frac{\hbar}{V} \sum_{\mathbf{k}} \hat{k}_i v_{\mathbf{k},\text{T}}^z \left(F_{\mathbf{k},\text{RH}}^{(1)} - F_{\mathbf{k},\text{LH}}^{(1)} \right) \quad (99)$$

$$= \hbar v_{\text{T}} \int \frac{d^3 \mathbf{k}}{(2\pi)^3} \hat{k}_i \hat{k}_z \left[(B_{\mathbf{k},\text{RH}} - B_{\mathbf{k},\text{LH}}) + \Theta_{\text{H}}(-k_z) \left(C_{\mathbf{k},\text{RH}} e^{-z/(\tau v_{\mathbf{k},\text{RH}}^z)} - C_{\mathbf{k},\text{LH}} e^{-z/(\tau v_{\mathbf{k},\text{LH}}^z)} \right) \right] \quad (100)$$

$$\simeq \hbar v_{\text{T}} \int \frac{d^3 \mathbf{k}}{(2\pi)^3} \hat{k}_i \hat{k}_z \left[(B_{\mathbf{k},\text{RH}} - B_{\mathbf{k},\text{LH}}) + \Theta_{\text{H}}(-k_z) e^{-z/(\tau v_{\text{T}} \hat{k}_z)} (C_{\mathbf{k},\text{RH}} - C_{\mathbf{k},\text{LH}}) \right] \quad (101)$$

$$= \hbar v_{\text{T}} \int_{k_z < 0} \frac{d^3 \mathbf{k}}{(2\pi)^3} \hat{k}_i \hat{k}_z e^{-z/(\tau v_{\text{T}} \hat{k}_z)} (C_{\mathbf{k},\text{RH}} - C_{\mathbf{k},\text{LH}}), \quad (102)$$

which gives the SAM flux in the CC. Here $\Theta_{\text{H}}(w)$ is the Heaviside step function (14). In Eq. (102), we omit the uniform part of the SAM flux, since $\hat{k}_i \hat{k}_z (B_{\mathbf{k},\text{RH}} - B_{\mathbf{k},\text{LH}})$ is odd in \mathbf{k} .

As for the SAM flux in the ACC, we again use Eqs. (75), (81b), and (83b) to obtain

$$J_i^{\text{SAM}}(z > 0) \simeq \hbar c_{\text{T}} \int_{q_z > 0} \frac{d^3 \mathbf{q}}{(2\pi)^3} \hat{q}_i \hat{q}_z e^{-z/(\tilde{\tau} c_{\text{T}} \hat{q}_z)} (D_{\mathbf{q},\text{RH}} - D_{\mathbf{q},\text{LH}}). \quad (103)$$

For later convenience, we change the variables in Eq. (103) from the wavevector \mathbf{q} of the transmitted transverse wave with $q_z > 0$ to the wavevector \mathbf{k} of the incident transverse wave with $k_z > 0$. Since $\omega_{\mathbf{q}\text{T}} = \Omega_{\mathbf{k}\text{T}}$ and

$q_{\parallel} = k_{\parallel}$ hold, the integrating factor is given as

$$d^3 \mathbf{q} = \frac{d\omega_{\mathbf{q}\text{T}} d^2 \mathbf{q}_{\parallel}}{c_{\text{T}} \cos \Theta} = d^3 \mathbf{k} \frac{v_{\text{T}} \cos \theta}{c_{\text{T}} \cos \Theta(\mathbf{k})} \quad (104)$$

where θ and Θ are angles that \mathbf{k} and \mathbf{q} form with the z -axis, respectively. In particular, $\sin \Theta(\mathbf{k}) \equiv c_{\text{T}} |\mathbf{k}_{\parallel}| / \Omega_{\mathbf{k},\text{T}}$ according to Snell's law. We also rearrange the direction $\hat{\mathbf{q}}$ as

$$\hat{\mathbf{q}}(\mathbf{k}) = \frac{\mathbf{k}_{\parallel} + \sqrt{(\Omega_{\mathbf{k}\text{T}}/c_{\text{T}})^2 - |\mathbf{k}_{\parallel}|^2} \cdot \hat{z}}{\Omega_{\mathbf{k}\text{T}}/c_{\text{T}}}. \quad (105)$$

We thus transform Eq. (103) into

$$J_i^{\text{SAM}}(z > 0) = \hbar v_{\text{T}} \int_{k_z > 0} \frac{d^3 \mathbf{k}}{(2\pi)^3} \frac{\cos \theta}{\cos \Theta(\mathbf{k})} \hat{q}_i(\mathbf{k}) \hat{q}_z(\mathbf{k}) e^{-z/[\tilde{\tau} c_{\text{T}} \hat{q}_z(\mathbf{k})]} \times [D_{+,\text{RH}}(\Omega_{\mathbf{k},\text{T}}, \mathbf{k}_{\parallel}) - D_{+,\text{LH}}(\Omega_{\mathbf{k},\text{T}}, \mathbf{k}_{\parallel})]. \quad (106)$$

By using the boundary condition (88) and the symmetry of reflectance and transmittance (16), we can simplify the difference in the localized distribution around the interface between the RH and LH modes:

$$C_{\mathbf{k},\text{RH}} - C_{\mathbf{k},\text{LH}} = C_{-,\text{RH}}(\Omega_{\mathbf{k},\text{RH}}, \mathbf{k}_{\parallel}) - C_{-,\text{LH}}(\Omega_{\mathbf{k},\text{LH}}, \mathbf{k}_{\parallel}) \quad (107)$$

$$\simeq C_{-,\text{RH}}(\Omega_{\mathbf{k},\text{T}}, \mathbf{k}_{\parallel}) - C_{-,\text{LH}}(\Omega_{\mathbf{k},\text{T}}, \mathbf{k}_{\parallel}) \quad (108)$$

$$= - [B_{-,\text{RH}}(\Omega_{\mathbf{k},\text{T}}, \mathbf{k}_{\parallel}) - B_{-,\text{LH}}(\Omega_{\mathbf{k},\text{T}}, \mathbf{k}_{\parallel})] + \sum_m [\mathcal{R}_{\text{RH},m}(\Omega_{\mathbf{k},\text{T}}, \mathbf{k}_{\parallel}) - \mathcal{R}_{\text{LH},m}(\Omega_{\mathbf{k},\text{T}}, \mathbf{k}_{\parallel})] \times B_{+,m}(\Omega_{\mathbf{k},\text{T}}, \mathbf{k}_{\parallel}) \quad (109)$$

$$\simeq - (B_{\mathbf{k},\text{RH}} - B_{\mathbf{k},\text{LH}}) + [\mathcal{R}_{\text{RH},\text{RH}}(\Omega_{\mathbf{k},\text{T}}, \mathbf{k}_{\parallel}) - \mathcal{R}_{\text{LH},\text{RH}}(\Omega_{\mathbf{k},\text{T}}, \mathbf{k}_{\parallel})] \times (B_{\bar{\mathbf{k}},\text{RH}} - B_{\bar{\mathbf{k}},\text{LH}}) \quad (110)$$

with $\bar{\mathbf{k}} \equiv (k_x, k_y, -k_z)$ and

$$D_{+,\text{RH}}(\Omega_{\mathbf{k},\text{T}}, \mathbf{k}_{\parallel}) - D_{+,\text{LH}}(\Omega_{\mathbf{k},\text{T}}, \mathbf{k}_{\parallel}) \simeq [\mathcal{T}_{\text{RH},\text{RH}}(\Omega_{\mathbf{k},\text{T}}, \mathbf{k}_{\parallel}) - \mathcal{T}_{\text{LH},\text{RH}}(\Omega_{\mathbf{k},\text{T}}, \mathbf{k}_{\parallel})] \times \Theta_{\text{H}}(k_z) (B_{\mathbf{k},\text{RH}} - B_{\mathbf{k},\text{LH}}). \quad (111)$$

To clarify that the reflectance/transmittance are functions of the angle of incidence, let us write $\mathcal{R}_{nm}(\omega, \mathbf{k}_{\parallel}) = \mathcal{R}_{nm}(\theta_m)$ and $\mathcal{T}_{nm}(\omega, \mathbf{k}_{\parallel}) = \mathcal{T}_{nm}(\theta_m)$ with $\sin \theta_m = v_m |\mathbf{k}_{\parallel}| / \omega$. Substituting Eqs.(96), (110), and (111) into Eqs. (102) and (106), we obtain the following expression of the SAM flux:

$$\begin{aligned}
\frac{J_i^{\text{SAM}}(z < 0)}{\frac{3}{2}\alpha v_{\text{T}}} &= \left\{ Ei_5 \left(\left| \frac{z}{\tau v_{\text{T}}} \right| \right) + \int_0^{\pi/2} d\theta \sin \theta \cos^3 \theta [\mathcal{R}_{\text{RH,RH}}(\theta) - \mathcal{R}_{\text{LH,RH}}(\theta)] e^{-\frac{|z/\tau v_{\text{T}}|}{\cos \theta}} \right\} \delta_{i,z} \frac{\partial T}{\partial z} \\
&+ \left\{ \left[Ei_3 \left(\left| \frac{z}{\tau v_{\text{T}}} \right| \right) - Ei_5 \left(\left| \frac{z}{\tau v_{\text{T}}} \right| \right) \right] - \int_0^{\pi/2} d\theta \sin^3 \theta \cos \theta [\mathcal{R}_{\text{RH,RH}}(\theta) - \mathcal{R}_{\text{LH,RH}}(\theta)] e^{-\frac{|z/\tau v_{\text{T}}|}{\cos \theta}} \right\} \\
&\times \left(\frac{\delta_{i,x}}{2} \frac{\partial T}{\partial x} + \frac{\delta_{i,y}}{2} \frac{\partial T}{\partial y} \right), \tag{112a}
\end{aligned}$$

$$\begin{aligned}
\frac{J_i^{\text{SAM}}(z > 0)}{\frac{3}{2}\alpha v_{\text{T}}} &= \int_0^{\pi/2} d\theta \sin \theta \cos^2 \theta \sqrt{1 - \left(\frac{c_{\text{T}}}{v_{\text{T}}} \sin \theta \right)^2} [\mathcal{T}_{\text{RH,RH}}(\theta) - \mathcal{T}_{\text{LH,RH}}(\theta)] e^{-\frac{|z/\tilde{\tau} c_{\text{T}}|}{\sqrt{1 - \left(\frac{c_{\text{T}}}{v_{\text{T}}} \sin \theta \right)^2}}} \delta_{i,z} \frac{\partial T}{\partial z} \\
&+ \frac{c_{\text{T}}}{v_{\text{T}}} \int_0^{\pi/2} d\theta \sin^3 \theta \cos \theta [\mathcal{T}_{\text{RH,RH}}(\theta) - \mathcal{T}_{\text{LH,RH}}(\theta)] e^{-\frac{|z/\tilde{\tau} c_{\text{T}}|}{\sqrt{1 - \left(\frac{c_{\text{T}}}{v_{\text{T}}} \sin \theta \right)^2}}} \left(\frac{\delta_{i,x}}{2} \frac{\partial T}{\partial x} + \frac{\delta_{i,y}}{2} \frac{\partial T}{\partial y} \right). \tag{112b}
\end{aligned}$$

Here we have used $\alpha(T)$ in (97) and introduced an integral $Ei_n(w)$ defined by

$$Ei_n(w) \equiv \int_1^\infty \frac{e^{-wt}}{t^n} dt, \quad \text{Re } w > 0. \tag{113}$$

The constitutive equation (86) now leads to the SAM

density in the junction:

$$\boldsymbol{\ell}^{\text{SAM}}(z) = \begin{cases} \boldsymbol{\ell}_0 + \boldsymbol{\ell}_1(z) & z < 0 \\ \boldsymbol{\ell}_2(z) & z > 0 \end{cases} \tag{114a}$$

with $\boldsymbol{\ell}_0$ given in Eq. (97) and

$$\begin{aligned}
\boldsymbol{\ell}_1(z) &= -\frac{3\alpha}{2} \left\{ Ei_4 \left(\left| \frac{z}{\tau v_{\text{T}}} \right| \right) + \int_0^{\pi/2} d\theta \sin \theta \cos^2 \theta [\mathcal{R}_{\text{RH,RH}}(\theta) - \mathcal{R}_{\text{LH,RH}}(\theta)] \exp \left(-\frac{|z/\tau v_{\text{T}}|}{\cos \theta} \right) \right\} \frac{\partial T}{\partial z} \hat{\boldsymbol{z}} \\
&- \frac{3\alpha}{4} \left\{ Ei_2 \left(\left| \frac{z}{\tau v_{\text{T}}} \right| \right) - Ei_4 \left(\left| \frac{z}{\tau v_{\text{T}}} \right| \right) - \int_0^{\pi/2} d\theta \sin^3 \theta [\mathcal{R}_{\text{RH,RH}}(\theta) - \mathcal{R}_{\text{LH,RH}}(\theta)] \exp \left(-\frac{|z/\tau v_{\text{T}}|}{\cos \theta} \right) \right\} \\
&\times \left(\frac{\partial T}{\partial x} \hat{\boldsymbol{x}} + \frac{\partial T}{\partial y} \hat{\boldsymbol{y}} \right), \tag{114b}
\end{aligned}$$

$$\begin{aligned}
\boldsymbol{\ell}_2(z) &= 3\alpha \int_0^{\pi/2} \frac{\sin \theta d\theta}{2} [\mathcal{T}_{\text{RH,RH}}(\theta) - \mathcal{T}_{\text{LH,RH}}(\theta)] \exp \left[-\frac{|z/\tilde{\tau} c_{\text{T}}|}{\sqrt{1 - \left(\frac{c_{\text{T}}}{v_{\text{T}}} \sin \theta \right)^2}} \right] \\
&\times \left[\frac{v_{\text{T}}}{c_{\text{T}}} \cos^2 \theta \frac{\partial T}{\partial z} \hat{\boldsymbol{z}} + \frac{\sin^2 \theta \cos \theta / 2}{\sqrt{1 - \left(\frac{c_{\text{T}}}{v_{\text{T}}} \sin \theta \right)^2}} \left(\frac{\partial T}{\partial x} \hat{\boldsymbol{x}} + \frac{\partial T}{\partial y} \hat{\boldsymbol{y}} \right) \right]. \tag{114c}
\end{aligned}$$

We illustrate the spatial profile of the SAM density

and flux when both ∇T and $\boldsymbol{\ell}^{\text{SAM}}$ are normal to the in-

interface as orange dashed curves in Fig. 5(a). Moreover, in Fig. 5(b), we illustrate the spatial profile of the SAM density (red solid curves) and the SAM flux (blue dashed curves) when both ∇T and ℓ^{SAM} are parallel to the interface. We selected quartz as the CC occupying the region $z < 0$ while we selected vacuum (in the case of free end), platinum, lead, and quartz itself (in the case of perfect transmission of every mode) as the ACC in $z > 0$. The SAM density ℓ^{SAM} , irrespective of its direction, diffuses from the bulk of the CC subject to the thermal gradient into the interface and adjacent ACC on the whole. The SAM flux J_i^{SAM} is, on the other hand, finite only around the interface, since J_i^{SAM} increases with the drop of ℓ^{SAM} from its bulk value in accordance with the constitutive equation (86).

The other key ingredients indicated by Figs. 5(a) and (b) are threefold: (i) the SAM diffuses through the interface whether or not there is a thermal flux flowing normal to the interface; (ii) in the ACC, the z -component of the SAM density can be increased at the interface, while the other components of the SAM density and SAM flux have constant upper bounds; (iii) there is a jump in the SAM flux at the interface. We detail each of them in the following.

First, a finite SAM is transmitted through the interface even when no thermal flux flows normal to the interface. This is the case of Fig. 5(b): the application of $\partial T/\partial x$ or $\partial T/\partial y$ to the CC results in a thermal flux parallel to the interface (xy -plane). Nevertheless, the SAM density and flux diffuse into the z -direction. This is because spin-conserving transmittance $\mathcal{T}_{\text{RH,RH}}$ and spin-flipping transmittance $\mathcal{T}_{\text{LH,RH}}$ are different according to the elastic theory; this difference enables the transfer of imbalance in phonon distribution between the RH and LH modes from the bulk of the CC into the ACC [see Eq. (111)]. The setup here is quite similar to the experiment in Ref. [30], the mechanism of which we shall discuss in Sect. VIII.

Second, in the quartz/lead junction shown in Fig. 5(a), the SAM density in the ACC near the interface exceeds the bulk SAM density ℓ_0 in the CC. This excess results from a factor $v_{\text{T}}/c_{\text{T}}$ in Eq. (114c), which becomes large in the quartz/lead junction. Since the difference in the transmittance $\mathcal{T}_{\text{RH,RH}} - \mathcal{T}_{\text{LH,RH}}$ does not vanish even in the limit $v_{\text{T}}/c_{\text{T}} \rightarrow \infty$ according to Eqs. (4), $\ell_z^{\text{SAM}}(z = +0)$ shown in Eqs. (114c) increases as $v_{\text{T}}/c_{\text{T}} \rightarrow \infty$. In other words, we can amplify the SAM density that is diffused to the ACC and is polarized normal to the interface by choosing crystals with low transverse-wave velocity $c_{\text{T}} \ll v_{\text{T}}$.

Considering other components of the SAM density and flux in the ACC, their upper bounds are independent of the ratio $v_{\text{T}}/c_{\text{T}}$:

$$\frac{J_i^{\text{SAM}}(z > 0)}{\alpha v_{\text{T}} \cdot \partial T/\partial r_i} \leq \begin{cases} 3/16 & i = x, y \\ 1/2 & i = z \end{cases}, \quad (115a)$$

$$\frac{\ell_i^{\text{SAM}}(z > 0)}{\alpha \cdot \partial T/\partial r_i} \leq \begin{cases} 1/2 & i = x, y \\ v_{\text{T}}/(2c_{\text{T}}) & i = z \end{cases}. \quad (115b)$$

We can derive the above inequalities by using Eqs. (112), (114), and an inequality $\mathcal{T}_{\text{RH,RH}} - \mathcal{T}_{\text{LH,RH}} \leq 1$, together with consideration of critical angles. In particular, the SAM density and flux polarized in the x - or y -direction at $z = +0$ have the maximum in the case of perfect transmittance of transverse modes $\mathcal{T}_{\text{RH,RH}} - \mathcal{T}_{\text{LH,RH}} = 1$.

Third, the SAM flux is discontinuous at the interface, irrespective of the direction of spin polarization. For the interface of two different crystals, phonon distributions at the interface follow the boundary condition shown in Eq. (87). This condition, however, does not satisfy the conservation of SAM: the sum of SAM carried by phonons reflected and transmitted from the interface is different from the initial SAM carried by phonons incident to the interface. The jump of the SAM flux density at the interface thus follows even when its polarization is normal to the interface.

This result seems to contradict to the existence of continuous rotational symmetry of the interface around the z -axis. We shall detail in the next section that this contradiction is resolved by introducing orbital angular momentum (OAM) in the phonon reflection/transmission.

Note that an exceptional case is the interface of the same crystals, shown in the bottom of Figs. 5(a) and (b). Here the perfect transmission allows the phonon distributions in both sides to become the same for each mode n and each wavevector $\mathbf{k} = \mathbf{q}$: $F_{\mathbf{k}n}(z = -0) = f_{\mathbf{q}n}(z = +0)$. Every physical quantity including the SAM flux is thus continuous at the interface in this case.

VII. PHONON ANGULAR MOMENTUM CONSERVATION AT THE INTERFACE

In this section we address the conservation law of the phonon angular momentum (AM) at the interface of the chiral crystal (CC)/achiral crystal (ACC) junction when a thermal gradient normal to the interface $\nabla T = (\partial T/\partial z)\hat{z}$ is applied to the CC. This conservation law is complementary to the phonon transport in the junction considered in Sect. VI.

The smooth, flat interface between the CC and ACC has a continuous rotational symmetry around the interface normal \hat{z} . The conservation of AM thus follows at the interface. As a corollary, a phonon AM flux density, with both of its flow and polarization being normal to the interface, does not have any source or sink and is continuous at the interface.

Let us recall the AM conservation law of elastic paraxial beams at the smooth and flat interface (see Sect. III for details). The circular polarization of each beam provides the spin angular momentum (SAM), while the transverse spatial shift of reflected/transmitted beams yields the orbital angular momentum (OAM). The sum of the SAM flux and OAM flux for each beam (43)

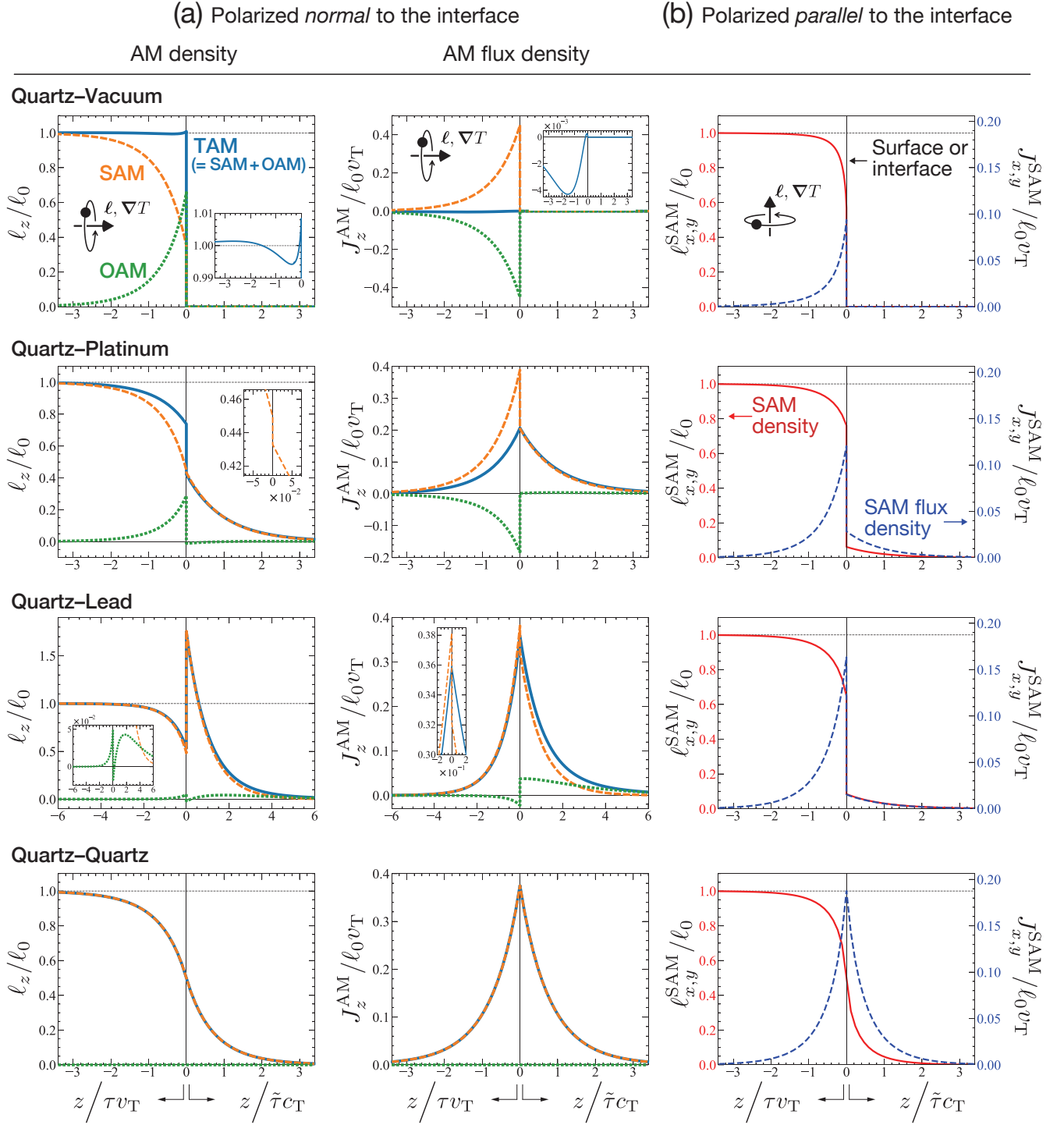


FIG. 5. (a) Spatial profile of phonon angular momentum (AM) density $\ell_z = \ell_z^{\text{SAM}}, \ell_z^{\text{OAM}},$ and ℓ_z^{TAM} , and its flux density $J_z^{\text{AM}} = J_z^{\text{SAM}}, J_z^{\text{OAM}},$ and J_z^{TAM} , illustrated for some examples of interfaces. Their AM are polarized normal to the interface. (b) Spatial profile of phonon spin angular momentum (SAM) density $\ell_{x,y}^{\text{SAM}}$ and its flux density $J_{x,y}^{\text{SAM}}$, illustrated for some examples of interfaces. Their AM are polarized parallel to the interface. In both (a) and (b), the AM diffuses from a chiral crystal (CC) in $z < 0$ subject to a thermal gradient ∇T into an adjacent achiral crystal in $z > 0$. The magnitudes of the AM densities and fluxes are normalized by using the bulk AM density $\ell_0 = |\ell_0|$ [see Eqs. (85) and (97)] or the transverse-wave velocity v_T in the CC. The total AM (TAM) density/flux consists of two parts, SAM part and orbital angular momentum (OAM) part; the former arises from the circular polarization, while the latter arises from the transverse shift at the interface. We set parameters as $v_L/v_T = 1.59$ and [Quartz–Vacuum] $\zeta_T/Z_T = 0$, [Quartz–Platinum] $c_L/c_T = 2.25$, $c_T/v_T = 0.493$, and $\zeta_T/Z_T = 3.99$, [Quartz–Lead] $c_L/c_T = 2.84$, $c_T/v_T = 0.183$, and $\zeta_T/Z_T = 0.947$, [Quartz–Quartz] $c_L/v_T = 1.59$ and $c_T/v_T = \zeta_T/Z_T = 1$.

satisfies a conservation law. In particular, the ratio of the total AM flux of the reflected/transmitted beam to that of the incident beam is equal to the power reflectance/transmittance.

Similar to the elastic beams, we consider that phonon reflected/transmitted at the interface experiences the same transverse shift and satisfies the total AM conservation. We thus introduce an OAM flux carried by phonons. We shall call the sum of the SAM and OAM the total angular momentum (TAM). We hereafter consider only SAM, OAM, and TAM carried by non-equilibrium part of the phonon distribution proportional to $\partial T/\partial z$. We also confine ourselves to a steady state without a rigid body rotation, i.e., macroscopic rotation of the entire junction, for simplicity.

We first consider the OAM and TAM flux incident upon the interface. Since phonon coming from the bulk has not experienced boundary scatterings before or lost the memory of preceding boundary scatterings, the OAM flux is not accompanied by the incident phonons. There is still a possibility of thermal gradient-induced intrinsic OAM in the bulk of the CC, but we here neglect this effect.

The TAM flux in the CC carried by phonons with $k_z > 0$ thus becomes the same as the corresponding SAM flux. Its element contributed from phonons of mode n spread around a central frequency ω and wavevector parallel to the interface \mathbf{k}_{\parallel} with a range $d\omega d^2\mathbf{k}_{\parallel}$ is given as

$$\ell_{\mathbf{k}n}^z v_{\mathbf{k}n}^z B_{\mathbf{k}n} \frac{d^3\mathbf{k}}{(2\pi)^3} = \ell_{+,n}^z(\omega, \mathbf{k}_{\parallel}) B_{+,n}(\omega, \mathbf{k}_{\parallel}) \frac{d\omega d^2\mathbf{k}_{\parallel}}{(2\pi)^3} \quad (116)$$

with the help of Eq. (104). Here we put $\ell_{\mathbf{k}n}^z = \ell_{+,n}^z(\omega, \mathbf{k}_{\parallel})$. According to the boundary condition (88), $B_{\mathbf{k}n}$ is only the phonon distribution that is proportional to $\partial T/\partial z$ and is incident to the interface.

By applying the balance of the TAM flux (43) to the phonon transport, the TAM flux accompanied by the phonons reflected from the interface with $k_z < 0$ and

mode n spread around $(\omega, \mathbf{k}_{\parallel})$ is defined as

$$-\sum_m \mathcal{R}_{nm}(\omega, \mathbf{k}_{\parallel}) \cdot \ell_{+,m}^z(\omega, \mathbf{k}_{\parallel}) B_{+,m}(\omega, \mathbf{k}_{\parallel}) \frac{d\omega d^2\mathbf{k}_{\parallel}}{(2\pi)^3}, \quad (117)$$

while the TAM flux accompanied by phonons transmitted from the interface with $q_z > 0$ and mode n spread around $(\omega, \mathbf{q}_{\parallel})$ is defined as

$$\sum_m \mathcal{T}_{nm}(\omega, \mathbf{q}_{\parallel}) \cdot \ell_{+,m}^z(\omega, \mathbf{q}_{\parallel}) B_{+,m}(\omega, \mathbf{q}_{\parallel}) \frac{d\omega d^2\mathbf{q}_{\parallel}}{(2\pi)^3}. \quad (118)$$

We assume that the reflected and transmitted OAM fluxes fade away as they flow inside and vanish in the bulk of the CC and ACC. This is because the extrinsic OAM, cross product of position and momentum \mathbf{k}_{\parallel} or \mathbf{q}_{\parallel} , is lost in a momentum relaxation time by the scattering at other (grain) boundaries or Umklapp scattering. It then follows that the OAM flux decays in a mean free path away from the interface. The SAM flux also decays inside of the CC and ACC [see Eqs. (112)], and so does the TAM flux.

It is worth noting that the TAM of the entire system is conserved under the continuous rotational symmetry and in the absence of dissipation of phonon AM to other excitations [39, 40]. In this ideal case, the steady TAM flux becomes spatially constant. In crystals, however, the continuous rotational symmetry is broken at the microscopic scale due to anisotropy of the crystal structure and anisotropic disorders inside. The TAM flux thus decays at the mesoscale. We are not concerned here with detailed relaxation mechanism of the AM. Instead, we approximate that the relaxation mechanism is represented by relaxation time constants τ and $\tilde{\tau}$.

Within the distribution functions (81a) and (81b), only the terms with coefficients $C_{\mathbf{k}n}$ and $D_{\mathbf{q}n}$ describe this loss of the memory along path by the length $|\tau v_{\mathbf{k}n}^z|$ or $|\tilde{\tau} c_{\mathbf{q}n}^z|$. The OAM is thus carried only by the localized distributions with $C_{\mathbf{k}n}$ or $D_{\mathbf{q}n}$, and not by the uniform distribution $B_{\mathbf{k}n}$. As for the SAM, however, all of $B_{\mathbf{k}n}$, $C_{\mathbf{k}n}$ and $D_{\mathbf{q}n}$ terms contribute to its transport, since the SAM $\ell_{\mathbf{k}n}$ or $\tilde{\ell}_{\mathbf{q}n}$ stems from the circular polarization inherent in the phonon state.

Let us write $L_{\mathbf{k}n}^z = L_{-,n}^z(\Omega_{\mathbf{k}n}, \mathbf{k}_{\parallel})$ and $\tilde{L}_{\mathbf{q}n}^z = \tilde{L}_{+,n}^z(\omega_{\mathbf{q}n}, \mathbf{q}_{\parallel})$ to represent the OAM carried by the state (\mathbf{k}, n) and (\mathbf{q}, n) , respectively. With the help of the TAM flux at the interface (117) and (118), the detailed balance of the TAM flux at the interface is expressed as

$$\begin{aligned} & - \left\{ \ell_{-,n}^z(\omega, \mathbf{k}_{\parallel}) [B_{-,n}(\omega, \mathbf{k}_{\parallel}) + C_{-,n}(\omega, \mathbf{k}_{\parallel})] + L_{-,n}^z(\omega, \mathbf{k}_{\parallel}) C_{-,n}(\omega, \mathbf{k}_{\parallel}) \right\} \frac{d\omega d^2\mathbf{k}_{\parallel}}{(2\pi)^3} \\ & = - \sum_m \mathcal{R}_{nm}(\omega, \mathbf{k}_{\parallel}) \cdot \ell_{+,m}^z(\omega, \mathbf{k}_{\parallel}) \cdot B_{+,m}(\omega, \mathbf{k}_{\parallel}) \frac{d\omega d^2\mathbf{k}_{\parallel}}{(2\pi)^3}, \end{aligned} \quad (119a)$$

$$\left[\tilde{\ell}_{+,n}^z(\omega, \mathbf{q}_{\parallel}) + \tilde{L}_{+,n}^z(\omega, \mathbf{q}_{\parallel}) \right] D_{+,n}(\omega, \mathbf{q}_{\parallel}) \frac{d\omega d^2 \mathbf{q}_{\parallel}}{(2\pi)^3} = \sum_m \mathcal{T}_{nm}(\omega, \mathbf{q}_{\parallel}) \cdot \ell_{+,m}^z(\omega, \mathbf{q}_{\parallel}) B_{+,m}(\omega, \mathbf{q}_{\parallel}) \frac{d\omega d^2 \mathbf{q}_{\parallel}}{(2\pi)^3}. \quad (119b)$$

The OAM $L_{-,n}^z$ and $\tilde{L}_{+,n}^z$ are now determined by using the boundary condition (88) and the detailed balance of the TAM flux (119). Even the phonons of the longitudinal mode have the OAM, since the reflectance \mathcal{R}_{LRH} ,

\mathcal{R}_{LLH} , and the transmittance \mathcal{T}_{LRH} , \mathcal{T}_{LLH} are finite in general. By taking the sum over the phonon states, the OAM flux density is expressed as

$$J_z^{\text{OAM}}(z) = \begin{cases} -\sum_n \int \frac{d\omega d^2 \mathbf{k}_{\parallel}}{(2\pi)^3} L_{-,n}^z(\omega, \mathbf{k}_{\parallel}) C_{-,n}(\omega, \mathbf{k}_{\parallel}) \exp \left[z / |\tau v_n \cos \theta_n(\omega, \mathbf{k}_{\parallel})| \right] & z < 0 \\ \sum_n \int \frac{d\omega d^2 \mathbf{q}_{\parallel}}{(2\pi)^3} \tilde{L}_{+,n}^z(\omega, \mathbf{q}_{\parallel}) D_{+,n}(\omega, \mathbf{q}_{\parallel}) \exp \left[-z / |\tilde{\tau} c_n \cos \Theta_n(\omega, \mathbf{q}_{\parallel})| \right] & z > 0 \end{cases}. \quad (120)$$

Here $\theta_n(\omega, \mathbf{k}_{\parallel})$ and $\Theta_n(\omega, \mathbf{q}_{\parallel})$ are the angle of reflection/refraction of the scattered wave labeled by the mode n , respectively. The angles satisfy $\sin \theta_n(\omega, \mathbf{k}_{\parallel}) = v_n |\mathbf{k}_{\parallel}| / \omega$ and $\sin \Theta_n(\omega, \mathbf{q}_{\parallel}) = c_n |\mathbf{q}_{\parallel}| / \omega$. The OAM density is also obtained by dividing the integrand of Eqs. (120) by the group velocity and then summing over the states again:

$$\ell_z^{\text{OAM}}(z) = \begin{cases} \sum_n \int \frac{d\omega d^2 \mathbf{k}_{\parallel}}{(2\pi)^3} \frac{L_{-,n}^z(\omega, \mathbf{k}_{\parallel})}{|v_n \cos \theta_n(\omega, \mathbf{k}_{\parallel})|} C_{-,n}(\omega, \mathbf{k}_{\parallel}) \exp \left[z / |\tau v_n \cos \theta_n(\omega, \mathbf{k}_{\parallel})| \right] & z < 0 \\ \sum_n \int \frac{d\omega d^2 \mathbf{q}_{\parallel}}{(2\pi)^3} \frac{\tilde{L}_{+,n}^z(\omega, \mathbf{q}_{\parallel})}{|c_n \cos \Theta_n(\omega, \mathbf{q}_{\parallel})|} D_{+,n}(\omega, \mathbf{q}_{\parallel}) \exp \left[-z / |\tilde{\tau} c_n \cos \Theta_n(\omega, \mathbf{q}_{\parallel})| \right] & z > 0 \end{cases}. \quad (121)$$

Then the TAM flux and TAM density are given as $J_z^{\text{TAM}}(z) = J_z^{\text{SAM}}(z) + J_z^{\text{OAM}}(z)$ and $\ell_z^{\text{TAM}}(z) =$

$\ell_z^{\text{SAM}}(z) + \ell_z^{\text{OAM}}(z)$. We finally obtain the TAM flux in the junction analytically:

$$J_z^{\text{TAM}}(z < 0) = \frac{3}{2} \alpha v_{\text{T}} \frac{\partial T}{\partial z} \left(Ei_5(|z/\tau v_{\text{T}}|) - \int_0^{\pi/2} d\theta \sin \theta \cos^3 \theta \right. \\ \left. \times \left\{ \mathcal{R}_{\text{L,RH}}(\theta) \exp \left(-\frac{|z/\tau v_{\text{L}}|}{\sqrt{1 - \left(\frac{v_{\text{L}}}{v_{\text{T}}} \sin \theta\right)^2}} \right) + [\mathcal{R}_{\text{RH,RH}}(\theta) + \mathcal{R}_{\text{LH,RH}}(\theta)] \exp \left(-\frac{|z/\tau v_{\text{T}}|}{\cos \theta} \right) \right\} \right), \quad (122a)$$

$$J_z^{\text{TAM}}(z > 0) = \frac{3}{2} \alpha v_{\text{T}} \frac{\partial T}{\partial z} \int_0^{\pi/2} d\theta \sin \theta \cos^3 \theta \\ \times \left\{ \mathcal{T}_{\text{L,RH}}(\theta) \exp \left(-\frac{|z/\tilde{\tau} c_{\text{L}}|}{\sqrt{1 - \left(\frac{c_{\text{L}}}{v_{\text{T}}} \sin \theta\right)^2}} \right) + [\mathcal{T}_{\text{RH,RH}}(\theta) + \mathcal{T}_{\text{LH,RH}}(\theta)] \exp \left(-\frac{|z/\tilde{\tau} c_{\text{T}}|}{\sqrt{1 - \left(\frac{c_{\text{T}}}{v_{\text{T}}} \sin \theta\right)^2}} \right) \right\}. \quad (122b)$$

The TAM density is also derived by using a constitutive

equation

$$\ell_z^{\text{TAM}}(z) = \begin{cases} \ell_0 - \tau \frac{\partial J_z^{\text{TAM}}}{\partial z} & z < 0 \\ -\tilde{\tau} \frac{\partial J_z^{\text{TAM}}}{\partial z} & z > 0 \end{cases}. \quad (123)$$

It is worth noting that the OAM density and flux addressed here, polarized normal to the interface, is independent of the choice of origin. This is related to the absence of heat current perpendicular to the thermal gradient in isotropic media; the statistical average of wavevector component parallel to the interface \mathbf{k}_{\parallel} over phonon states vanishes when $\partial T/\partial z$ is applied to the CC. It follows that the statistical average of additional OAM $(\Delta\mathbf{r}_O \times \hbar\mathbf{k}_{\parallel})_z$ with constant shift of the origin $\Delta\mathbf{r}_O$ disappears. The z -component of the OAM density is thus a well-defined quantity invariant under the translation. The OAM flux polarized in the z -direction is also shown to be invariant under the translation of the coordinate system [72].

Figure 5(a) shows spatial profile of the OAM density (TAM density) and OAM flux (TAM flux) as green dotted curves (blue solid curves). As we assumed, both OAM density and flux are localized around the interface $z = 0$. We notice that in the quartz/lead junction, the density and flux of the diffused OAM partially exceed those of the diffused SAM. Therefore, not only the SAM but also the OAM could be important in the interfacial transport of phonon AM.

It is also read from Fig. 5(a) that a SAM flux or OAM flux alone is discontinuous at the interface, but their sum, TAM flux, is continuous at the interface. The continuity of the TAM flux at $z = 0$ is also derived analytically:

$$\begin{aligned} & \frac{J_z^{\text{TAM}}(z = -0) - J_z^{\text{TAM}}(z = +0)}{\frac{3}{2}\alpha v_T \frac{\partial T}{\partial z}} \\ &= E i_5(0) - \int_0^{\pi/2} d\theta \sin\theta \cos^3\theta [\mathcal{R}_{L,RH} + \mathcal{R}_{RH,RH} \\ & \quad + \mathcal{R}_{LH,RH} + \mathcal{T}_{L,RH} + \mathcal{T}_{RH,RH} + \mathcal{T}_{LH,RH}] \quad (124) \\ &= 0. \quad (125) \end{aligned}$$

We used the energy conservation law (15) in the last line.

VIII. DISCUSSION AND SUMMARY

We have elaborated on the interfacial transport of angular momentum (AM) mediated by acoustic phonon on the basis of both elastic theory and Boltzmann formalism. In particular, we have built a theoretical framework for (i) the boundary condition for phonon distribution functions at smooth, flat interfaces, (ii) the spatial profile of phonon AM diffusion in junction systems, and (iii) the total AM conservation at the interface (see also Fig. 2).

Let us summarize each section. We have first addressed acoustic analog of the Imbert–Fedorov shift in Sect. III. By considering scatterings experienced by each plane wave component in the beam, we have derived the transverse shift. This allows us to correctly describe the redistribution of the AM flux from incident waves into reflected/transmitted waves.

In Sect. IV we have derived the boundary condition for phonon distribution functions at the smooth, flat interface. Our derivation is based on a comparison of the

energy flux carried by wave packets and by monochromatic plane waves. The S -matrix for elastic waves then turns into a restriction to the physical Fock space of the junction after the quantization. By taking the trace in the restricted Fock space, we have finally obtained the boundary condition for the reduced density matrices and for the distribution functions. The boundary condition for the reduced density matrices would be important if we rigorously analyze the interfacial transport between degenerate phonon bands, as an analogue of spin mixing conductance in electron spintronics [73, 74].

In Sect. V and VI we have described the diffusion of spin angular momentum (SAM), stemming from the circular polarization of phonon, across the interface in the chiral–achiral crystal junction. We have shown that the SAM diffuses through the interface even without a heat flow normal to the interface. Furthermore, the injected SAM polarized normal to the interface can be amplified in the vicinity of the interface when we use crystals with relatively low velocities as the achiral crystal.

In the latest section (Sect. VII) we have introduced the extrinsic orbital angular momentum (OAM) of phonon, assuming that the phonon reflected/transmitted at the interface also experiences the transverse shift addressed in Sect. III. We have demonstrated that the sum of the SAM and OAM polarized normal to the interface is continuous at the interface.

The boundary condition provided here [see Eqs. (68) and (87)] will be helpful to explain phonon drag effect across interfaces [75, 76]. We expect that our boundary condition is quantitatively valid at a sufficiently low temperature of about 1 K, where phonons are less scattered [37].

Finally, we discuss an issue how to detect the phonon spin we have considered so far. Although we have neglected all the effects of electrons in the present paper, we expect that in heavy metals with strong spin–orbit interaction, there exist mechanisms by which a part of the phonon spin is converted into the electron spin. For example, the phonon spin in the metals will be transferred to the itinerant-electron spin via a spin–orbit coupling under the potential of bond-bending forces [77, 78], which are non-central forces that break the AM conservation of the lattice. We will not go into the details here, but these mechanisms in the bulk will convert a phonon SAM flux into an electron spin current, which will be detected electrically by the inverse spin Hall effect.

Ohe et al. have recently detected the inverse spin Hall voltage induced at a platinum or a tungsten electrode adjacent to an α -quartz subject to a thermal gradient [30]. Here the α -quartz and electrodes play the roles of the CC and ACC, respectively. As can be read from Figs. 5, the phonon SAM generated in the α -quartz will diffuse into the heavy-metal electrodes. We thus expect that the observed inverse spin Hall voltage results from the phonon spin diffused into the bulk of the heavy metal. Together with a study of spin conversion at the interface [34], the spin conversion mechanism in the bulk proposed above

will explain this experiment.

ACKNOWLEDGMENTS

We wish to thank M. Kato, H. Matsuura, S. Murakami, E. Saitoh, H. Shishido, J. Kishine, Y. Togawa, and H. Kusunose for helpful discussions. In particular, J. Kishine for information on earlier phonon angular momentum studies, H. Matsuura for communication on

boundary condition and interfacial phonon drag [75, 76], and S. Murakami for his comments on total angular momentum conservation at the interface. This work was supported by JSPS KAKENHI Grants No. JP20K03855, No. JP21H01032, No. JP22KJ0856, No. JP23K13056, No. JP23K03333, and No. 24KJ1036 and JST CREST Grant No. JPMJCR19T2. This research was also supported by Joint Research by the Institute for Molecular Science (IMS program No. 23IMS1101). This research was also supported by the grant of OML Project by the National Institutes of Natural Sciences (NINS program No. OML012301).

-
- [1] D. L. Portigal and E. Burstein, *Phys. Rev.* **170**, 673 (1968).
- [2] L. Zhang and Q. Niu, *Phys. Rev. Lett.* **112**, 085503 (2014).
- [3] L. Zhang and Q. Niu, *Phys. Rev. Lett.* **115**, 115502 (2015).
- [4] J. Kishine, A. S. Ovchinnikov, and A. A. Tereshchenko, *Phys. Rev. Lett.* **125**, 245302 (2020).
- [5] A. S. Pine, *Phys. Rev. B* **2**, 2049 (1970).
- [6] S.-Y. Chen, C. Zheng, M. S. Fuhrer, and J. Yan, *Nano Lett.* **15**, 2526 (2015).
- [7] H. Zhu, J. Yi, M.-Y. Li, J. Xiao, L. Zhang, C.-W. Yang, R. A. Kaindl, L.-J. Li, Y. Wang, and X. Zhang, *Science* **359**, 579 (2018).
- [8] Y. Chen, J. L. G. Schneider, M. F. Groß, K. Wang, S. Kalt, P. Scott, M. Kadic, and M. Wegener, *Adv. Funct. Mater.* **34**, 2302699 (2024).
- [9] M. Hamada, E. Minamitani, M. Hirayama, and S. Murakami, *Phys. Rev. Lett.* **121**, 175301 (2018).
- [10] M. Hamada and S. Murakami, *Phys. Rev. B* **101**, 144306 (2020).
- [11] S. Park and B.-J. Yang, *Nano Lett.* **20**, 7694 (2020).
- [12] H. Zhang, C. Xu, C. Carnahan, M. Sretenovic, N. Suri, D. Xiao, and X. Ke, *Phys. Rev. Lett.* **127**, 247202 (2021).
- [13] H. Chen, W. Wu, J. Zhu, Z. Yang, W. Gong, W. Gao, S. A. Yang, and L. Zhang, *Nano Lett.* **22**, 1688 (2022).
- [14] D. Yao and S. Murakami, *Phys. Rev. B* **105**, 184412 (2022).
- [15] C. P. Romao, R. Catena, N. A. Spaldin, and M. Matas, *Phys. Rev. Res.* **5**, 043262 (2023).
- [16] S. V. Vonsovskii and M. S. Svirskii, *Fiz. Tverd. Tela* **3**, 2160 (1961), [*Sov. Phys. Solid State* **3**, 7 (1962)].
- [17] A. D. Levine, *Nuovo Cimento* **26**, 190 (1962).
- [18] T. Ishii, *Bussei-Kenkyu* **23**, 217 (1975).
- [19] A. McLellan, *J. Phys. C: Solid State Phys.* **21**, 1177 (1988).
- [20] T. Zhang and S. Murakami, *Phys. Rev. Res.* **4**, L012024 (2022).
- [21] K. Ishito, H. Mao, Y. Kousaka, Y. Togawa, S. Iwasaki, T. Zhang, S. Murakami, J.-i. Kishine, and T. Satoh, *Nat. Phys.* **19**, 35 (2023).
- [22] K. Ishito, H. Mao, K. Kobayashi, Y. Kousaka, Y. Togawa, H. Kusunose, J. Kishine, and T. Satoh, *Chirality* **35**, 338 (2023).
- [23] E. Oishi, Y. Fujii, and A. Koreeda, *Phys. Rev. B* **109**, 104306 (2024).
- [24] A. Kato and J.-i. Kishine, *J. Phys. Soc. Jpn.* **92**, 075002 (2023).
- [25] V. L. Korenev, M. Salewski, I. A. Akimov, V. F. Sapega, L. Langer, I. V. Kalitukha, J. Debus, R. I. Dzhiyev, D. R. Yakovlev, D. Müller, C. Schröder, H. Hövel, G. Karzewski, M. Wiater, T. Wojtowicz, Y. G. Kusrayev, and M. Bayer, *Nat. Phys.* **12**, 85 (2016).
- [26] J. Holanda, D. Maior, A. Azevedo, and S. Rezende, *Nat. Phys.* **14**, 500 (2018).
- [27] R. Sasaki, Y. Nii, and Y. Onose, *Nat. Commun.* **12**, 2599 (2021).
- [28] S. G. Jeong, J. Kim, A. Seo, S. Park, H. Y. Jeong, Y.-M. Kim, V. Lauter, T. Egami, J. H. Han, and W. S. Choi, *Science Advances* **8**, 4 (2022).
- [29] K. Kim, E. Vetter, L. Yan, C. Yang, Z. Wang, R. Sun, Y. Yang, A. H. Comstock, X. Li, J. Zhou, L. Zhang, W. You, D. Sun, and J. Liu, *Nat. Mater.* **22**, 322 (2023).
- [30] K. Ohe, H. Shishido, M. Kato, S. Utsumi, H. Matsuura, and Y. Togawa, *Phys. Rev. Lett.* **132**, 056302 (2024).
- [31] M. Hamada and S. Murakami, *Phys. Rev. Res.* **2**, 023275 (2020).
- [32] J. Fransson, *Phys. Rev. Res.* **5**, L022039 (2023).
- [33] D. Yao and S. Murakami, *J. Phys. Soc. Jpn.* **93**, 034708 (2024).
- [34] T. Funato, M. Matsuo, and T. Kato, *Phys. Rev. Lett.* **132**, 236201 (2024).
- [35] W. A. Little, *Can. J. Phys.* **37**, 334 (1959).
- [36] I. M. Khalatnikov, *An Introduction to the Theory of Superfluidity*, Frontiers in Physics (W.A. Benjamin, New York, 1965) translated by P.C. Hohenberg.
- [37] E. T. Swartz and R. O. Pohl, *Rev. Mod. Phys.* **61**, 605 (1989).
- [38] K. Y. Bliokh and V. D. Freilikher, *Phys. Rev. B* **74**, 174302 (2006).
- [39] D. A. Garanin and E. M. Chudnovsky, *Phys. Rev. B* **92**, 024421 (2015).
- [40] J. J. Nakane and H. Kohnno, *Phys. Rev. B* **97**, 174403 (2018).
- [41] B. T. Hefner and P. L. Marston, *J. Acoust. Soc. Am.* **106**, 3313 (1999).
- [42] J.-L. Thomas and R. Marchiano, *Phys. Rev. Lett.* **91**, 244302 (2003).
- [43] M. K. Ayub, S. Ali, and J. T. Mendonca, *Phys. Plasmas* **18**, 102117 (2011).
- [44] W. Wang, Y. Tan, B. Liang, G. Ma, S. Wang, and J. Cheng, *Phys. Rev. B* **104**, 174301 (2021).

- [45] F. I. Fedorov, *J. Opt.* **15**, 014002 (2013), [Dokl. Akad. Nauk SSSR **105** 465 (1955)].
- [46] H. Schilling, *Ann. Phys.* **16**, 122 (1965).
- [47] C. Imbert, *Phys. Rev. D* **5**, 787 (1972).
- [48] M. Onoda, S. Murakami, and N. Nagaosa, *Phys. Rev. Lett.* **93**, 083901 (2004).
- [49] See Supplemental Material at [url] for supporting information—behavior of the power reflectance/transmittance for elastic waves, and the spatial profile of phonon energy transport in the case of thermal boundary resistance and when thermal gradient is applied to only one side of the junction.
- [50] L. D. Landau, E. M. Lifshitz, J. B. Sykes, W. H. Reid, A. M. Kosevich, and L. P. Pitaevskii, *Theory of Elasticity*, 3rd ed., Course of Theoretical Physics, Vol. 7 (Butterworth-Heinemann, Oxford, UK, 1995).
- [51] A. Sommerfeld, *Mechanics of Deformable Bodies*, Lectures on Theoretical Physics, Vol. 2 (Academic Press, New York, 1964).
- [52] C. G. Knott, *Lond. Edinb. Dubl. Phil. Mag.* **48**, 64 (1899).
- [53] K. Zieppitz, *Nachrichten von der Gesellschaft der Wissenschaften zu Göttingen, Mathematisch-Physikalische Klasse* **1**, 66 (1919).
- [54] W. Ewing, W. S. Jardetzky, and F. Press, *Elastic Waves in Layered Media*, Lamont Geological Observatory Contribution No. 189 (McGraw-Hill, New York, 1957).
- [55] J. L. Synge, *Proc. Roy. Irish Acad.* **58**, 13 (1956).
- [56] K. Y. Bliokh and A. Aiello, *J. Opt.* **15**, 014001 (2013).
- [57] A. Schoch, *Schallreflexion, Schallbrechung und Schallbeugung*, Ergebnisse der exakten Naturwissenschaften, Vol. 23 (Springer, Heidelberg, 1950) pp. 127–234, Chapter 20.
- [58] F. Goos and H. Hänchen, *Ann. Phys.* **1**, 333 (1947).
- [59] M. I. D'yakonov and V. I. Perel', *ZhETF Pis. Red.* **13**, 657 (1971), [*JETP Lett.* **13**, 467 (1971)].
- [60] S. Murakami, N. Nagaosa, and S.-C. Zhang, *Science* **301**, 1348 (2003).
- [61] J. Sinova, D. Culcer, Q. Niu, N. A. Sinitsyn, T. Jungwirth, and A. H. MacDonald, *Phys. Rev. Lett.* **92**, 126603 (2004).
- [62] W. Ledermann, *Proc. R. Soc. Lond. A* **182**, 362 (1944).
- [63] R. E. Peierls, *Quantum Theory of Solids*, International Series of Monographs on Physics (Clarendon Press, Oxford, UK, 1955).
- [64] J. Zhong, H. Sun, Y. Pan, Z. Wang, X. Xu, L. Zhang, and J. Zhou, *Phys. Rev. B* **107**, 125147 (2023).
- [65] A. J. Minnich, G. Chen, S. Mansoor, and B. S. Yilbas, *Phys. Rev. B* **84**, 235207 (2011).
- [66] C. Hua, *Exploring Thermal Phonon Transport from Atomic to Macroscopic Scales for Energy Conversion and Management*, PhD Thesis, California Institute of Technology (2016).
- [67] J. M. Ziman, *Electrons and Phonons: the Theory of Transport Phenomena in Solids*, International Series of Monographs on Physics (Clarendon Press, Oxford, UK, 1960) Chapter 11.
- [68] G. Kluge and G. Scholz, *Acta Acust. United Ac.* **16**, 60 (1965).
- [69] J. Joffrin and A. Levelut, *Solid State Commun.* **8**, 1573 (1970).
- [70] A. S. Pine, *J. Acoust. Soc. Am.* **49**, 1026 (1971).
- [71] H. Tsunetsugu and H. Kusunose, *J. Phys. Soc. Jpn.* **92**, 023601 (2023).
- [72] The same argument shows that, in a crystal under an external thermal gradient, the phonon OAM density stemming from the interfacial scattering is well-defined only if its polarization is parallel to the thermal gradient. Furthermore, by using the constitutive equation, the OAM flux flowing through the interface is well-defined only if its polarization is parallel to the thermal gradient. For this reason, we did not discuss the conservation of the OAM polarized normal to the interface for the case when the thermal gradient is applied in the direction parallel to the interface [see also Fig. 5(b)].
- [73] Y. Tserkovnyak, A. Brataas, and G. E. Bauer, *Phys. Rev. Lett.* **88**, 117601 (2002).
- [74] Y. Tserkovnyak, A. Brataas, G. E. W. Bauer, and B. I. Halperin, *Rev. Mod. Phys.* **77**, 1375 (2005).
- [75] G. Wang, L. Endicott, H. Chi, P. Lošt'ák, and C. Uher, *Phys. Rev. Lett.* **111**, 046803 (2013).
- [76] M. Kimura, X. He, T. Katase, T. Tadano, J. M. Tomczak, M. Minohara, R. Aso, H. Yoshida, K. Ide, S. Ueda, H. Hiramatsu, H. Kumigashira, H. Hosono, and T. Kamiya, *Nano Lett.* **21**, 9240 (2021).
- [77] P. N. Keating, *Phys. Rev.* **145**, 637 (1966).
- [78] R. M. Martin, *Phys. Rev. B* **1**, 4005 (1970).

Supplemental Materials for:

Theory of phonon angular momentum transport across smooth interfaces between crystals

S1. EXAMPLES OF POWER REFLECTANCE/TRANSMITTANCE FOR ELASTIC WAVES

In the main text we defined power reflectance/transmittance for elastic waves \mathcal{R}_{nm} , \mathcal{R}'_{nm} , \mathcal{T}_{nm} , and \mathcal{T}'_{nm} . For some sets of velocities and acoustic impedances, we have plotted their behavior with respect to the angle of incidence in Figs. S1 and S2. Here the reflectance/transmittance by using the angle of incidence are denoted by $\mathcal{R}_{nm}(\omega, \mathbf{k}_{\parallel}) = \mathcal{R}_{nm}(\theta_m)$ and $\mathcal{T}_{nm}(\omega, \mathbf{k}_{\parallel}) = \mathcal{T}_{nm}(\theta_m)$ with $\sin \theta_m = v_m |\mathbf{k}_{\parallel}| / \omega$ or $\mathcal{R}'_{nm}(\omega, \mathbf{q}_{\parallel}) = \mathcal{R}'_{nm}(\Theta_m)$ and $\mathcal{T}'_{nm}(\omega, \mathbf{q}_{\parallel}) = \mathcal{T}'_{nm}(\Theta_m)$ with $\sin \Theta_m = c_m |\mathbf{q}_{\parallel}| / \omega$.

Note that the reflectance/transmittance satisfy two symmetries: one is a Helmholtz reciprocity $\mathcal{R}_{nm} = \mathcal{R}_{mn}$, $\mathcal{R}'_{nm} = \mathcal{R}'_{mn}$ and $\mathcal{T}_{nm} = \mathcal{T}'_{mn}$; the other is an invariance of \mathcal{R}_{nm} , \mathcal{R}'_{nm} , \mathcal{T}_{nm} and \mathcal{T}'_{nm} under a replacement of subscripts n, m from (L, RH, LH) into (L, LH, RH). In order to prevent duplication of the same figure brought on by the latter symmetry, we omit the cases of reflection/transmission between LH modes in Fig. S1 as well as the cases of reflection/transmission between L and LH modes in Fig. S2. We can also read the former symmetry, the Helmholtz reciprocity, from Fig. S2 if we compare the curves with the same color in the first and second columns

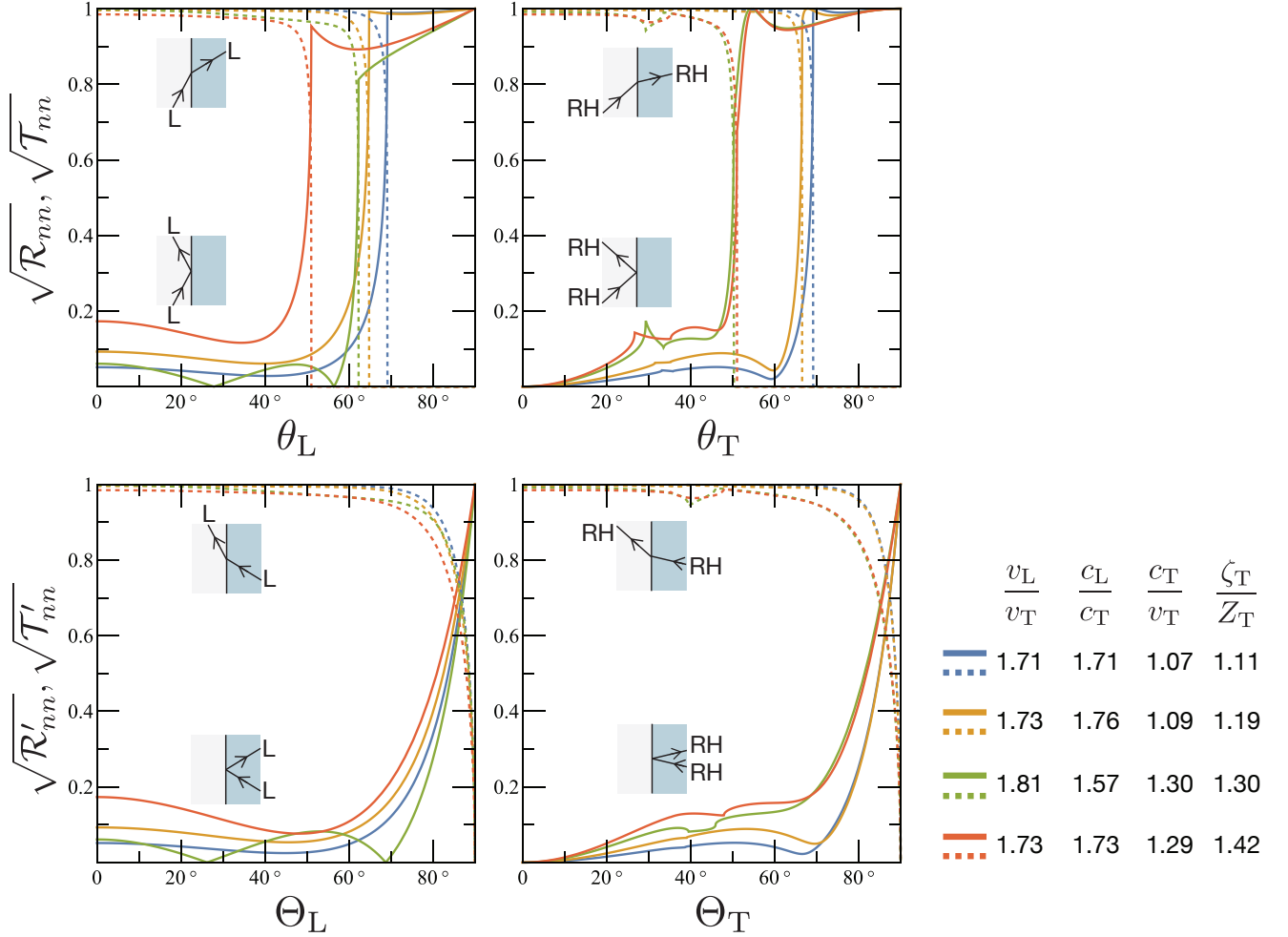


FIG. S1. Square roots of reflected/transmitted energy flow divided by incident energy flow if no change in elastic wave modes occurs. The wave modes here consist of longitudinal (L) and right-handed (RH)/left-handed (LH) circularly polarized transverse modes.

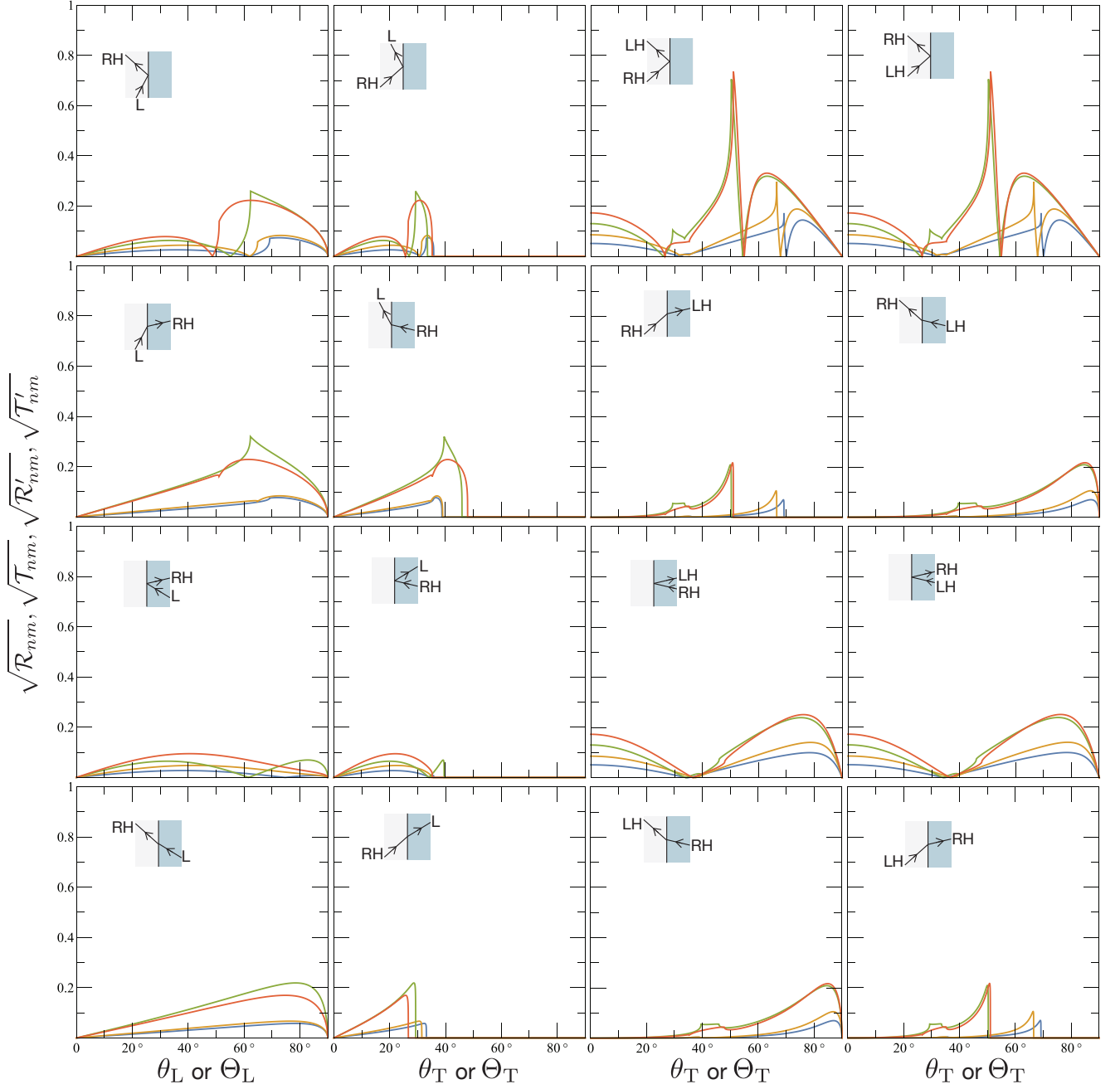


FIG. S2. Square roots of reflected/transmitted energy flow divided by incident energy flow if incident and reflected/transmitted waves are of different mode. The wave modes here consist of longitudinal (L) and right-handed (RH)/left-handed (LH) circularly polarized transverse modes. Parameters for each colored curve are the same as Fig. S1.

or the third and fourth columns, properly converting their angles of incidence according to Snell's law.

S2. ENERGY DIFFUSION FROM CHIRAL CRYSTAL SUBJECT TO THERMAL GRADIENT

Instead of the phonon angular momentum transport examined in the main text, we here explore spatial diffusion of energy in the chiral crystal (CC)–achiral crystal (ACC) junction, generated by the thermal gradient ∇T solely applied within the CC. We only consider the case when ∇T is parallel to the interface normal (z -axis). This is because rotational symmetry of the junction around the z -axis forbids the energy flux normal to the interface when

$\partial T/\partial z = 0$ in the linear response region. For the same reason, the spatial modulation of energy density in the z -direction is forbidden when ∇T is applied parallel to the interface. We thus safely focus on the case $\nabla T \parallel \mathbf{z}$.

First, let us remind ourselves about a constitutive equation between the energy density and energy flux, derived from the Boltzmann equation. The energy density without zero-point energy contributions \mathbf{u} and the energy flux normal to the interface J^u are written as

$$\mathbf{u}(z) \equiv \begin{cases} \frac{1}{V} \sum_{\mathbf{k},n} \hbar\Omega_{\mathbf{k}n} F_{\mathbf{k}n}(z) & z < 0 \\ \frac{1}{\tilde{V}} \sum_{\mathbf{q},n} \hbar\omega_{\mathbf{q}n} f_{\mathbf{q}n}(z) & z > 0 \end{cases}, \quad J^u(z) \equiv \begin{cases} \frac{1}{V} \sum_{\mathbf{k},n} \hbar\Omega_{\mathbf{k}n} v_{\mathbf{k}n}^z F_{\mathbf{k}n}(z) & z < 0 \\ \frac{1}{\tilde{V}} \sum_{\mathbf{q},n} \hbar\omega_{\mathbf{q}n} c_{\mathbf{q}n}^z f_{\mathbf{q}n}(z) & z > 0 \end{cases}, \quad (\text{S1})$$

while the distribution functions $F_{\mathbf{k}n}$ and $f_{\mathbf{q}n}$ follow the Boltzmann equation for each crystal

$$v_{\mathbf{k}n}^z \frac{\partial F_{\mathbf{k}n}^{(1)}}{\partial z} + \mathbf{v}_{\mathbf{k}n} \cdot \nabla T \frac{\partial F_{\mathbf{k}n}^{(0)}}{\partial T} = -\frac{F_{\mathbf{k}n}^{(1)}}{\tau} \quad (z < 0), \quad (\text{S2a})$$

$$c_{\mathbf{q}n}^z \frac{\partial f_{\mathbf{q}n}^{(1)}}{\partial z} = -\frac{f_{\mathbf{q}n}^{(1)}}{\tilde{\tau}} \quad (z > 0). \quad (\text{S2b})$$

If we multiply energy $\hbar\Omega_{\mathbf{k}n}$ or $\hbar\omega_{\mathbf{q}n}$ by both sides of the Boltzmann equation and sum up for states (\mathbf{k}, n) or (\mathbf{q}, n) , we obtain the following relations:

$$\frac{\partial}{\partial z} \left(\frac{1}{V} \sum_{\mathbf{k},n} \hbar\Omega_{\mathbf{k}n} v_{\mathbf{k}n}^z F_{\mathbf{k}n}^{(1)} \right) + \nabla T \cdot \underbrace{\frac{\partial}{\partial T} \left(\frac{1}{V} \sum_{\mathbf{k},n} \hbar\Omega_{\mathbf{k}n} \mathbf{v}_{\mathbf{k}n} F_{\mathbf{k}n}^{(0)} \right)}_0 = -\frac{1}{\tau} \left(\frac{1}{V} \sum_{\mathbf{k},n} \hbar\Omega_{\mathbf{k}n} F_{\mathbf{k}n}^{(1)} \right), \quad (\text{S3a})$$

$$\frac{\partial}{\partial z} \left(\frac{1}{\tilde{V}} \sum_{\mathbf{q},n} \hbar\omega_{\mathbf{q}n} v_{\mathbf{q}n}^z f_{\mathbf{q}n}^{(1)} \right) = -\frac{1}{\tilde{\tau}} \left(\frac{1}{\tilde{V}} \sum_{\mathbf{q},n} \hbar\omega_{\mathbf{q}n} f_{\mathbf{q}n}^{(1)} \right). \quad (\text{S3b})$$

As there is no energy flux in equilibrium, the term proportional to ∇T vanishes. We thus obtain the constitutive equation

$$\Delta \mathbf{u} = \begin{cases} \mathbf{u} - \mathbf{u}_{<0}^{\text{eq}} = -\tau \frac{\partial J^u}{\partial z} & z < 0 \\ \mathbf{u} - \mathbf{u}_{>0}^{\text{eq}} = -\tilde{\tau} \frac{\partial J^u}{\partial z} & z > 0 \end{cases}, \quad (\text{S4})$$

which represents a balance between the sink of the energy flow and energy dissipation. The bulk equilibrium energy density in each crystal $\mathbf{u}_{<0}^{\text{eq}}$ or $\mathbf{u}_{>0}^{\text{eq}}$ is given as

$$\mathbf{u}_{<0}^{\text{eq}} = \sum_n \int \frac{d^3 \mathbf{k}}{(2\pi)^3} \frac{\hbar\Omega_{\mathbf{k}n}}{e^{\hbar\Omega_{\mathbf{k}n}/k_B T} - 1} \simeq \frac{4\pi}{(2\pi)^3} k_B T \sum_n \left(\frac{k_B T}{\hbar v_n} \right)^3 \int_0^\infty \frac{w^3 dw}{e^w - 1} = \frac{C_V(T)}{V} \cdot \frac{T}{4}, \quad (\text{S5})$$

$$\mathbf{u}_{>0}^{\text{eq}} \simeq \frac{\tilde{C}_V(T)}{\tilde{V}} \cdot \frac{T}{4} \quad (\text{S6})$$

in low-temperature limit. Here specific heat follows the Debye T^3 law

$$C_V(T) = \frac{12\pi^4}{5} N \left(\frac{T}{\Theta_D} \right)^3 k_B, \quad \tilde{C}_V(T) = \frac{12\pi^4}{5} \tilde{N} \left(\frac{T}{\tilde{\Theta}_D} \right)^3 k_B \quad (\text{S7})$$

with number of unit cells N , \tilde{N} and the Debye temperature Θ_D , $\tilde{\Theta}_D$ for the CC and ACC, respectively. As the constitutive equation (S4) allows us to derive $\mathbf{u}(z)$ as a spatial derivative of $J^u(z)$, we now focus on the spatial distribution of the energy flux $J^u(z)$.

In the CC ($z < 0$), the energy flux has three components:

$$J^u(z < 0) = \frac{1}{V} \sum_{\mathbf{k},n} \hbar\Omega_{\mathbf{k}n} v_{\mathbf{k}n}^z F_{\mathbf{k}n}^{(1)} = J_0^u + J_1^u(z) + J_2^u(z) \quad (\text{S8})$$

with

$$J_0^u \equiv \sum_n \int \frac{d^3 \mathbf{k}}{(2\pi)^3} \hbar \Omega_{\mathbf{k}n} v_n \cos \theta \cdot B_{\mathbf{k}n}, \quad (\text{S9a})$$

$$J_1^u(z) \equiv - \sum_n \int_{k_z < 0} \frac{d^3 \mathbf{k}}{(2\pi)^3} \hbar \Omega_{\mathbf{k}n} v_n \cos \theta B_{\mathbf{k}n} \exp \left[\frac{|z/\tau v_n|}{\cos \theta} \right], \quad (\text{S9b})$$

$$J_2^u(z) \equiv \sum_n \int_{k_z < 0} \frac{d^3 \mathbf{k}}{(2\pi)^3} \hbar \Omega_{\mathbf{k}n} v_n \cos \theta \cdot \exp \left[\frac{|z/\tau v_n|}{\cos \theta} \right] \sum_m \mathcal{R}_{nm}(\Omega_{\mathbf{k}n}, \mathbf{k}_{\parallel}) B_{+,m}(\Omega_{\mathbf{k}n}, \mathbf{k}_{\parallel}). \quad (\text{S9c})$$

In the following calculations, we neglect the small band splitting of transverse modes RH and LH, since J_0^u , J_1^u , J_2^u are finite even in the absence of the splitting.

The bulk energy flux J_0^u is generated only in the direction parallel to the thermal gradient

$$J_0^u \simeq \frac{4\pi}{(2\pi)^3} \cdot \frac{-\tau \hbar}{3} \frac{1}{T} \frac{\partial T}{\partial z} \sum_n v_n^3 \left(\frac{k_B T}{\hbar v_n} \right)^4 \int_0^\infty dw \frac{w^4 e^w}{(e^w - 1)^2} = \frac{2\pi^2}{45} \tau \left(\frac{k_B T}{\hbar} \right)^3 k_B \left(-\frac{\partial T}{\partial z} \right) \sum_n \frac{1}{v_n} = \kappa \left(-\frac{\partial T}{\partial z} \right) \quad (\text{S10})$$

with a well-known thermal conductivity formula

$$\kappa = \frac{1}{3} \cdot \frac{C_V}{V} \tau \cdot \frac{\frac{1}{v_L} + \frac{2}{v_T}}{\frac{1}{v_L^3} + \frac{2}{v_T^3}}. \quad (\text{S11})$$

The second term $J_1^u(z)$ describes decrease of the energy flux in the vicinity of the interface, irrespective of the effect of reflections. This term is also generated only in the direction parallel to the thermal gradient:

$$J_1^u(z) \simeq \frac{4\pi}{(2\pi)^3} \frac{\tau \hbar}{T} \frac{\partial T}{\partial z} \sum_n v_n^3 \left(\frac{k_B T}{\hbar v_n} \right)^4 \int_0^\infty dw \frac{w^4 e^w}{(e^w - 1)^2} \int_{-1}^0 \frac{d(\cos \theta)}{2} \cos^2 \theta \exp \left[\frac{|z/\tau v_n|}{\cos \theta} \right] \quad (\text{S12})$$

$$= \frac{\kappa}{2} \frac{\frac{3Ei_4(|z/\tau v_L|)}{v_L} + \frac{6Ei_4(|z/\tau v_T|)}{v_T}}{\frac{1}{v_L} + \frac{2}{v_T}} \frac{\partial T}{\partial z} \quad (\text{S13})$$

where we introduced $Ei_n(w)$, a kind of exponential integral, defined by

$$Ei_n(w) \equiv \int_1^\infty \frac{e^{-wt}}{t^n} dt, \quad \text{Re } w > 0. \quad (\text{S14})$$

The third term $J_2^u(z)$ involves the reflectance at the interface. We first replace the variable in the integral with the incident wavevector \mathbf{k}' from the reflected wavevector \mathbf{k}

$$J_2^u(z) = \sum_{n, m, k_z < 0} \int \frac{d\omega d^2 \mathbf{k}_{\parallel}}{(2\pi)^3} \frac{\hbar \omega \cdot v_n \cos \theta}{|v_n \cos \theta|} \cdot \exp \left[\frac{|z/\tau v_n|}{\cos \theta} \right] \mathcal{R}_{nm}(\omega, \mathbf{k}_{\parallel}) B_{+,m}(\omega, \mathbf{k}_{\parallel}) \quad (\text{S15})$$

$$= - \sum_{n, m, k'_z > 0} \int \frac{d^3 \mathbf{k}'}{(2\pi)^3} \hbar \Omega_{\mathbf{k}'m} v_m \cos \theta' \cdot \exp \left[\frac{-|z/\tau v_n|}{\sqrt{1 - \left(\frac{v_n}{v_m} \sin \theta' \right)^2}} \right] \mathcal{R}_{nm}(\theta') B_{\mathbf{k}'m} \quad (\text{S16})$$

by using the property

$$d^3 \mathbf{k} = \frac{d\omega d^2 \mathbf{k}_{\parallel}}{|v_n \cos \theta|} = \left| \frac{v_m \cos \theta'}{v_n \cos \theta} \right| d^3 \mathbf{k}'. \quad (\text{S17})$$

Substitution of $B_{\mathbf{k}'n} = -\tau \mathbf{v}_{\mathbf{k}'n} \cdot \nabla T \frac{\partial F_{\mathbf{k}'n}^{(0)}}{\partial T}$ finally yields

$$J_2^u(z) = \kappa \left(\frac{1}{3} \sum_n \frac{1}{v_n} \right)^{-1} \sum_{n,m} \frac{1}{v_m} \int_0^1 \frac{d(\cos \theta)}{2} \mathcal{R}_{nm}(\theta) \cos^2 \theta \cdot \exp \left[\frac{-|z/\tau v_n|}{\sqrt{1 - \left(\frac{v_n}{v_m} \sin \theta \right)^2}} \right] \frac{\partial T}{\partial z}. \quad (\text{S18})$$

In the ACC, on the other hand, the energy flux is described as

$$J^u(z > 0) = \frac{1}{V} \sum_{\mathbf{q}, n} \hbar \omega_{\mathbf{q}n} c_{\mathbf{q}n}^z f_{\mathbf{q}n}^{(1)} \quad (\text{S19})$$

$$= \sum_n \int_{q_z > 0} \frac{d^3 \mathbf{q}}{(2\pi)^3} \hbar \omega_{\mathbf{q}n} c_n \cos \Theta \cdot D_{\mathbf{q}n} \exp \left[-\frac{|z/\tilde{\tau} c_n|}{\cos \Theta} \right] \quad (\text{S20})$$

$$= \sum_n \int_{q_z > 0} \frac{d\omega d^2 \mathbf{q}_{\parallel}}{(2\pi)^3} \hbar \omega \cdot \exp \left[-\frac{|z/\tilde{\tau} c_n|}{\cos \Theta} \right] \sum_m \mathcal{T}_{nm}(\omega, \mathbf{q}_{\parallel}) B_{+,m}(\omega, \mathbf{q}_{\parallel}) \quad (\text{S21})$$

$$= \sum_{n,m} \int_{k_z > 0} \frac{d^3 \mathbf{k}}{(2\pi)^3} \hbar v_m k \cdot v_m \cos \theta \cdot \exp \left[-\frac{|z/\tilde{\tau} c_n|}{\sqrt{1 - \left(\frac{c_n}{v_m} \sin \theta \right)^2}} \right] \mathcal{T}_{nm}(\theta) B_{\mathbf{k}m} \quad (\text{S22})$$

$$= \kappa \left(\frac{1}{3} \sum_n \frac{1}{v_n} \right)^{-1} \sum_{n,m} \frac{1}{v_m} \int_0^1 \frac{d(\cos \theta)}{2} \cos^2 \theta \cdot \mathcal{T}_{nm}(\theta) \cdot \exp \left[-\frac{|z/\tilde{\tau} c_n|}{\sqrt{1 - \left(\frac{c_n}{v_m} \sin \theta \right)^2}} \right] \left(-\frac{\partial T}{\partial z} \right). \quad (\text{S23})$$

We have plotted spatial distributions of the energy flux for some interfaces as blue dashed curves in Fig. S3(a). It is worth noting that continuity of the energy flux holds even at the interface, since $\sum_n (\mathcal{R}_{nm}(\theta) + \mathcal{T}_{nm}(\theta)) = 1$:

$$\begin{aligned} & J^u(z = -0) - J^u(z = +0) \\ &= \kappa \left(-\frac{\partial T}{\partial z} \right) \left[\frac{1}{2} - \left(\frac{1}{3} \sum_n \frac{1}{v_n} \right)^{-1} \sum_m \frac{1}{v_m} \int_0^1 \frac{d(\cos \theta)}{2} \cos^2 \theta \sum_n (\mathcal{R}_{nm}(\theta) + \mathcal{T}_{nm}(\theta)) \right] = 0. \end{aligned} \quad (\text{S24})$$

Finally, we derive the energy density $u(z)$ from the constitutive equation (S4). For differentiation of the exponential integrals, we use a relation $dEi_{n+1}(w)/dw = -Ei_n(w)$. It follows that

$$\begin{aligned} & u(z < 0) - u_{<0}^{\text{eq}} \\ &= \kappa \left(-\frac{\partial T}{\partial z} \right) \left\{ \frac{3}{4} \frac{\frac{2Ei_3(|z/\tau v_L|)}{v_L^2} + \frac{4Ei_3(|z/\tau v_T|)}{v_T^2}}{\frac{1}{v_L} + \frac{2}{v_T}} \right. \\ & \quad \left. + \left(\frac{1}{3} \sum_n \frac{1}{v_n} \right)^{-1} \sum_{n,m} \frac{1}{v_n v_m} \int_0^1 \frac{d(\cos \theta)}{2} \frac{\mathcal{R}_{nm}(\theta) \cos^2 \theta}{\sqrt{1 - \left(\frac{v_n}{v_m} \sin \theta \right)^2}} \cdot \exp \left[\frac{-|z/\tau v_n|}{\sqrt{1 - \left(\frac{v_n}{v_m} \sin \theta \right)^2}} \right] \right\}, \end{aligned} \quad (\text{S25})$$

$$\begin{aligned} & u(z > 0) - u_{>0}^{\text{eq}} \\ &= \kappa \left(-\frac{\partial T}{\partial z} \right) \left(\frac{1}{3} \sum_n \frac{1}{v_n} \right)^{-1} \sum_{n,m} \frac{1}{v_m c_n} \int_0^1 \frac{d(\cos \theta)}{2} \frac{\mathcal{T}_{nm}(\theta) \cos^2 \theta}{\sqrt{1 - \left(\frac{c_n}{v_m} \sin \theta \right)^2}} \cdot \exp \left[\frac{-|z/\tilde{\tau} c_n|}{\sqrt{1 - \left(\frac{c_n}{v_m} \sin \theta \right)^2}} \right]. \end{aligned} \quad (\text{S26})$$

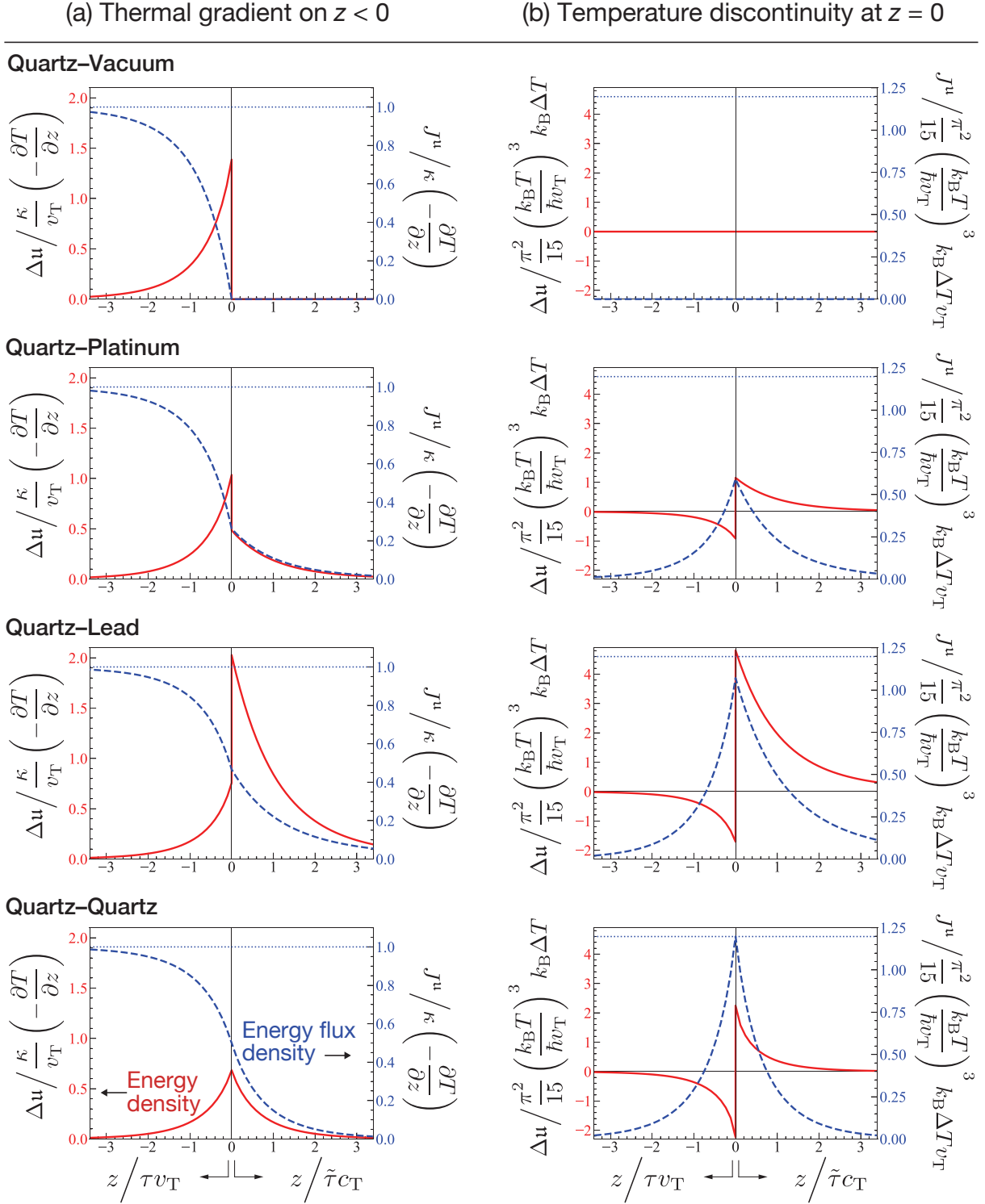


FIG. S3. Energy flux and energy density deviated from equilibrium (a) when a thermal gradient normal to the interface is applied on $z < 0$ or (b) when there is a difference in temperatures between adjacent two crystals. κ denotes the thermal conductivity. We set the parameters as $v_L/v_T = 1.59$ and [Quartz–Vacuum] $\zeta_T/Z_T = 0$, [Quartz–Platinum] $c_L/c_T = 2.25$, $c_T/v_T = 0.493$, and $\zeta_T/Z_T = 3.99$, [Quartz–Lead] $c_L/c_T = 2.84$, $c_T/v_T = 0.183$, and $\zeta_T/Z_T = 0.947$, [Quartz–Quartz] $c_L/v_T = 1.59$ and $c_T/v_T = \zeta_T/Z_T = 1$.

For some interfaces, we have depicted the spatial distribution of the energy density as red solid curves in Fig. S3(a). The energy flux is continuous at the interface but energy density is discontinuous. The exception is for interfaces between the same crystals; the phonon distribution functions of each mode at $z = \pm 0$ coincide in this case and every quantities are continuous at the interface.

S3. ENERGY DIFFUSION IN THE CASE OF THERMAL BOUNDARY RESISTANCE

Let us consider another situation when two crystals in contact have different temperatures and energy diffuses across the interface accordingly. In this case, the energy flow is measured by the thermal boundary resistance (also called the interfacial thermal resistance or Kapitza resistance). Since the theory of the energy flow at smooth, flat interface, known as acoustic mismatch model, is established by earlier studies [35–37], we can use this topic as a benchmark to check the validity of our boundary condition, given in the main text. We also aim to present the spatial profile of both energy density and energy flux from the bulk to the interface in the case of the thermal boundary resistance, since their spatial profile was overlooked by the earlier studies.

Suppose two semi-infinite crystals are in contact at a plane $z = 0$. The crystal in the left-hand side ($z < 0$) has a temperature T_1 in the bulk, while the crystal in the right-hand side ($z > 0$) has a lower temperature T_2 ($< T_1$) in the bulk. We assume that the drop of the temperature $\Delta T = T_1 - T_2$ is small compared to $T = (T_1 + T_2)/2$.

The phonon distribution function in the left-hand-side crystal $F_{\mathbf{k}n}(z)$ and that in the right-hand-side crystal $f_{\mathbf{q}n}(z)$ follow the Boltzmann equation with a constant relaxation time and without external fields. They have a stationary solution deviated from the Bose distribution function $f^{\text{eq}}(\omega, T) = [\exp(\hbar\omega/k_B T) - 1]^{-1}$, given as

$$F_{\mathbf{k}n} = f^{\text{eq}}(\Omega_{\mathbf{k}n}, T_1) + \begin{cases} C_{\mathbf{k}n} \exp\left[z/(-\tau v_{\mathbf{k}n}^z)\right] & v_{\mathbf{k}n}^z < 0 \\ 0 & v_{\mathbf{k}n}^z > 0 \end{cases}, \quad (\text{S27})$$

$$f_{\mathbf{q}n} = f^{\text{eq}}(\omega_{\mathbf{q}n}, T_2) + \begin{cases} 0 & c_{\mathbf{q}n}^z < 0 \\ D_{\mathbf{q}n} \exp\left[-z/\tilde{\tau} c_{\mathbf{q}n}^z\right] & c_{\mathbf{q}n}^z > 0 \end{cases} \quad (\text{S28})$$

with amplitudes of the deviation localized around the interface $C_{\mathbf{k}n}$, $D_{\mathbf{q}n}$ to be determined.

For distribution functions $F_{\mathbf{k}n}(z)$ and $f_{\mathbf{q}n}(z)$ satisfying $\Omega_{\mathbf{k}n} = \omega_{\mathbf{q}n}$ and $\mathbf{k}_{\parallel} = \mathbf{q}_{\parallel}$, our boundary condition yields the following linear relation:

$$\begin{cases} F_{-,n} = \sum_m [\mathcal{R}_{nm} F_{+,m} + \mathcal{T}'_{nm} f_{-,m}] \\ f_{+,n} = \sum_m [\mathcal{T}_{nm} F_{+,m} + \mathcal{R}'_{nm} f_{-,m}] \end{cases} \quad (\text{S29})$$

where we write $F_{\mathbf{k}n}(z = -0)$ and $f_{\mathbf{q}n}(z = +0)$ as

$$F_{\mathbf{k}n} = \begin{cases} F_{+,n}(\Omega_{\mathbf{k}n}, \mathbf{k}_{\parallel}) & v_{\mathbf{k}n}^z > 0 \\ F_{-,n}(\Omega_{\mathbf{k}n}, \mathbf{k}_{\parallel}) & v_{\mathbf{k}n}^z < 0 \end{cases}, \quad f_{\mathbf{q}n} = \begin{cases} f_{+,n}(\omega_{\mathbf{q}n}, \mathbf{q}_{\parallel}) & c_{\mathbf{q}n}^z > 0 \\ f_{-,n}(\omega_{\mathbf{q}n}, \mathbf{q}_{\parallel}) & c_{\mathbf{q}n}^z < 0 \end{cases} \quad (\text{S30})$$

with \mathbf{k}_{\parallel} and \mathbf{q}_{\parallel} wavevector components parallel to the interface.

Since sum of the reflectance and transmittance is unity, i.e., $\sum_m [\mathcal{R}_{nm} + \mathcal{T}'_{nm}] = 1$ and $\sum_m [\mathcal{T}_{nm} + \mathcal{R}'_{nm}] = 1$ hold, we obtain the amplitudes of the localized phonon distribution around the interface

$$\begin{cases} C_{-,n}(\omega, \mathbf{k}_{\parallel}) = \left[\sum_m \mathcal{T}'_{nm}(\omega, \mathbf{k}_{\parallel}) \right] \cdot [f^{\text{eq}}(\omega, T_2) - f^{\text{eq}}(\omega, T_1)] \\ D_{+,n}(\omega, \mathbf{q}_{\parallel}) = \left[\sum_m \mathcal{T}_{nm}(\omega, \mathbf{q}_{\parallel}) \right] \cdot [f^{\text{eq}}(\omega, T_1) - f^{\text{eq}}(\omega, T_2)] \end{cases}. \quad (\text{S31})$$

It follows from the Helmholtz reciprocity $\mathcal{T}_{nm} = \mathcal{T}'_{mn}$ that

$$\begin{cases} C_{\mathbf{k}n} = -\Delta T \cdot \frac{\partial f^{\text{eq}}(\hbar v_n k/k_B T)}{\partial T} \left[\sum_m \mathcal{T}_{mn}(\Omega_{\mathbf{k}n}, \mathbf{k}_{\parallel}) \right] & (k_z < 0) \\ D_{\mathbf{q}n} = \Delta T \cdot \frac{\partial f^{\text{eq}}(\hbar c_n q/k_B T)}{\partial T} \left[\sum_m \mathcal{T}'_{mn}(\omega_{\mathbf{q}n}, \mathbf{q}_{\parallel}) \right] & (q_z > 0) \end{cases}. \quad (\text{S32})$$

The energy flux is thus calculated as

$$J^u(z < 0) = \sum_n \int_{k_z < 0} \frac{d^3 \mathbf{k}}{(2\pi)^3} \hbar \Omega_{\mathbf{k}n} v_{\mathbf{k}n}^z C_{\mathbf{k}n} \exp \left[- \left| \frac{z}{\tau v_{\mathbf{k}n}^z} \right| \right] \quad (\text{S33})$$

$$= \frac{2\pi^2}{15} \frac{(k_B T)^3 k_B \Delta T}{\hbar^3} \sum_n \frac{1}{v_n^2} \int_0^1 \frac{d(\cos \theta)}{2} \cos \theta \exp \left[- \frac{|z/\tau v_n|}{\cos \theta} \right] \sum_m \mathcal{T}_{mn}(\theta) \quad (\text{S34})$$

in the left-hand side, while the energy flux in the right-hand side is

$$J^u(z > 0) = \sum_n \int_{q_z > 0} \frac{d^3 \mathbf{q}}{(2\pi)^3} \hbar \omega_{\mathbf{q}n} c_{\mathbf{q}n}^z D_{\mathbf{q}n} \exp \left[- \left| \frac{z}{\tilde{\tau} c_{\mathbf{q}n}^z} \right| \right] \quad (\text{S35})$$

$$= \frac{2\pi^2}{15} \frac{(k_B T)^3 k_B \Delta T}{\hbar^3} \sum_n \frac{1}{c_n^2} \int_0^1 \frac{d(\cos \Theta)}{2} \cos \Theta \exp \left[- \frac{|z/\tilde{\tau} c_n|}{\cos \Theta} \right] \sum_m \mathcal{T}'_{mn}(\Theta). \quad (\text{S36})$$

Spatial distributions of the energy flux for some interfaces are illustrated in Fig. S3(b) with blue dashed curves. It is worth noting that continuity of the energy flux holds even at the interface:

$$J^u(z = -0) / \frac{\pi^2}{15} \frac{(k_B T)^3 k_B \Delta T}{\hbar^3} = \sum_{n,m} \int_0^1 \frac{\cos \theta_n d(\cos \theta_n)}{v_n^2} \mathcal{T}_{mn}(\theta_n), \quad (\text{S37a})$$

$$J^u(z = +0) / \frac{\pi^2}{15} \frac{(k_B T)^3 k_B \Delta T}{\hbar^3} = \sum_{n,m} \int_0^1 \frac{\cos \Theta_m d(\cos \Theta_m)}{c_m^2} \mathcal{T}'_{nm}(\Theta_m). \quad (\text{S37b})$$

First, the Helmholtz reciprocity leads to $\mathcal{T}_{mn}(\theta_n) = \mathcal{T}'_{nm}(\Theta_m)$. Second, Snell's law provides $\sin \theta_n / v_n = \sin \Theta_m / c_m$. Third, for a small difference in the angles, Snell's law again provides $\cos \theta_n d\theta_n / v_n = \cos \Theta_m d\Theta_m / c_m$. The product of these three relations yields

$$\frac{\cos \theta_n d(\cos \theta_n)}{v_n^2} \mathcal{T}_{mn}(\theta_n) = \frac{\cos \Theta_m d(\cos \Theta_m)}{c_m^2} \mathcal{T}'_{nm}(\Theta_m). \quad (\text{S38})$$

We thus find the two expressions (S37) equivalent, i.e., $J^u(z = -0) = J^u(z = +0)$.

Let us write $1/\mathcal{V}^2$ to represent the right-hand sides of the two equations (S37). Then the thermal resistivity of the boundary is proportional to T^{-3} :

$$k_B \Delta T = \frac{15\mathcal{V}^2}{\pi^2} \left(\frac{\hbar}{k_B T} \right)^3 J^u(z = 0), \quad (\text{S39})$$

which leads to the appearance of a temperature jump at a boundary, whenever there is a flux of heat from one crystal to the other. The above equation (S39) agrees well with the result of the acoustic mismatch model [35, 36].

We also obtain the energy density deviated from equilibrium $\Delta u(z)$ as a spatial derivative of the energy flux, since the constitutive equation (S4) also holds in the case of the thermal boundary resistance:

$$\mathbf{u} - \mathbf{u}_{<0}^{\text{eq}} = - \frac{\pi^2}{15} \left(\frac{k_B T}{\hbar v_T} \right)^3 k_B \Delta T \sum_{n,m} \int_0^1 d(\cos \theta) \left(\frac{v_T}{v_n} \right)^3 \mathcal{T}_{mn}(\theta) \exp \left[- \frac{|z/\tau v_T|}{\cos \theta} \right], \quad (\text{S40a})$$

$$\mathbf{u} - \mathbf{u}_{>0}^{\text{eq}} = \frac{\pi^2}{15} \left(\frac{k_B T}{\hbar v_T} \right)^3 k_B \Delta T \sum_{n,m} \int_0^1 d(\cos \Theta) \left(\frac{v_T}{c_n} \right)^3 \mathcal{T}'_{mn}(\Theta) \exp \left[- \frac{|z/\tilde{\tau} c_T|}{\cos \Theta} \right], \quad (\text{S40b})$$

where bulk equilibrium energy density in each crystal is given as $\mathbf{u}_{<0}^{\text{eq}} = C_V(T_1)T_1/4V$ and $\mathbf{u}_{>0}^{\text{eq}} = \tilde{C}_V(T_2)T_2/4V$ with specific heat $C_V(T_1)$, $\tilde{C}_V(T_2)$ given in Eqs. (S7).

For some interfaces, the spatial distributions of $\Delta u(z)$ are shown in Fig. S3(b) with red solid curves. Note that energy density $\mathbf{u}(z)$ is continuous at the interface between the same crystals; the jump in $\Delta u(z)$ compensates for the difference in bulk equilibrium energy density between two crystals.